Politecnico di Torino

Politecnico di Torino

MSc in Biomedical Engineering

Context-Dependent Variations in Gait and Head Motion During Real-World Walking

Candidate: Davide Ronco

Supervisors: Prof. Andrea Cereatti
Ing. Paolo Tasca

Academic Year 2024/25

Abstract

In recent years, gait analysis has increasingly shifted its focus toward real-world observations, which allow for a more comprehensive evaluation of individual motor performance. However, the influence of daily-life activities on such performance, and the consequent cognitive load are still scarcely investigated.

To address this gap, this study aims to investigate differences in gait parameters based on the activities performed in real-world conditions. Considering that navigation in real-world environments requires significant exploratory trunk and head movements to manage multiple concurrent visual and auditory stimuli, this work also includes the quantitative observation of head, trunk, and lower back movements.

A total of 11 young adults (60% females, 20-31 years) wore a multi-sensor system, including pressure insoles, distance sensors and 5 magneto-inertial measurement units positioned on the head, chest, lower back, and feet (100 Hz), along with smart glasses for video recording. Data from the feet and lower-back sensors were used to segment strides.

Video data was used to identify and annotate six real-world walking situations: 1) road crossing, 2) texting, 3) phone calls, 4-5) navigation through fixed and moving obstacles and 6) visual search within a supermarket.

Each subject completed four straight walking trials in a lab setting and a 2.5-hour real-world session.

Walking parameters along with head, trunk and lower back parameters were estimated on a stride-by-stride basis, covering five characteristic domains: i) Amplitude, ii) Attenuation, iii) Symmetry, iv) Smoothness and v) Regularity.

A comprehensive dataset was built from the collected data, associating information on concurrent activities to quantitative information on walking and trunk motion parameters on a stride-by-stride basis.

For each of the six annotated types of activity, the computed stride-by-stride parameters were averaged per subject. Real-world situations were compared with each other and with lab walking for all parameters with a one-way repeated measures analysis of variance.

Analysis showed that statistically significant differences are found in all the evaluated domains except for Smoothness measures. Gait parameters (e.g., stride duration) and amplitude measures (e.g., relative yaw angle between head and chest) showed the greatest number of significant differences among activities. For instance, stride duration distributions during visual search (median: 1.378 s, inter-quartile range: 0.268 s) significantly differed from texting (median: 1.029 s, inter-quartile range: 0.094 s), while yaw angle distributions during road crossing (median: 20.762°, inter-quartile range: 11.612°) differed from straight walking (median: 9.925°, inter-quartile range: 1.168°).

These findings demonstrate that gait and trunk and head motion parameters vary substantially depending on the specific activity performed in real-world contexts. As such, aggregating movement data across heterogeneous daily-life situations risks obscuring critical behavioral adaptations. This underscores the importance of incorporating contextual information into real-world gait analysis to ensure accurate, ecologically valid interpretation of motor performance.

Contents

Chapter 1

Introduction

1.1 General introduction and motivation

Human locomotion and head orientation are fundamental to navigate dynamic environments and engaging with the world. The ability to walk efficiently, maintain balance, and stabilize one's gaze is crucial for independent living, occupational performance, and overall quality of life. Understanding these processes is a cornerstone of fields ranging from rehabilitation and sports science to robotics and human-computer interaction. Notably, human movement is rarely a singular task; individuals often simultaneously engage in cognitive or motor tasks while ambulating, a phenomenon known as dual-tasking. These concurrent demands can significantly affect gait parameters and head stability, often revealing subtle deficits in motor control and cognitive-motor integration that may not be apparent under single-task conditions. Or, more simply, they can highlight different strategies and prioritization while handling an additional task while walking.

1.2 Knowledge gap

Despite extensive research into human gait already exists, a significant knowledge gap persists due to a reliance on laboratory-based studies. Although controlled laboratory environments offer precision and reproducibility, they often fail to replicate the inherent complexity, variability, and ecological demands of daily life. The highly constrained nature of lab settings can lead to "white coat effects" on gait, where individuals alter their natural walking patterns, and may not capture the adaptive responses to unpredictable stimuli encountered in real-world scenarios. Moreover, traditional motion capture systems, while highly accurate, are typically confined to limited spaces, making long-term unconstrained monitoring outside the laboratory impractical. Although dual-task paradigms have been widely used to assess cognitive-motor interference, secondary tasks often involve abstract cognitive demands such as serial subtractions or memory recall. These tasks, while valuable for assessing fundamental cognitive load, are often quite different from the rich and varied multimodal stimuli and cognitive demands one encounters in daily activities, such as avoiding obstacles, navigating a crowded street or exploring a supermarket. In recent years, many studies have analyzed real world gait in order to get a more comprehensive insight into individual motor performance, but the influence of daily activities, and the consequent cognitive load, over this performance is still scarcely

investigated. The usual approach based on aggregating movement data across heterogeneous daily-life situations risks obscuring critical behavioral adaptations.

1.3 Aim of the study

This thesis addresses these limitations by investigating the relationship between gait and head movement in response to different activities in real world settings. Exploiting magneto-inertial sensors (MIMUs), paired with indirect monitoring through scene-recording glasses, this research aims to explore this field of growing interest, providing a comprehensive observation of human locomotion and head stabilization in ecologically valid scenarios, focusing on conditions that are hard to reproduce in controlled settings.

Chapter 2

Background

2.1 Gait and postural control during walking

Gait, defined as the manner or style of walking or moving on foot[1], is the fundamental locomotor pattern in humans [2]. Its essential function is to provide efficient and stable forward propulsion of the body, allowing for movement across various surfaces while minimizing energy expenditure[2].

2.1.1 Gait Cycle

The gait cycle is the basic unit of human locomotion and represents the series of events that occur as one limb moves from initial contact with the ground to the next initial contact of the same limb.
The interval between these two events is also referred to as **Stride**. A **Step** is the sequence of events that occurs within successive heel contacts of opposite feet, therefore a stride is composed by two steps, left and right [2].

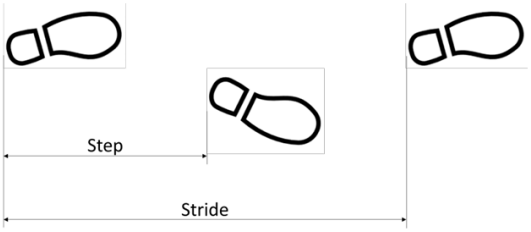

Figure 2.1: Graphic representation of step and stride

The gait cycle is divided into two principal phases: the **stance phase** and the **swing phase**, which are further subdivided into specific subphases, each characterized by distinct biomechanical actions and temporal contributions.

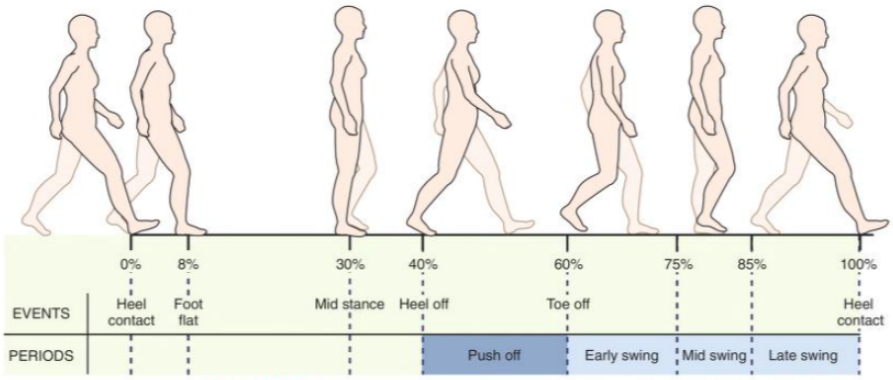

Figure 2.2: stride phases according to Neumann [2]

The **stance phase** constitutes approximately 60-62 % of the gait cycle, representing the period during which the foot is in contact with the ground, providing support and facilitating propulsion [3]. This phase is divided into five subphases[4]:

- **Initial Contact (Heel Strike) [0% to 2%]**:
  Its primary role is to establish contact with the ground and begin the process of weight acceptance, effectively absorbing the initial impact of the limb's interaction with the surface[2].

- **Loading Response (Foot Flat) [2% to 12%]** :
  During this period, the entire foot progressively makes contact with the ground, and the limb functions as a crucial shock absorber, adapting to the terrain and distributing weight. This interval also encompasses the first period of double-limb support[2][3][4].

- **Midstance [12% to 31%]**:
  The body's center of gravity passes directly over the supporting limb, which is the sole foot in contact with the ground [2][3][4]. The primary objective of this subphase is to maintain stability and facilitate the forward progression of the body over the fixed foot [5].

- **Terminal Stance (Heel Off)[31% to 50%]**:
  The body continues its forward advancement over the forefoot, preparing for the propulsive push-off. During this time, the heel continues to rise, and the center of gravity shifts anteriorly relative to the foot [5].

- **Pre-Swing (Toe Off) [50% to 62%]**:
  It signifies the transition from stance to swing, beginning with the initial contact of the contralateral limb and concluding with the reference foot's toe leaving the ground [4]. This subphase is critical for generating the final propulsion to clear the limb from the ground and is part of the second period of double-limb support [4][5].

The **swing phase** comprises the remaining 38-40% of the gait cycle, during which the foot is not in contact with the ground and is actively advanced forward [3]. It is composed of three significant subphases:

- **Initial Swing [62% to 75%]**:
  This subphase begins immediately after toe-off and persists until the swinging foot is opposite the stance limb, coincident with maximal knee flexion.The essential function here is to ensure foot clearance from the ground and initiate the forward advancement of the limb [2].

- **Mid-Swing [75% to 87%]**:
  Mid-swing involves the continued forward progression of the swinging limb, reaching a point where the tibia becomes vertical or perpendicular to the ground [4]. The foot remains clear of the ground as the limb continues its trajectory [2].

- **Terminal Swing [87% to 100%]**: begins when the tibia is vertical and ends just before the next initial contact of the foot with the ground. During this period, the limb decelerates, precisely positioning the foot for the subsequent initial contact and completing the gait cycle [2][5].

Spatio-temporal gait parameters

Gait can be quantitatively evaluated in terms of local parameters (i.e., parameters that quantify gait at the local level of joints or muscles) and global parameters (i.e., parameters that quantify gait globally). Among global parameters, spatio-temporal parameters of gait provide critical insights into an individual's movement patterns, efficiency, and stability. Among these, **stride speed**, **stride length**, and **stride duration** are cornerstone measurements, offering a comprehensive understanding of its temporal and spatial characteristics.

- **Stride length** is defined as the distance covered by one foot during a gait cycle i.e., the distance covered from the initial contact of the foot to the subsequent initial contact of the same foot. It is a key indicator of mobility and can be influenced by various factors, including limb length, muscle strength, joint range of motion (particularly at the hip and knee), and balance [6]. In clinical settings, a reduced stride length can be indicative of pain, weakness, neurological impairment, or a strategy to maintain stability [7]. Maximizing or optimizing stride length, without compromising stability or increasing energy cost, is often a goal in rehabilitation to improve mobility and gait efficiency.

- **Stride duration** is the elapsed time of a gait cycle i.e., the time between an initial contact of one foot and the following initial contact of the same foot. It is directly related to stride frequency, being its mathematical inverse: $StrideDuration = 1/StrideFrequency$. A shorter stride duration implies a quicker turnover of the legs and a higher stride frequency, contributing to faster gait speed [6]. In gait analysis, examining stride duration, along with other temporal parameters like swing phase duration and stance phase duration, provides detailed information about the timing and coordination of movements within the gait cycle. Alterations in stride duration can denote inefficient motor control, compensatory strategies, or underlying neuromuscular

impairments [8], making it an essential parameter for comprehensive assessment.

- **Stride speed**, often expressed in meters per second [m/s], represents the velocity of progression during one gait cycle. It is a direct indicator of locomotor performance [9] and is intrinsically linked to both stride length and stride duration. Physiologically, an optimal stride speed typically reflects an efficient use of energy[10], and deviations can indicate underlying musculoskeletal issues, neurological impairments, or even compensatory mechanisms [6]. For instance, a significantly reduced stride speed might suggest pain, weakness, or a deliberate effort to increase stability, while an unusually high speed could point to a less controlled or rushed gait.

2.2 Head and trunk movements: physiological roles

During gait, the body can be modeled as two separate units with separate functions:

- **The locomotor unit**:
  Constituted by the pelvis and the lower limbs, its role is to alternatively support the body and drive its progression forward. In addition to the propulsive role, it also ensures the absorption of impact of the heel strike, vertical stability and energy conservation, acting as an inverse pendulum.

- **The passenger unit**:
  Consists in arms, head and Trunk. By maintaining the alignment between upper and lower body segments, it reduces unnecessary oscillations of the center of mass. The arms swinging counterweights the rotations induced by the lower limbs [6].

(a) Locomotor Unit (b) Passenger Unit

Figure 2.3: Distinction between locomotor(a) and passenger unit(b) according to Perry [6]

Head stabilization, a dynamic process of maintaining an equilibrium position of the head-in-space [11], is achieved through coordinated head and trunk movements

[12]. This coordination allows the sensory systems to orient for optimal function and maintain a stable reference frame [13] [11].
In healthy gait, head rotates to compensate body traslations, in both sagittal and horizontal plane [11][14]. Head-on-trunk rotations also ensure head stability in space, particularly at higher frequencies of trunk motion where it is significantly challenged [12]. For example, studies suggest that during locomotion, reflexive head movements operate to minimize horizontal head translation and simultaneously compensate for vertical translation by pitching the head [13]. The trunk plays a crucial role in minimizing head motion by attenuating gait-related oscillations, acting as a low-pass filter for gait-related harmonics [14]. This attenuation process is gradual from inferior to superior body segments. In healthy young adults, head accelerations are smoother and have a greater proportion of power at lower frequencies compared to trunk accelerations [15].
The differences in power spectral properties between the head and trunk are most pronounced in the mediolateral direction. Head accelerations in the mediolateral direction are characterized by a peak frequency corresponding to half of the peak frequency for the vertical and anterior-posterior directions. This is due to the intrinsic biphasic nature of gait [16]: during a stride the center of mass endures two perturbations on the vertical and anterior posterior axis, one for each step. On the mediolateral instead the oscillation is monophasic (left-right-left or opposite) and results in the frequency profile described before.
In addition, upper body coordination plays a crucial role in stabilizing and optimizing sensory inputs during walking. In particular visual and vestibular stability are crucial for effective balance and locomotion [15].

2.2.1 Gaze and visual exploration

Visual exploratory movements are a complex, coordinated process involving the eyes, head, and often the entire body, all working together to actively gather information from the surrounding environment. This active information-seeking behavior is crucial for perception, object recognition and spatial awareness [17].

Figure 2.4:
Visual exploration is a key part of environmental interaction (AI generated image)

The primary components typically include:

- **Eye Movements (Saccades and Fixations)**:
  The eyes make rapid, jerky movements called saccades to quickly shift gaze from one point to another, interspersed with brief pauses called fixations, during which visual information is acquired [18]. These eye movements allow for scanning and detailed analysis of specific areas of interest within a scene. Saccades are one of the fastest movements produced by the human eye, with normal speeds of about 300-400°/s [19].

- **Head Movements**:
  For larger shifts in gaze beyond the oculomotor range of the eyes (approximately ±40° horizontally), head movements become increasingly important [17]. The head can rotate to expand the field of view and orient the eyes more effectively towards a target. This coordination allows for more extensive exploration of the environment [17].

- **Body Movements**:
  In naturalistic settings, the entire body may contribute to visual exploration. Reorienting the trunk or feet in space can facilitate even larger gaze shifts, allowing an individual to survey a vast or complex environment with purpose [17].

These components are not independent but rather operate in a coordinated and adaptive manner, influenced by both bottom-up (cues and sudde stimuli) and top-down (searching for a specific object) factors, as well as biomechanical and physiological ones [17].

2.3 Moving outside the lab: Walking in real world conditions

2.3.1 Multitasking: definitions

In everyday life, human locomotion frequently involves the simultaneous performance of a cognitive task, making multitasking during walking the norm rather than the exception [20]. This concurrent engagement in two tasks, defined as "dual-tasking," requires attention to be divided between motor and cognitive components, even though gait control is often considered automatic [21]. The addition of a cognitive load, which refers to the mental effort required to perform a task, can significantly impact an individual's ability to control dynamic balance and gait [22]. This competition for limited cognitive resources often leads to cognitive-motor interference (CMI), characterized by a deterioration in the performance of either the motor task (e.g., walking), the cognitive task, or both[23].

2.3.2 Multi-Tasks in controlled settings

Multi-task paradigms are designed to assess the impact of cognitive load on motor performance, and the type of cognitive task employed can significantly influence the observed interference [23]. These tasks generally fall into categories based on the nature of the cognitive demand, as systematically reviewed in the literature [24][20]:

- **Arithmetic Tasks**:
  Mental calculation is frequently used to impose a continuous cognitive load. Common examples include serial subtractions (e.g., subtracting 7s or 3s continuously from a given number) or counting backwards.

- **Verbal Fluency Tasks**:
  Assesses the ability to retrieve information from semantic memory. Participants are typically asked to generate words within a specific category (e.g., naming animals) or starting with a particular letter.

- **Memory Tasks**:
  Challenge of working memory and recall abilities. Examples include recalling a list of words or numbers, or spelling words backwards.

- **Reaction Time Tasks**:
  Measuring of the speed of response to a stimulus, often involving simple or choice reaction time to visual or auditory cues.

- **Executive Function Tasks**:
  These tasks engage higher-level cognitive processes such as inhibition, planning, and cognitive flexibility. In tests that rely on this kind of stimuli, usually patients are asked to produce responses that are discordant with given visual or auditory stimuli (ex. Stroop, Go/No-go test)

- **Motor-motor interference**:
  In this category fall those tasks that involve the execution of two motor activities simultaneously.

It is consistently demonstrated that an increase in cognitive load can result in altered walking patterns, such as reduced gait speed, increased gait variability, and changes in stride parameters, indicating a decrease in walking stability. [25][26][21]. Understanding these interactions is crucial, as the trade-offs between automaticity and cognitive control during walking have significant implications for various populations, particularly in assessing fall risk and designing effective preventive solutions [22][27].

2.3.3 Multi-tasking: Ecological paradigms

Although numerous protocols have been developed to assess the effects of multitasking in laboratory settings, they typically focus on high-level information processing. While this approach effectively demands a redistribution of cognitive resources, it represents only a narrow segment of the wide array of inputs encountered in everyday life.
Most of the time, people do not walk while solving complex calculations or spelling words backwards. Instead, they continuously gather and process the flow of sensory information from the environment to navigate it efficiently. Therefore, capturing the effects of environmental context becomes crucial to truly understanding how walking tasks are managed in real-world conditions. However, traditional dual-task paradigms often fail to reproduce the lower-level stimuli that are constantly present in ecological settings.

Real world navigation

Considerable efforts have been devoted to addressing this critical issue by replicating specific walking conditions(such as street crossings) in controlled environments. These experimental setups often include the simulation of ambient noise and the projection of real-world videos [28], or alternatively, the use of virtual reality techniques [29]. Such approaches aim to recreate realistic scenarios in a safe and controlled manner, thereby enabling a more accurate analysis of pedestrian behavior and the factors influencing it.

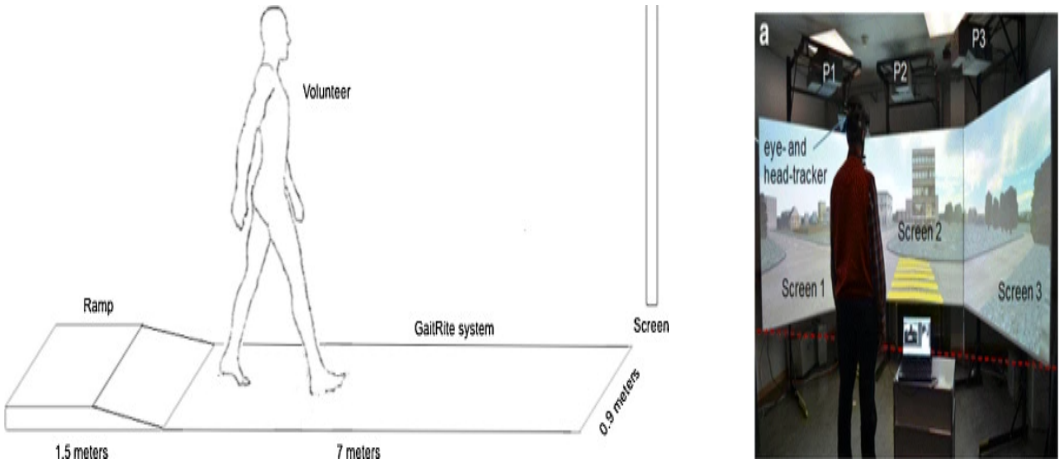

(a) (b)

Figure 2.5: Experimental setups of the studies from (a) Vieira et al. [28] and (b) Zito et al. [29]

Smarthone usage

Another important influencing factor in daily walking is phone usage. This ubiquitous integration of mobile technology into our lives has made "distracted walking" a growing concern, transforming what was once a simple task into a complex, multifaceted behavior.
Consequently, understanding the impact of smartphone use on ambulation has become an increasingly important area of study. Analyzing this condition in daily walking is crucial due to its implications for pedestrian safety, public health, and the design of urban environments.
For instance, some research involves collecting gait data during an instrumented walk, typically lasting a few minutes, with young adult participants. During these experiments, researchers compare normal walking conditions with walking while texting, measuring spatio-temporal parameters, ankle and knee kinematics, and the co-contraction of ankle antagonist muscles [30]. Other studies have been conducted in outdoor environments to provide more ecological validity, investigating gait and posture responses to various smartphone usage tasks with different cognitive loads. These outdoor experiments aim to understand how real-world smartphone interactions affect locomotion and posture [31]. The findings from such setups consistently show that smartphone use while walking can reduce gait speed, shorten stride length, and decrease toe clearance [30][31].

Context aware analyses

In recent years new datasets are providing recordings of human locomotion in various out-of-laboratory settings, including urban environments, public spaces, and obstacle courses. These datasets include full-body kinematics alongside egocentric vision and gaze data from everyday walk scenarios[32][33]. This shift acknowledges that human gait is significantly influenced by the environment and external factors, with individuals adapting their movements and gaze based on the complexity of their surroundings.

2.4 Wearable technologies for real world movement analysis

Instrumentation for ecological gait observation must be portable and minimally invasive. Wearable sensors are well suited to meet this need, as they enable the acquisition of large amounts of data over extended periods of time, ideally without interfering with the subject's movement or being restricted by the environment in which they are used.

2.4.1 Motion capture devices

Motion capture, often abbreviated as mocap, is a technology used to record the movement of objects or people and translate it into digital data. This process allows for the realistic animation of digital characters and the detailed analysis of human movement.

Magneto-inertial measurement units

Inertial Measurement Units (IMUs) directly measure acceleration and angular velocity, with respect to an inertial reference frame [34].Together with magnetometers, they are often embedded within MIMUs. Inertial systems offer greater portability and freedom of movement, making them suitable for outdoor or less controlled settings, at the cost of lesser accuracy compared to laboratory-based technologies.

These sensors incorporate three different technologies:

- **Accelerometer**
  Accelerometers measure acceleration along one, two, or three sensitive axes; those capable of measuring in all three spatial directions are commonly referred to as tri-axial accelerometers. They detect proper acceleration ($\vec{a}_p$), which is the vector difference between the coordinate acceleration ($\vec{a}_c$, the rate of change of the sensor's velocity) and the acceleration due to gravity ($\vec{g}$).

  $$\vec{a}_p = \vec{a}_c - \vec{g}$$

  As a result, the output of an accelerometer does not reflect the total acceleration experienced by the sensor, but rather the difference between that acceleration and gravity. For example, a 1D accelerometer in free fall, aligned with the gravitational axis, will output 0 m/s^2, while the same sensor at rest will read approximately $|\vec{g}| = 9.81 m/s^2$.

  An accelerometer can be modelled as a second order spring-mass-damper system with proof mass m, elasticity constant k and damping factor β . When a force $\vec{F}$ is applied to the system, the proof mass, the spring and the damper tend to react with forces opposed to the applied force. According to the Newton's second law - which states that the algebraic sum of all the forces equals the inertial force of the proof mass - the vectorial sum of the applied force and the forces exerted by the spring and by the damper (respectively $\vec{F}_k$ and $\vec{F}_\beta$) equals the inertial force acting on the proof mass $\vec{F}_I$:

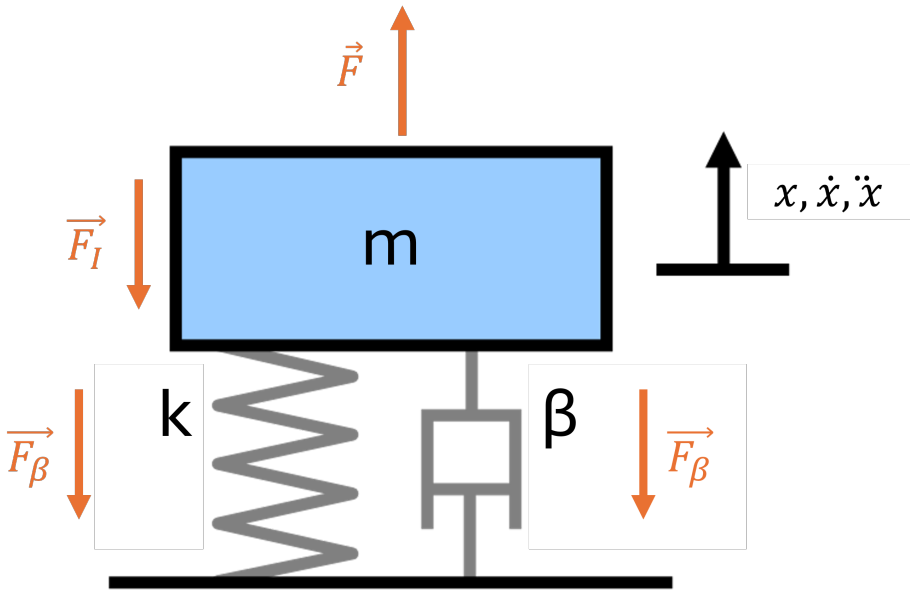

Figure 2.6: 2^{nd} order mechanical system

$$\vec{F} + \vec{F}_\beta + \vec{F}_k = \vec{F}_I$$

Linear displacement x, velocity $\dot{x}$ and acceleration $\ddot{x}$ of the mass can be rewritten by expliciting the definitions of the damping, elastic and inertial forces:

$$F - \beta\dot{x} - kx = m\ddot{x}$$

The applied force can be also written as the scalar product between the proof mass and the acceleration of the system a_c:

$$m\ddot{x} + \beta\dot{x} + kx = F = ma_c$$

The acceleration a_c represents the accelerometer input and - in absence of gravity - it corresponds both to coordinate and proper accelerations. If the sensitivity axis is parallel to gravity, the gravity acceleration exerts on the mass a force proportional to the mass itself. Then, the accelerometer will measure the proper acceleration a_p, which includes the gravity contribution:

$$m\ddot{x} + \beta\dot{x} + kx = m(a_c - g) = ma_p$$

Being the previous equation a second order non-homogeneous differential equation, its solution is hard to compute in the time domain, while it is easily done in the Laplace domain:

$$kx(s) + bsx(s) + ms^2x(s) = F(s) = ma(s)$$

By rearranging the terms, the ratio between the output displacement $x(s)$ and the input acceleration $a(s)$ can be easily obtained:

$$H(s) = \frac{x(s)}{a(s)} = \frac{1}{s^2 + \frac{\beta}{m}s + \frac{k}{m}} = \frac{1}{s^2 + \frac{\omega_0}{Q}s + \omega_0^2}$$

H(s) is the system transfer function, while Q and ω_0 correspond respectively to the quality factor and to the resonance angular frequency:

$$Q = \frac{m\omega_0}{\beta}$$

$$\omega_0 = \sqrt{\frac{k}{m}}$$

The transfer function of an accelerometer describes its dynamic sensitivity, which varies with the frequency of the input signal. Sensitivity decreases with the square of frequency, from a maximum value $H(0)$ for constant acceleration, down to zero as frequency approaches infinity. To ensure accurate measurements, accelerometers are typically operated well below their resonance frequency($\omega << \omega_0$). A higher resonance frequency allows for a wider bandwidth but reduces sensitivity, making accelerometer design a trade-off between bandwidth and sensitivity.

- **Gyroscope**
  Gyroscopes measure angular velocity along up to three sensitivity axis (gyroscopes that measure angular velocities in all the three directions are commonly called tri-axial gyroscopes). Angular velocities measurements are generally expressed in degrees per second (dps). the most common type of gyroscopes is based on the Coriolis force; hence, they are called *Coriolis vibrating gyroscopes* or *Vibrating forks gyroscopes*. Every time that an object with mass m rotates and translates respectively at angular rate $\vec{\omega}$ and linear speed $\vec{v_t}$, a force F_c named Coriolis force is applied to the object.

$$F_c = 2m\vec{v_t} \times \vec{\omega}$$

Vibrating forks gyroscopes include a pair of proof masses that oscillate with the same amplitude, but in opposite directions. At rest, the tines resonate in anti-phase in the plane of the fork (drive mode). When the sensor is put into rotation, the tines begin to oscillate also along the orthogonal direction to the plane. This oscillation generates a torque that triggers the torsional mode around the gyroscope stem. Forks can feature with one, two or more tines: the more the tines, the higher the sensitivity and rejection to common-mode errors.

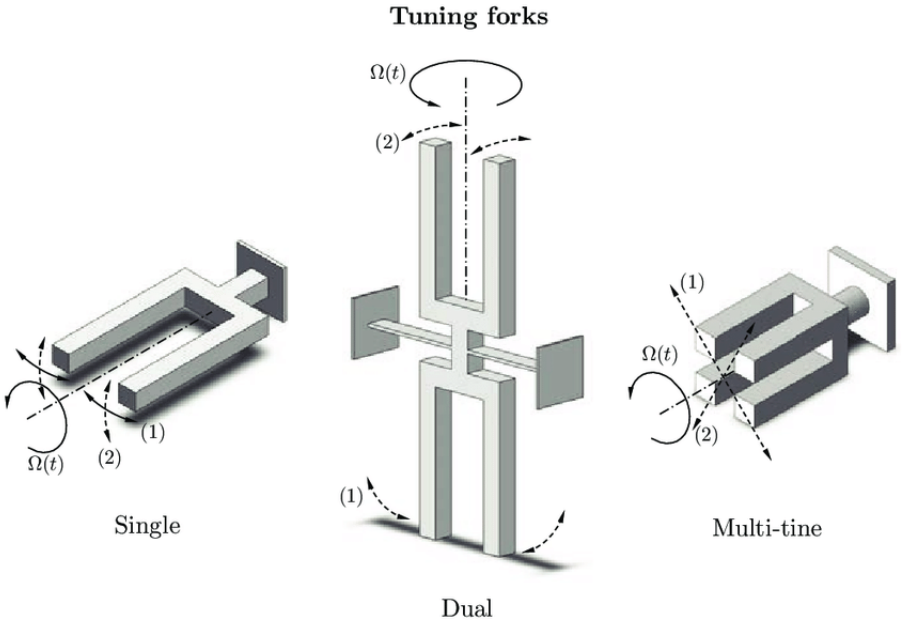

Figure 2.7: Different types of tuning forks [35]

- **Magnetometer**
  Magnetometers are instruments designed to measure magnetic fields. Their fundamental principle of functioning relies on various physical phenomena that are sensitive to the presence and strength of a magnetic field.One common principle involves the Hall effect. When a charged particle q is moving in a conductive plate with istantaneous speed $\vec{v}$ and is immersed in a magnetic field with magnetic flux density $\vec{B}$, the particle experiences a force $\vec{F_L}$ known as Lorentz force:

$$\vec{F_L} = q(\vec{v} \times \vec{B})$$

  Under this force, charged particles move in transverse direction and generate an electric field across the sides of the plate. The contribution of Lorentz force and the one of the electric field balance the charge distibution.

$$\vec{F}_{TOT} = q(\vec{v} \times \vec{B}) + q\vec{E}_{Hall}$$

  If those forces are at equilibrium $\vec{F}_{TOT} = 0$:

$$(\vec{v} \times \vec{B}) = -\vec{E}_{Hall}$$

  The Hall effect results in a voltage difference that can be measured across the sides of the plate.This voltage is directly proportional to the magnetic field strength, allowing the magnetometer to quantify it.

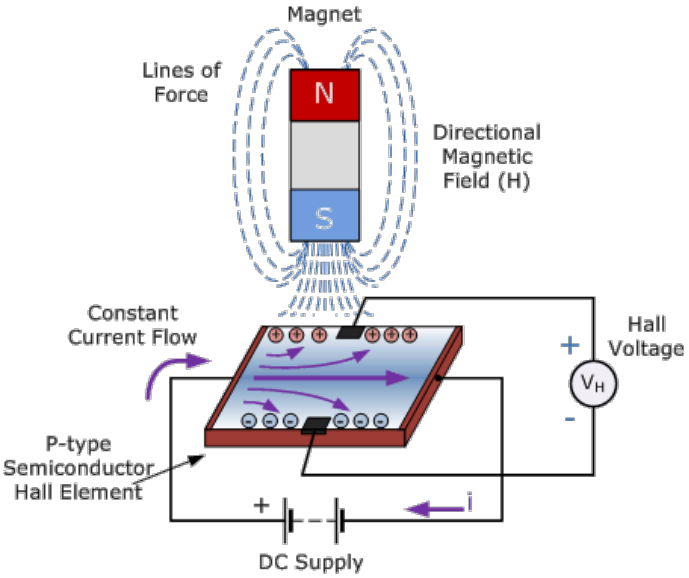

Figure 2.8: Visual scheme of the Hall effect

Pressure insoles

Pressure insoles are groups of force sensing resistors, usually embedded in a flexible plastic substrate. Their shape allows to insert them directly into the subject's shoe and adhere to the foot shape. They allow to describe the distribution of force exerted on the ground by the foot and identify heel strikes and toe offs during the gait cycle.

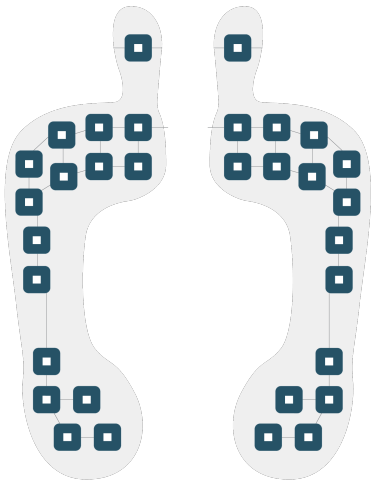

Figure 2.9: Pressure insoles from 221e

Barometers

Barometers measure the atmospheric pressure around them, usually used as environmental sensors or altimeters [36]. They are being recently included among wearable technologies as vertical position detectors [36] and center of mass trackers [37]. Pressure is measured through the deformation of a membrane using piezoresistors (piezoresistive barometers) or capacitance variation of parallel plate capacitors

(capacitive barometers) . In either case the pressure output $P(Pa)$ can be converted in the altimetric data $z(m)$ bi resolving the following equation [36].

$$P(z) = P_0 * e^{-\frac{z}{H}}$$

Where P_0 is the reference pressure at $z = 0$ and H is the *pressure scahe height*, namely the distance (vertical or radial) over which a physical quantity decreases by a factor of e.

$$H = \frac{k_b * T}{m * g}$$

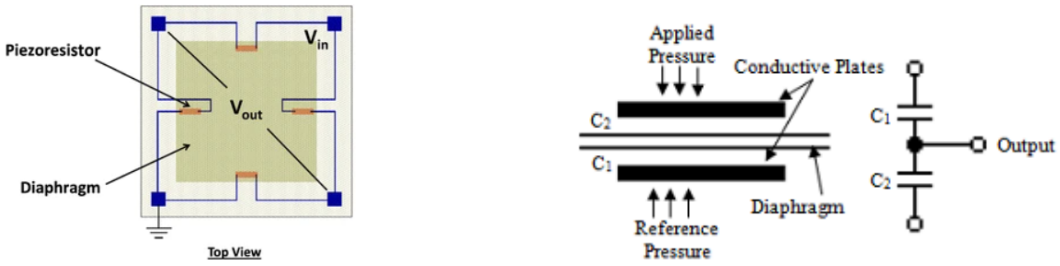

(a) Piezoresistive barometer [38] (b) Capacitive batometer [39]

Figure 2.10: Difference in barometer principle of functioning

Proximity sensors

Infrared proximity sensors are used in gait analysis for event detection and distance measuring [40] (e.g. base of support estimation[41]). The most recent technologies employ IR-time of flight devices. The distance is estimated by measuring the phase shift between the radiated and the reflected IR waves [42]. Emitter and receiver are built in the same hardware component and and allow to reduce overall encumbrance of the sensor.

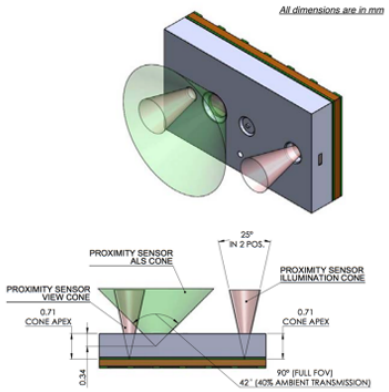

Figure 2.11: VL6180X distance sensor schematics

2.4.2 Scene-recording devices

Scene-recording devices allow to monitor the subject actions and environmental conditions without physically interfering with the activities. In order to grant ecological validity those devices must be worn by the subject and have minimum to no encumbrance.

Smart glasses

In recent years, smart glasses have gained increasing popularity due to their potential to seamlessly integrate digital information into user's everyday visual experience. Combining wearable technology with augmented reality capabilities, smart glasses are being adopted across a wide range of fields, from healthcare and industrial applications to research and personal use. Their ability to capture video, display real-time data, and support hands-free interaction makes them a valuable tool for both professional and everyday scenarios. They also find more and more applications in motion analysis. Commercial devices include both simpler models with a frontal camera in the glasses frame without other functionalities, and more complex ones with integrated IMUs and gaze tracking. Smart glasses are the less invasive option for context monitoring and provide an acceptable approximation of the user's field of view, but often have limited video resolution and reduced battery life.

(a) (b) (c)

Figure 2.12: Ray-Ban meta glasses(a), Doctorspy CAM.58 video recording glasses(b) and Tobii pro 3 wearable eye trackers(c)

Body mounted cameras

Body mouted cameras are widely used in sports to capture a first person perspective of athlete's actions and environments.These devices offer valuable insights into performance, technique, and decision-making by recording real-time visual and audio data from the athlete's point of view. They are widely adopted in training, performance analysis, and even broadcasting. Body mounted cameras have great video resolution and battery capacity, but are more bulky and heavy, making them less suitable for head-mounting.

(a) (b) (c)

Figure 2.13: GoPro Hero 13 (a), GoPro Chesty body harness(b) GoPro Head Strap 2.0 head mount(c)

Chapter 3

Materials and methods

The objective of this study was to acquire a comprehensive dataset of gait and upper body motion parameters, with a particular focus on head and trunk dynamics during real-world walking. To achieve this, a dedicated experimental setup and protocol were specifically designed and implemented to enable the collection of high-resolution motion data and the extraction of relevant biomechanical metrics. The following sections describe in detail the instrumentation used, the data acquisition procedures, the experimental protocol, and the processing steps applied to derive the parameters of interest.

3.1 Participants

Twenty-one healthy young adults (10 females, 11 males; age range: 20–31 years)[1] were enrolled in the study. All participants reported no history of neurological, musculoskeletal, or vestibular disorders that could affect gait or postural control. Prior to participation, each subject provided written informed consent. The study protocol was conducted in accordance with the Declaration of Helsinki.

3.2 Experimental setup

3.2.1 The INDIP system: Overview

All participants were equipped with the multi-sensor INDIP (INertial module with DIstance sensors and Pressure insoles) system [43]. The INDIP system is a multi-sensor wearable system designed by Università degli Studi di Sassari, widely used as a gold standard for the extraction of spatio-temporal parameters of gait in both laboratory and real-world conditions[44][45][46][47]. The core of the INDIP system is represented by 9-axes MIMU, serving as central gateaway for other peripherals. Peripherals can include other sensors for wearable motion capture, such as 16-channels force-sensing resistor pressure insoles, time-of-flight proximity sensors, load cells, or high-resolution barometers.

[1] Due to labeling or acquisition issues, only data of 11 subjects was analyzed.

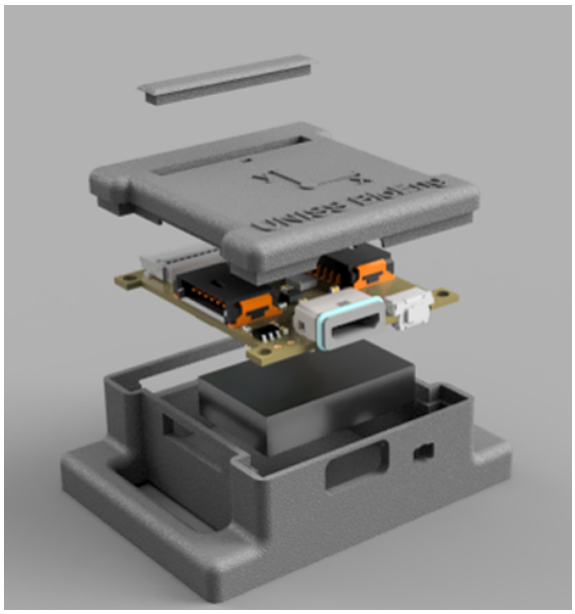

Figure 3.1: 3-D overview of an INDIP MIMU

TRI-AXIAL ACCELEROMETER	
Measurement range	Up to ±16 g selectable FSR
Zero-g offset	±40 mg
Rate noise density	1.8- 3.0 mg (Root Mean Squared (RMS))
Output data rate	1.6 to 6664 Hz
TRI-AXIAL GYROSCOPE	
Measurement range	Up to ±2000 dps selectable FSR
Zero-rate offset	±1 dps
RMS noise	0.075 dps
Output data rate	1.6 to 6664 Hz
TRI-AXIAL MAGNETOMETER	
Measurement range	U±50 G
Zero-G offset	dynamically cancelled
Rate noise density	3 mG (RMS)
Output data rate	10 to 100 Hz

3.2.2 INDIP configuration adopted in this study

In this study, the INDIP system configuration included 5 MIMU units and 2 force-sensing pressure insoles, positioned as follows:

- **Head**:
  A MIMU unit placed on the left temporal side of the head right above the ear. It was secured in position using a velcro strap or alternatively mounted on a cap with a sewn plastic support.

- **Chest**:
  A MIMU unit placed directly on the sternal manubrium and secured on clothing or directly on the skin with bi-adhesive tape.

- **Lower back**:
  A MIMU unit placed on the lower back in the correspondence of the 5^{th} lumbar vertebra with a velcro band of appropriate size.

- **Feet**
  Two MIMUs secured to laced shoes via custom support modules.

  - **Left foot**:
    The support consists in a 3D-printed clip applied to the shoelaces.
  - **Right foot**:
    The support consists in a 3D-printed L-shaped support base that the INDIP is secured to, along with two additional proximity sensors. The base itself is secured to the shoe using adhesive velcro bands.

  For both sides, a force-sensing pressure insole was connected to the hardware and inserted inside the shoe. A protective leather insole was added to protect the sensorized pressure insole.

All sensors sampled at 100 Hz.

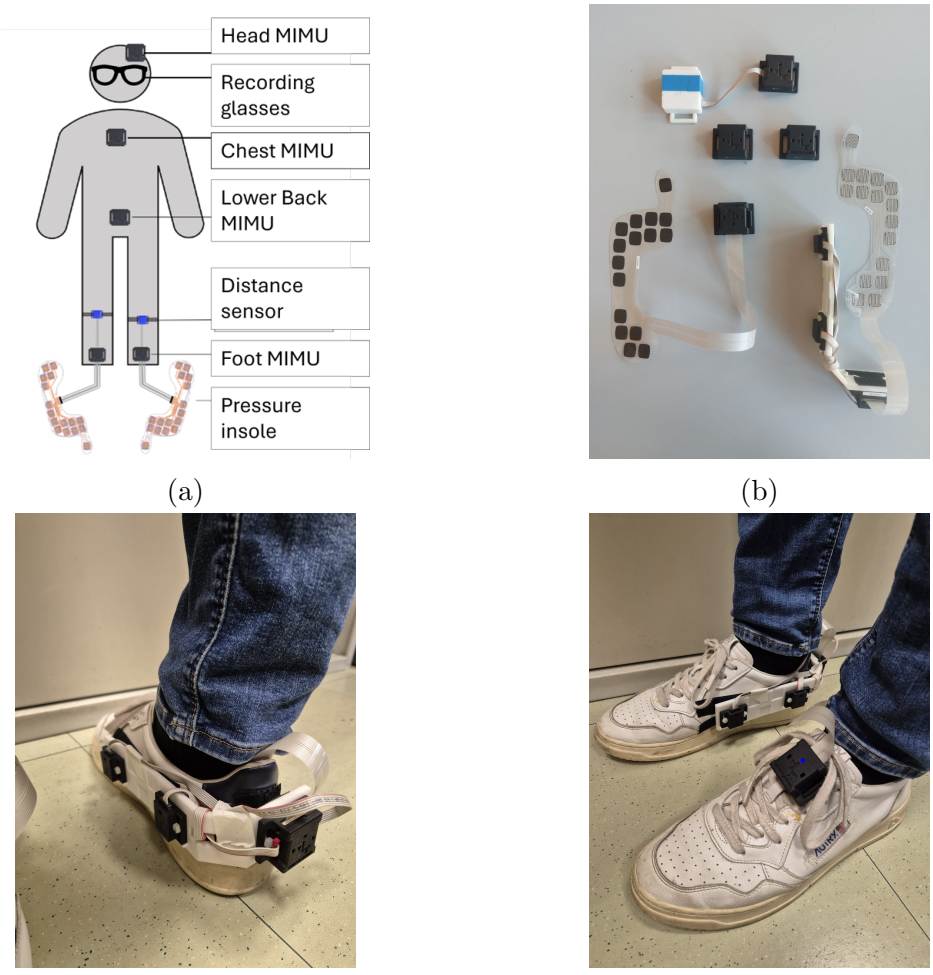

Figure 3.2: Sensor positioning on the body (a), top view of the INDIP setup (b), rear view of the right foot support (c) and view of both the instrumented feet (d)

3.2.3 Collecting data with the INDIP system

To collect time-synchronized data from multiple INDIP MIMUs and peripherals, it is necessary to set all the MIMUs' internal clocks to a common computer's timestamp. This can be done through a custom graphic user interface (GUI) previously developed in Matlab. Once that all MIMU have their internal clock set, sensors can be placed on the subject's body and connected via bluetooth low-energy (BLE) to a custom app developed in Matlab, which allows the user to trigger the acquisition of all the connected sensors. Once that the acquisition has started, the participant is free to move: the MIMUs disconnect when the participant walks too far from the computer; however, once that the sensors have started recording, they continue to log data offline. At the end of the recording, sensors may be reconnected to the app via BLE to stop the acquisition and then connected via USB to the GUI to download recorded data.
For more details regarding data collection with the INDIP system, see Section 3.4.

3.2.4 Scene-Recording Glasses

To enable contextual labeling of gait and motor behavior in naturalistic settings, all participants were equipped with a pair of video-recording glasses (DoctorSpy CAM.58). These glasses continuously captured both video and audio data from the wearer's point of view throughout all experimental sessions, without interfering with natural behavior or obstructing the visual field. The collected footage was later synchronized with sensor data and manually annotated to identify real-world walking activities and environmental events relevant to the analysis (for more details see Subsection 3.4.6). Table 3.1 summarizes the technical specifications of the scene-recording glasses used in this study.

(a) (b) (c)

Figure 3.3: DoctorSpy CAM.58 Video Glasses (a), front (b),and side (c) view of the head setup

Table 3.1: Technical Specifications of the DoctorSpy CAM.58 Video Glasses

Feature	**Specification**
Model	DoctorSpy CAM.58
Resolution	1920 × 1080 pixels (Full HD)
Frame Rate	30 frames per second (fps)
Audio Recording	Built-in mono microphone
File Format	avi (H.264 encoding)
Storage Capacity	MicroSD card up to 64 GB
Battery Life	Approximately 120 minutes per charge
Charging Interface	USB 2.0
Operating Temperature Range	-10°C to 50°C
Weight	34 grams
Form Factor	Integrated camera in eyeglass frame

3.3 Experimental protocol

The experimental protocol was designed to capture the natural variability of head, trunk, and gait movements in response to both induced tasks and spontaneous environmental stimuli and activities. To this end, data collection included both controlled laboratory acquisitions and an extended free-living session in real-world conditions. The laboratory trials ensured standardization and served as a reference for baseline gait and upper-body motion. The 2.5-hour real-world session aimed to reflect the complexity and unpredictability of daily-life contexts, enabling the observation of motor behavior under a wide range of sensory and cognitive demands. This combined approach allowed for a comprehensive analysis of how different environmental and activity-related factors influence locomotor and upper body dynamics.
All the acquisitions took place at the Department of Electronics and Telecommunications at Politecnico di Torino and the surrounding neighborhood in the city of Turin (TO, Italy).
All the recordings included a 5-seconds calibration phase at the start and end of the trial during which the subjects were asked to maintain standing position while keeping a neutral alignment between head, trunk and pelvis. This was done to ensure at least one static interval at the beginning of each recording to remove the gyroscope bias and initialize the head-MIMU orientation estimate.

3.3.1 In Lab

The *In lab* component consisted of a battery of standardized walking trials aimed to elicit specific visual or auditory stimuli, designed to investigate the influence of typical daily-life tasks on motor control. All tests (except for visual search) had a duration of 1 minute and were conducted along a 12-meter walkway set up in a university corridor.
In this time subjects were asked to walk back and forth at self selected speed, performing smooth U-turns when reaching the extremes of the route.
During the acquisitions, no constraints were imposed on the participants's head and trunk motion.
Tests included:

- **Straight Walking**
  walking back and forth at self-selected comfort speed for one minute with no additional stimuli.

- **Texting**
  walking for one minute while typing text messages.

- **Scrolling**
  walking for one minute while browsing a webpage or scrolling on their favorite social network without text generation.

- **Calling**
  walking for one minute while phone-calling a friend/colleague. The phone call was initiated before the start of the recording and ended after its completion, in order to avoid repetition of gestures similar to the previous two tasks.

- **Audio track comprehension**
  Listening to an audio track through earphones while walking for one minute[2]. The exact same audio was played for all participants. To ensure active listening, participants were informed that they would be asked questions about the content of the audio track at the end of the recording session.

- **Audio Disturb**
  This task was proposed to the subjects as a second straight walking trial. During the acquisition, without any warning, and when they were facing away from the experimenter, the latter called the subjects by their name in order to get their attention and induce a response. After that, they were instructed to continue to walk and the onset of the disturbance was annotated.

- **Visual search**
  The visual search task consisted in walking while actively trying to distinguish between tags reporting the letter "O" and the number "0" (Figure 3.4a and 3.4b) placed at different heights on the corridor walls where the tests were conducted. In this test, participants began the recording facing away from the walkway to prevent them from seeing the tag positions in advance. At the start signal, they were instructed to turn around and walk the path back and forth, while counting the tags of a predefined type. At the end of the recording, the participant was asked to report the number of counted "O"s and "0"s.

[2]The audio track was a listening exercise of an online Italian language course, available on the webpage of the website *"lingua.com"*: [`https://lingua.com/it/italiano/ascolto/mia-nuova-macchina/`].

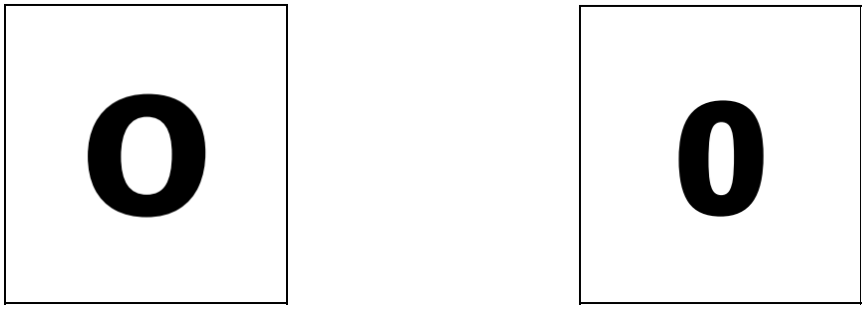

(a) (b)

Figure 3.4: Tags used in the visual search test. The font and text size have been selected to make the distinction between the two types challenging but feasible.

These structured tasks were used to establish reference movement patterns under repeatable conditions. The subsequent real-world session aimed to reflect the complexity and unpredictability of daily contexts, enabling the observation of motor behavior under a broader range of sensory and cognitive demands.

3.3.2 Out of Lab

The *Out of lab* session was designed to capture natural motor behavior in real-world environments, allowing for the assessment of gait and trunk and head movement in response to unstructured, ecologically valid stimuli.

Following a synchronization task[3], participants were completely free to move and behave naturally during a 2.5-hour unsupervised recording session. They were not given specific instructions regarding the type or duration of the activities to perform, in order to avoid altering their spontaneous behavior. The only required action was to visit a nearby supermarket and purchase a predetermined item. This step ensured that all participants were exposed to a similar visual search task, which was later used as a reference condition for comparison.

Throughout the session, participants wore the multi-sensor setup, including the INDIP system and scene-recording glasses, allowing for the continuous capture of gait-related parameters, head and trunk motion, and the surrounding environment. This protocol aimed to reflect the complexity, variability, and contextual richness of everyday life, providing an authentic framework for the investigation of context-dependent motor control.

3.4 Data Collection and Preprocessing

3.4.1 Data collection and synchronization

All data acquisition sessions were conducted using the custom-developed *INDIP App*, which enables the simultaneous connection and data logging of multiple INDIP MIMU via Bluetooth connection. This application allowed for efficient deployment

[3]At the start of the Out of lab recording, participants were asked to execute at least three full rotations on the spot before engaging in further activities. This action was required to align video and MIMU information for further analyses.

of the full multi-sensor setup in both laboratory and real-world scenarios[4] Once each acquisition was completed, the data were manually retrieved from each device using a custom USB-based graphical user interface (INDIP GUI). This interface was also employed to synchronize the internal clocks of all INDIP units prior to data collection[5].
Video recordings from the smart glasses were also retrieved and stored in a dedicated folder associated with the participant's ID.
Videos were downloaded and converted from `.avi` to `.mp4` format and compressed with lower resolution (from 1080p to 720p) using the Handbrake open source software, with a memory saving around 30-40%.

3.4.2 Anthropometric parameters

Alongside sensor data, various anthropometric parameters were recorded for each participant (Table 3.2). These parameters were later used to personalize gait and posture computations.

Table 3.2: Overview and description of the annotated anthropometric parameters.

Anthropometric parameters	
Parameter	**Description**
Foot length [cm]	distance between big toe and heel on the longitudinal axis
Shoe width [cm]	maximum medio-lateral distance of the shoe
Shoe length [cm]	maximum antero-posterior distance of the shoe
Participant age [years]	participant's chronological age at the time of data collection
Participant height [cm]	participant's height at the time of data collection
Participant weight [kg]	participant's weight at the time of data collection
Shoe size [EU]	size of the shoe reported using the European sizing system
Posterior waist width [cm]	width of the trunk at the height of the INDIP sensor on the person
Lower back sensor height [cm]	height of the MIMU on the lower back from the ground
Inter A.S.I.S. distance [cm]	distance between right and left Anterior-Superior Iliac Spines (A.S.I.S.)

[4]Although INDIP devices are connected to the app via Bluetooth for setup and initialization, they operate as standalone data loggers during recording. This approach is essential for Out of lab sessions, where the distance between the sensors and the acquisition computer often exceeds the Bluetooth range, rendering live streaming impractical.

[5]Synchronization was achieved by manually setting the timestamp of each device to match the current system time of the host PC, ensuring temporal alignment across all sensor data streams.

Anthropometric parameters (continued)	
Parameter	**Description**
Pelvis–Hip distance [cm]	distance between right A.S.I.S. and the greater trochanter
Thigh Length [cm]	distance between the greater trochanter and the lateral epicondyle
Shank Length [cm]	distance between the lateral epicondyle and the lateral malleolus
Foot Height [cm]	height of the lateral malleolus from the floor with the shoes on
Head-Chest sensor distance [cm]	vertical distance between the MIMUs mounted on the head and the chest

3.4.3 Data standardization

After retrieval, all raw data were standardized and organized into a hierarchical `data.mat` structure using MATLAB R2024A (The Mathworks Inc.). This structure consolidated all recordings and metadata related to a given participant into a single, organized file, thereby facilitating streamlined processing and analysis in the subsequent stages of the study. Inside this file, all sensor data are expressed in the reference frame proposed by Palmerini et al. [48].

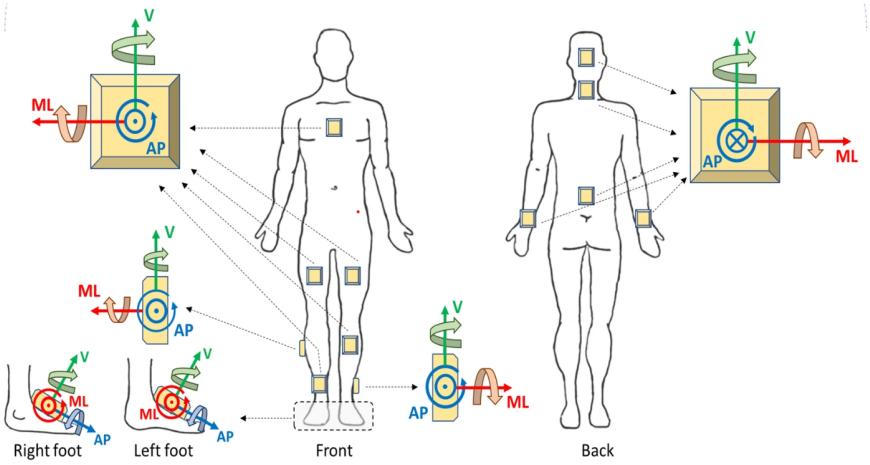

Figure 3.5: Sensors reference system orientation according to Palmerini [48].

The standardization process was performed using a custom written Matlab code. It gathered all sensor data from each recording, applied pre-computed calibration matrices for gain and drift correction, and synchronized them using a common timestamp. After that, data were resampled in order to have a sampling interval of exactly 0.01 s ($sf = 100Hz$), before being saved in an organized structure.

3.4.4 INDIP pipeline

Standardized data was processed with a validated algorithm pipeline for the estimation of spatio-temporal parameters of gait [43]. This pipeline processed the

calibrated inertial sensors recordings and data recorded by pressure insoles stored in the `data.mat` file to segment gait sequences and, for each gait sequence, derive a comprehensive set of spatio-temporal parameters of gait (Figure 7.3). For each processed recording, the output of the pipeline included:

- **Gait sequences**: Start and End timepoints of each continuous walking period within each recording.
- **Turns**: Start and End timepoints of each turning interval within each gait sequence.
- **Strides**: Start and End timepoints of each stride within each gait sequence.
- **Stride duration, stride length and stride speed**: Duration, length and speed associated to each stride within each gait sequence.

For more details regarding the definition of the output parameters see [43].

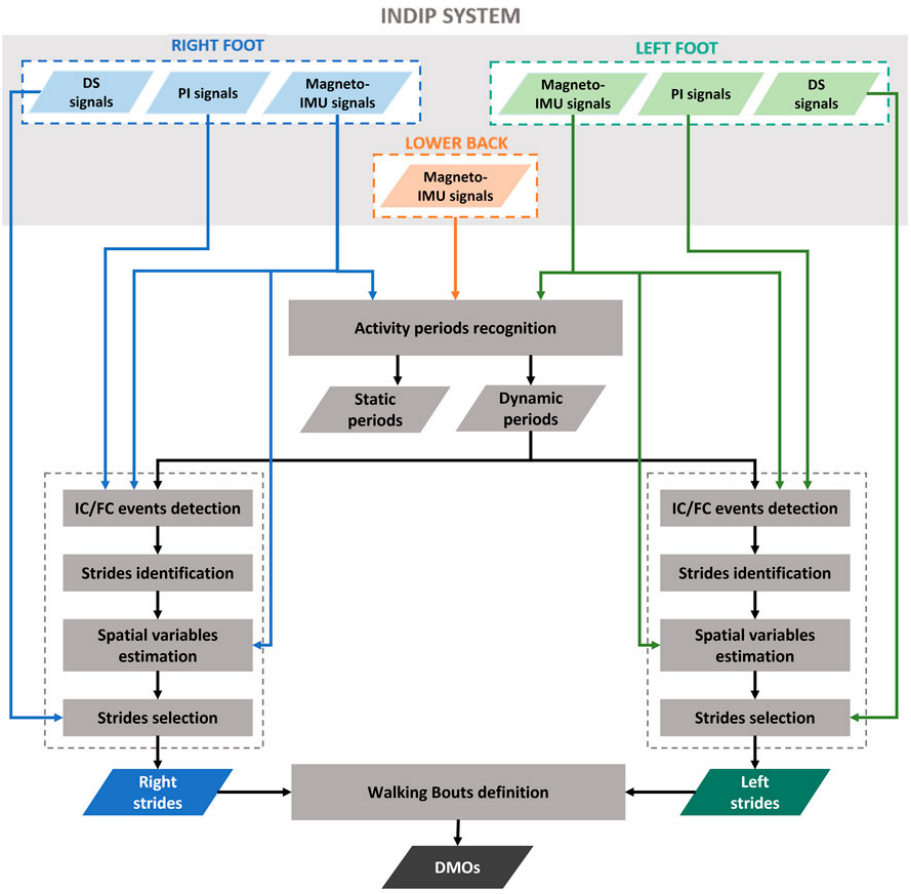

Figure 3.6: Workflow that shows the principal steps of INDIP algorithm [43].

3.4.5 Orientation estimation

The orientation of the MIMU on the upper body segments (head, chest and lower back) in the global reference system were derived using Madgwick's sensor fusion complementary filter [49]. The filter parameter β, representing the gyroscope weight

in the algorithm, was preliminarily tuned by comparing the orientation of the head-worn MIMU estimated by the algorithm against its orientation derived by a 14-cameras stereophotogrammetric motion capture system. The resulting optimal value of the parameter β was 0.04 (for more details regarding the procedures to tune β, see the Appendix). By integrating data from accelerometer, gyroscope and magnetometer, the orientation quaternions for each data point and segment were computed and used to remove the gravity contribution from accelerometric data. As a final step, the relative orientations between head, chest and lower back in the form of Euler angles (roll,pitch and yaw) were computed.

Raw acceleration data are reoriented in the lower back reference system for further elaboration. This choice is made in order to preserve the information of the anatomical axes on which accelerations are perceived.

Previous laboratory studies used a fixed reference frame aligned with the laboratory for acceleration data. However, this approach is only applicable to walking observations in which the subject does not change direction, and was therefore discarded. A global reference frame was also deemed unsuitable, as its horizontal directions depend on the Earth's magnetic field and cannot be effectively aligned with anatomical axes.

3.4.6 Video Labeling

Video recordings from smart glasses were manually labeled in order to characterize the activities and stimuli experienced by the subjects while walking. Both will be referred to as *contextual labels* in the following discussion.
A total of 17 labels were defined in advance (see Table 3.3). The purpose of the defined labels consisted in mapping the most relevant and frequent activities that could potentially affect gait, as well as environmental stimuli and contextual disturbance elements of that could alter motion pattern or the behavior of the subjects. The start and end of each identified label were noted on a dedicated `Labeling_ID.xlsx` Excel spreadsheet. Those instants were retrieved from the timestamp overlaid to the video interface and reported with a resolution of 1 second[6].
Given the coarse temporal resolution, the minimum duration for a label to be considered as valid was set to 2 seconds. If two or more stimuli/activities were concurrent (e.g., texting while avoiding moving pedestrians), all labels were annotated.
The video labeling was performed confidentially on anonymized data. Original video recordings were securely stored on an encrypted local server, and only the derived annotations were used for subsequent analysis, in accordance with data protection and privacy regulations.

[6]The output video-format did not allow to access timestamps, therefore information regarding the time instant associated to each frame was retrieved directly from the datetime overlaid to the video (format: HH:mm:ss).

Table 3.3: Overview of the contextual labels annotated from video recordings.

Labels		
Activity/stimulus/disturb	**Abbreviation**	**Description**
Search	SRC	Searching for a target item (e.g., a snack) in an indoor environment (usually a supermarket or shop), starting with entry into the area of interest and ending with target identification. This event generally included the subject's entire stay inside the supermarket until all the products to be purchased had been located.
Turning in place	ROT	In-place rotations were used as alignment points between inertial signals and video in case of signal distortion. Subject turns or changes of direction were not considered by this label.
Fixed obstacle	OBF	Planning and negotiation of various fixed obstacles, such as signs, furniture, and stationary people. This label included the planning phase when the subject focused on the obstacle and possibly analyzed its surroundings to decide on the path to take in order to pass by it.
Moving obstacle	OBM	Planning and negotiation of moving obstacles such as vehicles, pedestrians, and animals. This label included the planning phase when the subject focused on the moving obstacle and monitored its motion as well as the surrounding environment.
Audio stimulus response	AUX	Rapid head movements to localize sudden sound sources, such as car horns or other people calling the subject or attracting their attention without prior focused visual contact; a time window starting at the occurrence of the auditory stimulus and ending 2 seconds after its conclusion was reported.

Activity/stimulus/disturb	Abbreviation	Description
Door/gates crossing	PRT	Planning and crossing of doors and gates. The planning phase was observed when the subject focused on the door/gate to check for any people or vehicles that might be approaching or prepares to open the door. A necessary requirement was that the subject physically passed through the door/gate.
Texting/scrolling/reading	TXT	Use of smartphones or other objects/devices (e.g., books or notes) to read or write text, view images or maps. This label also considered the manipulation of objects that particularly demanded the subject's attention, such as searching for items inside a bag/backpack.
Calling	CLL	Answering to or making phone calls; the actions of reading the caller ID or dialing a number were considered as texting/scrolling if lasting longer than 1 second.
Approach to stairs	ASC	Planning the ascent/descent of stair ramps and/or ramps and slopes; considered as the moments when these become the dominant part of the visual field and when the subject raised or lowered their gaze to observe the slope, crowding, and any other relevant features.
Ascent/descent of stairs	SSC	The actual action of ascending or descending stairs and ramps, defined by the traversal of the inclined section. Separate ascending stair segments with landings where the next ramp is not visible were considered distinct. At the labeler's discretion, the descending sections of the same stairs was treated as a single event, as they were easier to observe and evaluate.

Activity/stimulus/disturb	Abbreviation	Description
Targeted head movements	TMV	Head movements targeted towards an object or point in space triggering the subject's attention could be identified, such as observing a place the subject was approaching to or prolonged observation of objects and people, whether stationary or moving, that were not directly on the subject's path. Separate events were identified for different targets, especially if they involved opposite head rotations.
Social interaction	SIN	Macro-event in which the subject walks in the company of other people, actively interacting with them.
Static head	STC	Moments, even brief ones, in which the subject was considered to be completely still. This is the only category that could and had to be assigned when the subject was not walking. The purpose of this category was to identify static intervals of head motion (for more details see Subsection).
Irregular surfaces	SIR	Walking on irregular and/or uneven surfaces with greater complexity than a smooth floor or paved road. This category included moments of walking on grass or other natural surfaces.
Generic head movement	GMV	Head movements not related to visual targets (e.g., cracking the neck, putting on clothing, etc.).
Various	VAR	Events considered relevant that do not fall into the previous categories. This includes all events that could affect sensor placement, such as impacts, stumbles, and similar occurrences.

For each participant, the result of the labeling process consisted in a table with annotated start and ending time instants in seconds from the video recording start.

3.4.7 Synchronization Between MIMU and Video Data

To synchronize the data recorded by the MIMU sensors with the video data captured by the scene-recording glasses, each participant was asked to perform a full rotation on the spot at the very beginning of the recording session. This rotation served as a common temporal reference across both modalities.

After data acquisition, the onset of this rotation was manually identified in the

video footage. All subsequent activities were then temporally referenced to the start of this rotation, establishing a common time zero.

In parallel, the IMU data from the head unit were inspected to identify the initial point of the vertical angular velocity peak (around the yaw axis), corresponding to the rotation performed by the participant. This peak was considered the MIMU-equivalent of the video-detected rotation onset.

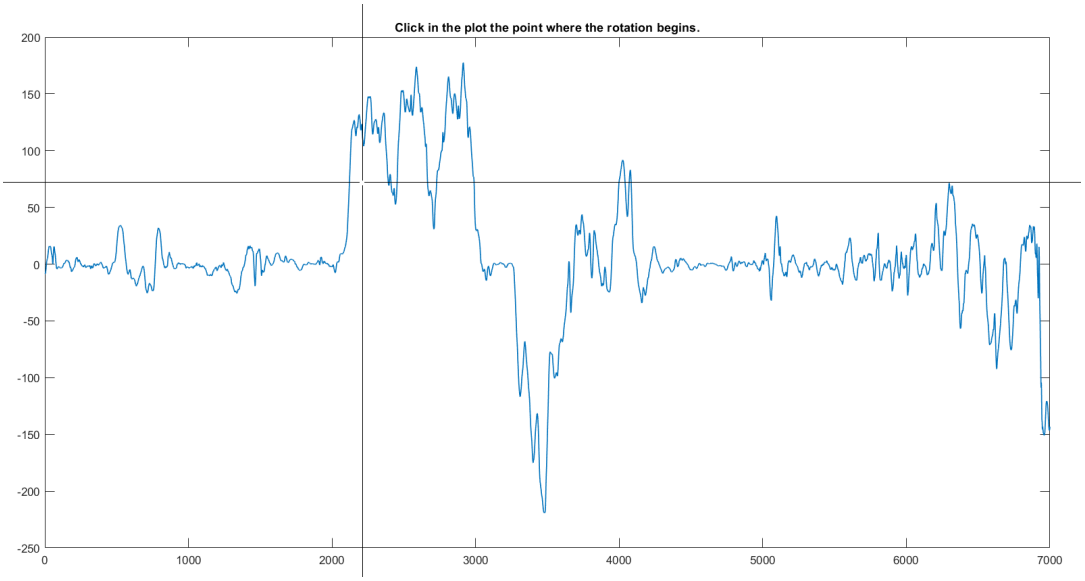

Figure 3.7: Algorithm interface plotting the vertical angular velocity from the head sensor to identify the rotation onset. Three positive peaks are clearly distinguishable and correspond to the three rotations performed by the subject.

The timestamp associated with this peak was aligned with time zero of the annotated activities, thereby synchronizing the video-based annotations with the inertial recordings.

Once that video-data was fully annotated, the starting sample of the in-place rotations was manually identified and used to compute the boundaries in samples of each label with respect to the in-place rotation.

To associate contextual information with locomotor data, a custom MATLAB function was developed. This function processed the outputs of the INDIP reference system, which detects walking bouts and identifies individual strides.

For each walking bout detected, the function retrieved the corresponding strides. Then, using the manually annotated labeling table derived from video recordings, the function assigned one or more contextual labels to each stride, as well as a yes/no label that denoted whether a specific stride belonged to a curvilinear gait portion.

This step ensured that every stride in the dataset was associated with its relevant real-world context, providing a rich basis for evaluating motor behavior under varying cognitive and environmental conditions.

3.5 Extraction of gait and upper body parameters

The extraction of gait and upper body motion parameters was performed to quantitatively characterize motor control strategies during both structured and unstruc-

tured walking. Particular attention was given to head and trunk movement, as they play a key role in maintaining balance, navigating the environment, and managing sensory inputs during real-world locomotion. Head and trunk movements were characterized according to the five domains proposed by Buckley et al. [50], namely: magnitude, regularity, attenuation, symmetry, and smoothness, which provide a comprehensive framework for describing upper body motor control during gait. To ensure consistency and reduce the influence of confounding variables, curved strides were excluded from the analysis in both lab-based and out-of-lab sessions. Additionally, the two strides immediately preceding and following each curvilinear walking segment were also discarded to avoid transitional effects. This preprocessing step allowed for a cleaner evaluation of steady-state, straight walking behavior.

3.5.1 Gait parameters

Gait parameters were extracted directly by the INDIP pipeline (see Subsection 3.4.4). For this study stride-by-stride duration, length and speed were considered. In addition, the Froude number FN was computed as a speed metric (see Subsubsection 3.5.1).

Froude number

First introduced by William Froude (1810–1879) as a non-dimensional parameter that served as the criterion for dynamic similarity when comparing boats of different hull lengths [51], Froude number has been used also in bipedal locomotion studies in recent years [15][51][52]. It is defined as the ratio between the square of velocity v and the product of the gravitational acceleration g and a characteristic length L.

$$FN = \frac{v^2}{gL}$$

In this study Froude number is evaluated as a gait speed metric that takes into account for possible differences due to stature differences. *Total leg length [m]* is used for the L variable, and is obtained as the sum of foot height, shank length and thigh length (see Table 3.2).

3.5.2 Magnitude

Magnitude parameters provide quantifiable information about the *Intensity* of movement, fundamental to understanding its characteristics and quality across a wide range of applications, from clinical diagnosis and rehabilitation to sports performance and daily activity monitoring. All magnitude parameters were calculated on a stride-by-stride basis.

Root mean square acceleration $[m/s^2]$

Root mean square acceleration (a_{rms}) of head (HD), chest (CH), and lower back (LB) was computed for each of the vertical (V), medial-lateral (ML) and anterior-

posterior (AP) axes, using the following formula:

$$a_{rms} = \sqrt{\sum_{k=1}^{N} a(k)^2}$$

Where a is the acceleration along a specific axis and N is the number of samples in one stride.

Rotational range of motion [°]

Yaw and pitch range of motion (ROM) was computed for head-in-chest, head-in-lower back and chest-in-lower back relative orientations. Given the relative orientation[7] of the segments during a stride $\theta(k)$ expressed in degrees, the range of motion was evaluated as:

$$ROM(\theta(k)) = max(\theta(k)) - min(\theta(k))$$

3.5.3 Attenuation

Attenuation parameters describe the coupling between head, chest and lower back and how the gait-related accelerations are transferred from the lower limbs to the segments above.

Attenuation coefficient [%]

The attenuation coefficient (AC) along the axis i is computed as the percentage reduction of the rms acceleration of segment X compared to segment Y [52]:

$$AC_iXY = \left(1 - \frac{a_{rms_{iX}}}{a_{rms_{iY}}}\right) * 100$$

With $i \in \{\text{AP}, \text{V}, \text{ML}\}$ and X and Y representing the lower-back, the chest or the head segments ($X \neq Y$).

3.5.4 Symmetry

Improved harmonic ratio

In order to asses the symmetry of gait, improved harmonic ratio (iHR) was computed using accelerometer data from the lower back. This index is based on the spectral analysis of the aforementioned signal, and defined as the ratio between the sum of its first 10 even harmonics and the sum of the first 10 even plus the first 10 odd harmonics:

$$iHR = \frac{\sum_{k=1}^{10} f_i^{even}}{\sum_{k=1}^{10} f_i^{even} + \sum_{k=1}^{10} f_i^{odd}}$$

[7] In this study, the relative orientation in quaternions between segments was obtained using a Madgwick complementary filter as described in 3.3 and then converted in the Euler's angles representation using the built-in Matlab function `quat2eul` available in the Navigation Toolbox.

This definition is valid for vertical and anterior-posterior components of the signal, but for the medio-lateral component the sum of even harmonics is used at the numerator instead:

$$iHR_{ML} = \frac{\sum_{k=1}^{10} f_i^{odd}}{\sum_{k=1}^{10} f_i^{even} + \sum_{k=1}^{10} f_i^{odd}}$$

This metric , proposed by Pasciuto et al. [53], has been chosen over the traditional harmonic ratio due to its limited value range ($iHR \in [0; 1]$), which makes it much easier to interpret, as a value of $iHR = 1$ reflects the perfect symmetry of the signal and $iHR = 0$ its perfect asymmetry.

iHR is calculated for each axis. Given the uncorrelation between gait and the highly present exploratory movements of head and chest, the parameter was not computed for those segments.

3.5.5 Smoothness

Movement smoothness is a key indicator in assessing motor control and detecting sensorimotor impairments, offering important information about the quality of movement. Defined by its continuity and lack of interruptions, smooth movement is widely regarded as a marker of intact motor function and successful motor learning [54].

Log dimensionless jerk

Jerk is defined as the first time derivative of acceleration or as the second time derivative of velocity:

$$\vec{j} = \frac{da\vec{(t)}}{dt} = \frac{d^2v\vec{(t)}}{dt^2}$$

A metric that is effectively representative of the signal shape must be dimensionless and independent of its amplitude and duration. Moreover, it must also be sensitive in the physiological range in which is applied [55]. To resolve this issue, *log dimensionless jerk* has been introduced:

$$LDLJ_v = -ln\left(\frac{t_2 - t_1}{v_{peak}^2}\int_{t_1}^{t_2}\left|\frac{d^2v\vec{(t)}}{dt^2}\right|^2 dt\right)$$

The values are normalized to the square of the signal peak velocity v_{peak} and the logarithm operation reduces the ceiling effect of data in the physiological range, increasing the sensitivity [55].

Generally $LDLJ_v$ is applied to stereophotogrammetric data, where movement velocity is easily computed, however its estimation from inertial data is way less reliable and prone to errors introduced by noise and drift. For this reason an alternative normalization to the square of the signal peak velocity a_{peak} has been introduced

[54][56]:

$$LDLJ_a = -ln\left(\frac{t_2 - t_1}{a_{peak}^2}\int_{t_1}^{t_2}\left|\frac{da(\vec{t})}{dt}\right|^2 dt\right)$$

$LDLJ_a$ was computed from acceleration data from the head for each axis.

3.5.6 Regularity

Entropy defines the level of regularity (e.g. complexity) in a time series. Multi-scale entropies determine the entropy as a function of scale and thus express how complexity in a time series changes with its temporal resolution.

Refined composite multiscale entropy

This metric, proposed by Wu et al. [57] and implemented through the matlab codes provided by Ihllen et al. [58], is computed throught the following steps:

- **Coarse graining of the time series:**
  To obtain the coarse-grained time series at a scale factor of τ, the original time series is divided into non-overlapping windows of length τ and the data points inside each window are averaged. Given a data vector $\vec{x}$, values of its k-th coarse-grained version $\vec{y}^{(\tau)}$ are obtained as follows:

$$y_k^{(\tau)}(j) = \sum_{i=(j-1)\tau+k}^{j\tau+k-1} x(i) \quad , \quad 1 \leq j \leq \frac{N}{\tau}, 1 \leq k \leq \tau$$

- **Calculation of matched vector pairs:**
  For a given time series $\vec{y}_k^{(\tau)}$, template vectors with dimension m are constructed as:

$$\vec{y}_{k,\tau}^m(j) = \{y_k^{(\tau)}(j) \qquad y_k^{(\tau)}(j+1) \qquad ... \qquad y_k^{(\tau)}(j+m-1)\}$$

  A match occurs when the distance between two template vectors ($\vec{y}_{k,\tau}^m(i)$, $\vec{y}_{k,\tau}^m(j)$) is smaller than a predefined tolerance r.

$$d_{ij}^m = ||\vec{y}_{k,\tau}^m(i) - \vec{y}_{k,\tau}^m(j)||_\infty < r$$

  For a given scale factor τ, the number of matched vector pairs, $n_{k,\tau}^{m+1}$ and $n_{k,\tau}^m$, are calculated for all coarse-grained series.

- **Averaging matched vector pairs:**
  The mean of $n_{k,\tau}^m$ (denoted as $\bar{n}_{k,\tau}^m$) and the mean of $n_{k,\tau}^{m+1}$ (denoted as $\bar{n}_{k,\tau}^{m+1}$) are calculated across all coarse-grained series for a given scale factor τ.

$$\bar{n}_{k,\tau}^m = \frac{1}{\tau}\sum_{k=1}^{\tau} n_{k,\tau}^m \qquad \bar{n}_{k,\tau}^{m+1} = \frac{1}{\tau}\sum_{k=1}^{\tau} n_{k,\tau}^{m+1}$$

- **RCMSE value definition:**
  The RCMSE value at a scale factor of τ is defined as the logarithm of the ratio of $\bar{n}_{k,\tau}^{m+1}$ and $\bar{n}_{k,\tau}^{m}$.

$$RCME(\vec{x}, \tau, m, r) = -ln\left(\frac{\bar{n}_{k,\tau}^{m+1}}{\bar{n}_{k,\tau}^{m}}\right) = -ln\left(\frac{\sum_{k=1}^{\tau} n_{k,\tau}^{m+1}}{\sum_{k=1}^{\tau} n_{k,\tau}^{m}}\right)$$

To avoid variations in the entropy result due to differences in signal length, all processed accelerometric data were resampled to 2000 data points using a radial basis function interpolation algorithm.
In this study $RCME(\vec{x}, \tau, m, r)$ was computed for head acceleration on each axis using template vectors of size $m = 2$, $\tau = [1:6]$ and $r = 0.2 * std(\vec{x})$. In order to obtain a single value that incorporates complexity information over the various scales, for a given signal $\vec{x}$ the overall entropy, always referred as RCME, was computed as the sum of $RCME(\tau)$ for each scale factor τ.

$$RCME(\vec{x}, m, r) = \sum_{\tau=1}^{6} RCME(\vec{x}, \tau, m, r)$$

3.6 Obtained Dataset

The completion of manual video labeling proved to be particularly time-consuming, with a highly variable duration depending on the activity level of each subject. As a result, labeling process was completed for 11 of the 21 acquired subjects.

For these subjects, two comprehensive datasets were organized in two separate `.csv` file, reporting the previously described parameters for a total of 50718 strides for the Out of Lab trial and 7587 strides for the In Lab tests. Information about the corresponding gait sequence and stride identified by the INDIP pipeline were added to allow for quick identification and verification within the dataset against the pipeline output.

3.7 Statistical analysis

In this study, the main effects of a subset of activities on the computed parameters were investigated.
Road crossings, **fixed and moving obstacle avoidance**, **texting**, **calling**, and **visual search** in free living conditions were compared to **laboratory straight walking**.

Data from In Lab simulated tests were **not** analyzed in this work, but were included in the produced dataset for future evaluations.

3.7.1 Filtering

The dataset was filtered to include only straight walking strides.
For each subject and each of the selected labels, strides were isolated and aggregated by computing the mean value of each parameter.
To guarantee the independence of the aggregated samples, strides with multiple labels among the evaluated ones were neglected.

Due to the absence of strides without multiple labels or the missing execution of specific activities, 3 more subjects were excluded, reducing the total number of valid subjects for the analysis to 8.

3.7.2 Assumption checks

Given the number of valid subjects, a distribution of 8 values was obtained for each parameter and label. Each distribution was checked for normality using a Shaphiro-Wilk test.
If the normality hypothesis was confirmed for each distribution of a given parameter, Mauchly's W was also computed to ensure the sphericity of the distribution. If this second condition was not satisfied, a Greenhouse-Geisser correction was applied to the data.

3.7.3 Statistical tests

If the normality hypothesis was confirmed for each distribution of a given parameter, a one way repeated measure ANOVA test was performed using the Jasp software.
Otherwise if the distributions were not normal a non-parametric analysis was performed with a Kruskal-Wallis test. A Holm post-hoc correction was applied to each analysis performed.

3.7.4 Effect size

If statistically significative difference were found among labels for a given parameter, its effect size was evaluated as the Cohen's D for each label combination.

Chapter 4

Results

4.1 Summary statistics by activity

Here are reported the values of each aggregated metric for all the subjects valid for the analysis.

4.1.1 Gait parameters

Stride speed

Table 4.1: Mean ± standard deviation of stride speed

Stride speed $[m/s]$							
ID	Crossroad	Texting	Calling	Search	Fixed obstacle	Moving obstacle	In Lab SW
5001	1.57 ± 1.57	1.38 ± 0.10	1.33 ± 0.13	0.88 ± 0.31	1.42 ± 0.28	1.57 ± 0.16	1.07 ± 0.08
5004	1.31 ± 1.31	1.25 ± 0.29	1.39 ± 0.09	1.04 ± 0.30	1.19 ± 0.32	1.18 ± 0.25	1.31 ± 0.12
5005	1.55 ± 1.55	1.54 ± 0.19	1.30 ± 0.36	1.08 ± 0.30	1.53 ± 0.19	1.41 ± 0.27	1.44 ± 0.11
5006	1.72 ± 1.72	1.68 ± 0.11	1.71 ± 0.11	0.91 ± 0.33	1.55 ± 0.42	1.70 ± 0.27	1.24 ± 0.07
5007	1.58 ± 1.58	1.39 ± 0.27	1.52 ± 0.18	1.09 ± 0.23	1.16 ± 0.51	1.34 ± 0.39	1.45 ± 0.12
5008	1.52 ± 1.52	1.24 ± 0.18	1.57 ± 0.10	0.72 ± 0.23	1.35 ± 0.26	1.41 ± 0.26	1.31 ± 0.10
5010	1.35 ± 1.35	0.88 ± 0.31	0.84 ± 0.34	0.71 ± 0.17	1.05 ± 0.41	1.29 ± 0.22	1.30 ± 0.12
5011	1.48 ± 1.48	1.52 ± 0.14	1.61 ± 0.21	0.81 ± 0.38	1.67 ± 0.22	1.65 ± 0.27	1.35 ± 0.11

Stride length

Table 4.2: Mean ± standard deviation of stride length

Stride length $[m]$							
ID	Crossroad	Texting	Calling	Search	Fixed obstacle	Moving obstacle	In Lab SW
5001	1.50 ± 1.50	1.41 ± 0.09	1.33 ± 0.09	1.08 ± 0.25	1.42 ± 0.21	1.52 ± 0.14	1.20 ± 0.07
5004	1.34 ± 1.34	1.27 ± 0.28	1.36 ± 0.09	1.18 ± 0.27	1.24 ± 0.28	1.25 ± 0.24	1.40 ± 0.16
5005	1.57 ± 1.57	1.57 ± 0.13	1.38 ± 0.29	1.27 ± 0.24	1.57 ± 0.14	1.50 ± 0.18	1.50 ± 0.10
5006	1.76 ± 1.76	1.73 ± 0.10	1.77 ± 0.11	1.21 ± 0.31	1.62 ± 0.34	1.74 ± 0.27	1.50 ± 0.08
5007	1.53 ± 1.53	1.41 ± 0.21	1.48 ± 0.18	1.21 ± 0.10	1.25 ± 0.38	1.39 ± 0.28	1.47 ± 0.11
5008	1.53 ± 1.53	1.35 ± 0.12	1.58 ± 0.10	1.00 ± 0.22	1.42 ± 0.21	1.46 ± 0.19	1.39 ± 0.09
5010	1.47 ± 1.47	1.08 ± 0.30	1.09 ± 0.32	1.00 ± 0.19	1.19 ± 0.41	1.41 ± 0.22	1.41 ± 0.14
5011	1.69 ± 1.69	1.73 ± 0.13	1.78 ± 0.13	1.12 ± 0.42	1.79 ± 0.15	1.77 ± 0.18	1.61 ± 0.08

Stride duration

Table 4.3: Mean ± standard deviation of stride duration

Stride duration $[s]$							
ID	Crossroad	Texting	Calling	Search	Fixed obstacle	Moving obstacle	In Lab SW
5001	0.97 ± 0.97	1.02 ± 0.02	1.00 ± 0.05	1.35 ± 0.40	1.02 ± 0.11	0.97 ± 0.05	1.20 ± 0.07
5004	1.03 ± 1.03	1.02 ± 0.11	0.98 ± 0.03	1.18 ± 0.23	1.08 ± 0.23	1.08 ± 0.15	1.40 ± 0.16
5005	1.02 ± 1.02	1.03 ± 0.08	1.11 ± 0.24	1.22 ± 0.18	1.03 ± 0.05	1.09 ± 0.17	1.50 ± 0.10
5006	1.03 ± 1.03	1.03 ± 0.02	1.04 ± 0.02	1.41 ± 0.31	1.10 ± 0.24	1.02 ± 0.03	1.50 ± 0.08
5007	0.99 ± 0.99	1.03 ± 0.12	0.97 ± 0.02	1.14 ± 0.19	1.24 ± 0.44	1.09 ± 0.22	1.47 ± 0.11
5008	1.01 ± 1.01	1.10 ± 0.09	1.00 ± 0.02	1.48 ± 0.35	1.07 ± 0.11	1.05 ± 0.09	1.39 ± 0.09
5010	1.10 ± 1.10	1.26 ± 0.15	1.38 ± 0.25	1.45 ± 0.19	1.21 ± 0.31	1.11 ± 0.07	1.41 ± 0.14
5011	1.16 ± 1.16	1.14 ± 0.06	1.11 ± 0.10	1.53 ± 0.40	1.08 ± 0.08	1.08 ± 0.09	1.61 ± 0.08

Froude number

Table 4.4: Mean ± standard deviation of Froude number

Froude number $[F_n]$							
ID	Crossroad	Texting	Calling	Search	Fixed obstacle	Moving obstacle	In Lab SW
5001	0.30 ± 0.30	0.22 ± 0.03	0.21 ± 0.04	0.10 ± 0.05	0.25 ± 0.08	0.29 ± 0.05	0.14 ± 0.02
5004	0.20 ± 0.20	0.18 ± 0.07	0.22 ± 0.03	0.13 ± 0.06	0.17 ± 0.07	0.16 ± 0.06	0.19 ± 0.03
5005	0.26 ± 0.26	0.26 ± 0.06	0.20 ± 0.09	0.14 ± 0.07	0.26 ± 0.06	0.22 ± 0.07	0.23 ± 0.03
5006	0.32 ± 0.32	0.30 ± 0.04	0.31 ± 0.04	0.10 ± 0.07	0.27 ± 0.11	0.32 ± 0.08	0.16 ± 0.02
5007	0.31 ± 0.31	0.24 ± 0.09	0.29 ± 0.07	0.15 ± 0.06	0.19 ± 0.13	0.24 ± 0.11	0.26 ± 0.04
5008	0.27 ± 0.27	0.18 ± 0.05	0.29 ± 0.04	0.07 ± 0.04	0.22 ± 0.07	0.24 ± 0.08	0.20 ± 0.03
5010	0.21 ± 0.21	0.10 ± 0.06	0.09 ± 0.06	0.06 ± 0.02	0.14 ± 0.09	0.19 ± 0.06	0.19 ± 0.03
5011	0.23 ± 0.23	0.24 ± 0.04	0.27 ± 0.07	0.08 ± 0.06	0.29 ± 0.07	0.29 ± 0.09	0.19 ± 0.03

4.1.2 Magnitude

Vertical rms acceleration of the head (a-rms HD-V)

Table 4.5: Mean ± standard deviation of a-rms HD-V

a-rms HD-V $[m/s^2]$							
ID	Crossroad	Texting	Calling	Search	Fixed obstacle	Moving obstacle	In Lab SW
5001	3.26 ± 3.26	2.09 ± 0.40	2.02 ± 0.19	1.43 ± 0.45	2.69 ± 0.84	3.05 ± 0.62	1.44 ± 0.16
5004	2.00 ± 2.00	2.37 ± 0.54	2.12 ± 0.19	1.23 ± 0.39	1.68 ± 0.53	1.64 ± 0.49	1.69 ± 0.18
5005	2.29 ± 2.29	2.19 ± 0.43	1.86 ± 0.53	1.33 ± 0.41	2.19 ± 0.38	2.03 ± 0.50	1.67 ± 0.29
5006	2.28 ± 2.28	2.20 ± 0.64	1.45 ± 0.51	1.05 ± 0.45	2.02 ± 0.90	1.88 ± 0.72	1.09 ± 0.31
5007	3.17 ± 3.17	1.92 ± 0.68	2.81 ± 0.33	1.85 ± 0.36	2.23 ± 1.21	2.52 ± 1.04	2.77 ± 0.25
5008	1.85 ± 1.85	1.95 ± 0.45	1.60 ± 0.29	0.89 ± 0.49	1.65 ± 0.58	1.75 ± 0.63	1.99 ± 0.26
5010	2.52 ± 2.52	1.68 ± 0.66	1.69 ± 0.52	1.12 ± 0.31	1.81 ± 0.74	2.21 ± 0.57	1.89 ± 0.28
5011	2.22 ± 2.22	2.42 ± 0.33	2.25 ± 0.53	1.20 ± 0.43	2.54 ± 0.66	2.61 ± 0.76	1.28 ± 0.21

Mediolateral rms acceleration of the head (a-rms HD-ML)

Table 4.6: Mean ± standard deviation of a-rms HD-ML

a-rms HD-ML $[m/s^2]$							
ID	Crossroad	Texting	Calling	Search	Fixed obstacle	Moving obstacle	In Lab SW
5001	1.11 ± 1.11	1.03 ± 0.17	1.03 ± 0.20	0.93 ± 0.33	0.99 ± 0.24	1.04 ± 0.27	0.87 ± 0.19
5004	1.04 ± 1.04	0.79 ± 0.19	0.81 ± 0.10	0.81 ± 0.23	0.89 ± 0.22	0.99 ± 0.30	0.72 ± 0.11
5005	1.10 ± 1.10	0.96 ± 0.24	1.17 ± 0.35	0.87 ± 0.27	1.11 ± 0.31	0.97 ± 0.19	0.83 ± 0.24
5006	2.66 ± 2.66	2.18 ± 0.85	2.13 ± 0.55	1.20 ± 0.43	2.11 ± 0.93	2.42 ± 0.85	0.99 ± 0.17
5007	1.13 ± 1.13	0.89 ± 0.28	0.77 ± 0.10	1.03 ± 0.26	0.88 ± 0.31	0.86 ± 0.25	0.67 ± 0.17
5008	1.46 ± 1.46	0.92 ± 0.26	1.58 ± 0.23	0.78 ± 0.23	1.17 ± 0.33	1.18 ± 0.36	0.84 ± 0.19
5010	1.59 ± 1.59	1.20 ± 0.31	1.22 ± 0.27	1.03 ± 0.28	1.35 ± 0.37	1.48 ± 0.39	1.36 ± 0.26
5011	1.33 ± 1.33	1.09 ± 0.16	1.17 ± 0.32	1.21 ± 0.35	1.54 ± 0.52	1.61 ± 0.53	1.30 ± 0.17

Anterior-posterior rms acceleration of the head (a-rms HD-AP)

Table 4.7: Mean ± standard deviation of a-rms HD-AP

a-rms HD-AP $[m/s^2]$							
ID	Crossroad	Texting	Calling	Search	Fixed obstacle	Moving obstacle	In Lab SW
5001	1.72 ± 1.72	1.64 ± 0.36	1.43 ± 0.40	1.09 ± 0.26	1.40 ± 0.55	1.71 ± 0.58	1.08 ± 0.31
5004	1.71 ± 1.71	1.03 ± 0.42	1.50 ± 0.24	1.14 ± 0.34	1.39 ± 0.45	1.43 ± 0.38	1.66 ± 0.27
5005	1.45 ± 1.45	1.31 ± 0.30	1.21 ± 0.31	0.96 ± 0.28	1.30 ± 0.36	1.18 ± 0.27	1.45 ± 0.37
5006	2.08 ± 2.08	1.66 ± 0.46	2.69 ± 0.40	1.19 ± 0.44	1.74 ± 0.77	2.06 ± 0.86	1.54 ± 0.31
5007	1.72 ± 1.72	1.92 ± 0.49	1.57 ± 0.37	1.12 ± 0.24	1.25 ± 0.65	1.44 ± 0.63	1.09 ± 0.36
5008	2.88 ± 2.88	1.15 ± 0.36	3.21 ± 0.18	1.16 ± 0.53	2.20 ± 0.70	2.32 ± 0.71	1.51 ± 0.37
5010	1.85 ± 1.85	1.25 ± 0.51	1.29 ± 0.35	1.13 ± 0.32	1.48 ± 0.53	1.88 ± 0.52	1.78 ± 0.24
5011	1.72 ± 1.72	1.40 ± 0.31	1.93 ± 0.52	0.91 ± 0.14	1.89 ± 0.56	1.80 ± 0.52	1.79 ± 0.36

Vertical rms acceleration of the chest (a-rms CH-V)

Table 4.8: Mean ± standard deviation of a-rms CH-V

a-rms CH-V $[m/s^2]$							
ID	Crossroad	Texting	Calling	Search	Fixed obstacle	Moving obstacle	In Lab SW
5001	3.39 ± 3.39	2.43 ± 0.26	2.35 ± 0.35	1.39 ± 0.44	2.87 ± 0.86	3.26 ± 0.55	1.63 ± 0.16
5004	2.42 ± 2.42	2.35 ± 0.51	2.37 ± 0.14	1.50 ± 0.51	1.99 ± 0.62	2.02 ± 0.44	2.05 ± 0.18
5005	2.43 ± 2.43	2.34 ± 0.39	1.82 ± 0.52	1.38 ± 0.43	2.36 ± 0.35	2.09 ± 0.48	1.99 ± 0.29
5006	2.15 ± 2.15	1.92 ± 0.29	2.05 ± 0.20	0.87 ± 0.31	1.91 ± 0.57	2.02 ± 0.35	1.32 ± 0.13
5007	3.71 ± 3.71	2.79 ± 0.61	3.14 ± 0.17	1.98 ± 0.38	2.51 ± 1.33	2.97 ± 1.11	2.83 ± 0.25
5008	2.68 ± 2.68	1.67 ± 0.41	2.52 ± 0.14	1.14 ± 0.55	2.17 ± 0.54	2.28 ± 0.57	1.91 ± 0.14
5010	2.56 ± 2.56	1.53 ± 0.65	1.59 ± 0.53	1.05 ± 0.35	1.82 ± 0.76	2.36 ± 0.55	2.09 ± 0.19
5011	2.18 ± 2.18	2.09 ± 0.29	2.11 ± 0.40	1.36 ± 0.54	2.52 ± 0.45	2.51 ± 0.59	1.78 ± 0.17

Mediolateral rms acceleration of the chest (a-rms CH-ML)

Table 4.9: Mean ± standard deviation of a-rms CH-ML

a-rms CH-ML $[m/s^2]$							
ID	Crossroad	Texting	Calling	Search	Fixed obstacle	Moving obstacle	In Lab SW
5001	1.33 ± 1.33	1.25 ± 0.21	1.16 ± 0.14	0.87 ± 0.17	1.18 ± 0.27	1.37 ± 0.23	1.01 ± 0.14
5004	1.18 ± 1.18	1.18 ± 0.20	1.16 ± 0.10	0.89 ± 0.20	1.07 ± 0.23	1.10 ± 0.26	1.16 ± 0.12
5005	1.22 ± 1.22	1.14 ± 0.25	1.14 ± 0.27	0.82 ± 0.23	1.24 ± 0.19	1.04 ± 0.22	1.30 ± 0.14
5006	1.64 ± 1.64	1.40 ± 0.21	1.46 ± 0.15	0.84 ± 0.25	1.52 ± 0.43	1.67 ± 0.36	0.92 ± 0.14
5007	1.08 ± 1.08	0.88 ± 0.21	1.02 ± 0.10	0.94 ± 0.18	0.96 ± 0.29	0.97 ± 0.22	1.01 ± 0.12
5008	1.58 ± 1.58	0.92 ± 0.29	1.42 ± 0.08	0.74 ± 0.26	1.34 ± 0.40	1.31 ± 0.40	1.30 ± 0.20
5010	1.39 ± 1.39	1.13 ± 0.24	1.02 ± 0.21	1.03 ± 0.21	1.18 ± 0.23	1.30 ± 0.19	1.27 ± 0.16
5011	1.42 ± 1.42	1.41 ± 0.19	1.33 ± 0.33	1.30 ± 0.43	1.67 ± 0.30	1.66 ± 0.43	1.28 ± 0.17

Anterior-posterior rms acceleration of the chest (a-rms CH-AP)

Table 4.10: Mean ± standard deviation of a-rms CH-AP

a-rms CH-AP $[m/s^2]$							
ID	Crossroad	Texting	Calling	Search	Fixed obstacle	Moving obstacle	In Lab SW
5001	2.39 ± 2.39	1.74 ± 0.26	1.31 ± 0.16	1.04 ± 0.31	1.85 ± 0.59	2.36 ± 0.45	1.20 ± 0.16
5004	1.30 ± 1.30	1.09 ± 0.21	0.92 ± 0.08	0.99 ± 0.20	1.05 ± 0.23	1.18 ± 0.25	1.67 ± 0.20
5005	1.81 ± 1.81	1.73 ± 0.26	1.63 ± 0.35	1.18 ± 0.27	1.76 ± 0.21	1.65 ± 0.24	1.71 ± 0.17
5006	3.33 ± 3.33	2.92 ± 0.34	3.07 ± 0.20	1.35 ± 0.52	2.77 ± 0.88	3.15 ± 0.45	1.61 ± 0.17
5007	1.85 ± 1.85	1.50 ± 0.26	1.59 ± 0.18	1.20 ± 0.15	1.43 ± 0.55	1.58 ± 0.39	1.63 ± 0.12
5008	2.63 ± 2.63	1.82 ± 0.39	2.96 ± 0.15	1.20 ± 0.52	2.19 ± 0.50	2.29 ± 0.53	2.13 ± 0.18
5010	2.29 ± 2.29	1.52 ± 0.47	1.60 ± 0.39	1.12 ± 0.26	1.71 ± 0.70	2.18 ± 0.46	2.22 ± 0.26
5011	2.03 ± 2.03	1.97 ± 0.27	2.25 ± 0.44	1.37 ± 0.48	2.34 ± 0.46	2.39 ± 0.55	1.75 ± 0.20

Vertical rms acceleration of the lower back (a-rms LB-V)

Table 4.11: Mean ± standard deviation of a-rms LB-V

a-rms LB-V $[m/s^2]$							
ID	Crossroad	Texting	Calling	Search	Fixed obstacle	Moving obstacle	In Lab SW
5001	4.10 ± 4.10	3.06 ± 0.37	2.48 ± 0.36	1.45 ± 0.50	3.32 ± 0.97	3.87 ± 0.51	1.76 ± 0.21
5004	2.94 ± 2.94	2.95 ± 0.62	2.97 ± 0.19	1.71 ± 0.66	2.41 ± 0.79	2.37 ± 0.57	2.58 ± 0.22
5005	3.50 ± 3.50	3.31 ± 0.61	2.75 ± 0.85	1.88 ± 0.66	3.49 ± 0.59	2.92 ± 0.78	2.69 ± 0.35
5006	3.79 ± 3.79	3.41 ± 0.44	3.38 ± 0.24	1.46 ± 0.54	3.22 ± 1.00	3.56 ± 0.43	1.89 ± 0.19
5007	4.57 ± 4.57	3.32 ± 0.83	3.91 ± 0.34	2.05 ± 0.39	2.94 ± 1.73	3.49 ± 1.39	3.56 ± 0.37
5008	3.58 ± 3.58	2.40 ± 0.57	3.81 ± 0.20	1.31 ± 0.77	2.88 ± 0.73	3.04 ± 0.76	2.63 ± 0.19
5010	3.35 ± 3.35	1.97 ± 0.85	1.88 ± 0.69	1.14 ± 0.34	2.32 ± 1.00	3.03 ± 0.69	2.82 ± 0.28
5011	3.15 ± 3.15	3.27 ± 0.51	3.28 ± 0.85	1.37 ± 0.64	3.69 ± 0.84	3.83 ± 1.08	2.44 ± 0.29

Mediolateral rms acceleration of the lower back (a-rms LB-ML)

Table 4.12: Mean ± standard deviation of a-rms LB-ML

a-rms LB-ML $[m/s^2]$							
ID	Crossroad	Texting	Calling	Search	Fixed obstacle	Moving obstacle	In Lab SW
5001	1.87 ± 1.87	1.48 ± 0.15	1.39 ± 0.18	1.10 ± 0.22	1.62 ± 0.35	1.72 ± 0.24	1.07 ± 0.11
5004	2.34 ± 2.34	2.33 ± 0.51	2.45 ± 0.22	1.55 ± 0.38	2.04 ± 0.55	2.02 ± 0.46	1.97 ± 0.21
5005	1.77 ± 1.77	1.60 ± 0.29	1.40 ± 0.37	1.15 ± 0.25	1.81 ± 0.33	1.46 ± 0.31	1.58 ± 0.19
5006	2.10 ± 2.10	1.85 ± 0.36	1.82 ± 0.23	1.24 ± 0.22	1.71 ± 0.49	1.89 ± 0.36	1.33 ± 0.14
5007	1.74 ± 1.74	1.44 ± 0.38	1.65 ± 0.16	1.20 ± 0.15	1.37 ± 0.47	1.47 ± 0.40	1.48 ± 0.16
5008	1.58 ± 1.58	1.16 ± 0.29	1.69 ± 0.18	0.95 ± 0.24	1.39 ± 0.29	1.39 ± 0.35	1.50 ± 0.17
5010	1.72 ± 1.72	1.38 ± 0.30	1.19 ± 0.25	1.32 ± 0.28	1.50 ± 0.37	1.52 ± 0.25	1.57 ± 0.16
5011	1.89 ± 1.89	1.98 ± 0.35	1.78 ± 0.36	1.71 ± 0.37	2.10 ± 0.35	2.13 ± 0.46	1.82 ± 0.19

Anterior-posterior rms acceleration of the lower back (a-rms LB-AP)

Table 4.13: Mean ± standard deviation of a-rms LB-AP

a-rms LB-AP $[m/s^2]$							
ID	Crossroad	Texting	Calling	Search	Fixed obstacle	Moving obstacle	In Lab SW
5001	2.92 ± 2.92	2.22 ± 0.27	1.91 ± 0.19	1.56 ± 0.39	2.45 ± 0.60	2.83 ± 0.33	1.55 ± 0.15
5004	2.10 ± 2.10	1.96 ± 0.31	1.97 ± 0.21	1.53 ± 0.35	1.76 ± 0.46	1.73 ± 0.32	1.97 ± 0.16
5005	2.44 ± 2.44	2.35 ± 0.34	1.93 ± 0.45	1.51 ± 0.40	2.48 ± 0.41	2.15 ± 0.44	2.07 ± 0.24
5006	3.09 ± 3.09	2.88 ± 0.36	2.79 ± 0.19	1.39 ± 0.40	2.58 ± 0.79	2.94 ± 0.47	1.70 ± 0.18
5007	2.52 ± 2.52	1.96 ± 0.41	2.32 ± 0.28	1.60 ± 0.20	1.86 ± 0.71	2.08 ± 0.55	2.26 ± 0.22
5008	2.43 ± 2.43	1.58 ± 0.30	2.48 ± 0.22	1.14 ± 0.32	1.96 ± 0.45	2.06 ± 0.50	1.64 ± 0.12
5010	2.25 ± 2.25	1.46 ± 0.39	1.32 ± 0.46	1.25 ± 0.24	1.76 ± 0.67	2.06 ± 0.39	1.87 ± 0.20
5011	3.43 ± 3.43	3.65 ± 0.63	3.70 ± 1.05	2.29 ± 0.83	4.09 ± 0.87	4.15 ± 1.14	2.94 ± 0.28

Head-in-lower back yaw range of motion (yaw ROM HD-LB)

Table 4.14: Mean ± standard deviation of yaw ROM HD-LB

yaw ROM HD-LB [*deg*]							
ID	Crossroad	Texting	Calling	Search	Fixed obstacle	Moving obstacle	In Lab SW
5001	18.07 ± 18.07	11.24 ± 6.83	12.83 ± 3.56	38.35 ± 24.81	14.48 ± 10.98	14.43 ± 8.37	14.47 ± 5.61
5004	24.23 ± 24.23	10.36 ± 6.48	9.93 ± 3.04	23.91 ± 16.66	20.15 ± 16.68	23.74 ± 19.98	8.63 ± 2.16
5005	21.98 ± 21.98	16.44 ± 7.13	12.63 ± 5.46	23.80 ± 15.31	20.30 ± 9.04	16.91 ± 7.99	19.44 ± 12.51
5006	42.71 ± 42.71	26.03 ± 12.31	23.35 ± 8.05	44.49 ± 25.73	29.08 ± 20.54	30.11 ± 16.82	21.09 ± 7.51
5007	30.33 ± 30.33	15.96 ± 10.57	16.23 ± 3.42	48.82 ± 26.00	25.81 ± 18.35	21.15 ± 14.12	16.41 ± 4.08
5008	28.59 ± 28.59	14.32 ± 4.81	28.09 ± 4.05	28.10 ± 13.64	24.47 ± 8.66	21.44 ± 6.07	18.82 ± 3.46
5010	32.13 ± 32.13	18.90 ± 13.11	21.05 ± 10.00	44.33 ± 18.91	30.12 ± 18.59	26.98 ± 17.19	17.81 ± 6.96
5011	32.03 ± 32.03	17.58 ± 4.27	18.30 ± 7.31	35.24 ± 24.80	20.60 ± 7.29	19.27 ± 7.47	21.14 ± 4.52

Head-in-lower back pitch range of motion (pitch ROM HD-LB)

Table 4.15: Mean ± standard deviation of pitch ROM HD-LB

pitch ROM HD-LB [*deg*]							
ID	Crossroad	Texting	Calling	Search	Fixed obstacle	Moving obstacle	In Lab SW
5001	17.05 ± 17.05	14.21 ± 12.49	10.41 ± 4.29	10.33 ± 5.70	15.02 ± 8.81	15.63 ± 10.74	10.25 ± 6.57
5004	12.35 ± 12.35	10.66 ± 6.70	8.48 ± 2.82	10.71 ± 5.69	11.68 ± 6.49	13.06 ± 7.74	8.29 ± 2.13
5005	13.99 ± 13.99	12.25 ± 8.88	13.30 ± 7.91	13.33 ± 8.96	14.74 ± 8.20	12.75 ± 6.84	13.84 ± 7.49
5006	20.70 ± 20.70	19.68 ± 10.53	15.89 ± 3.98	18.44 ± 8.24	16.38 ± 8.05	18.65 ± 8.06	8.51 ± 2.59
5007	18.15 ± 18.15	13.04 ± 10.92	15.83 ± 7.29	15.35 ± 5.96	16.68 ± 9.70	19.73 ± 11.67	7.50 ± 3.31
5008	9.34 ± 9.34	8.34 ± 7.77	7.52 ± 2.40	12.19 ± 7.37	10.23 ± 7.69	8.48 ± 4.86	7.85 ± 3.03
5010	13.10 ± 13.10	13.15 ± 10.50	14.54 ± 7.87	13.40 ± 6.48	12.50 ± 7.34	11.17 ± 7.79	8.59 ± 3.65
5011	15.00 ± 15.00	12.20 ± 6.12	12.59 ± 4.34	17.56 ± 6.50	14.93 ± 6.26	14.52 ± 5.78	12.20 ± 4.25

Chest-in-lower back yaw range of motion (yaw ROM CH-LB)

Table 4.16: Mean ± standard deviation of yaw ROM CH-LB

yaw ROM CH-LB [*deg*]							
ID	Crossroad	Texting	Calling	Search	Fixed obstacle	Moving obstacle	In Lab SW
5001	14.48 ± 14.48	14.22 ± 3.92	15.18 ± 1.95	10.84 ± 3.82	13.36 ± 3.44	16.84 ± 3.73	15.87 ± 2.53
5004	11.44 ± 11.44	7.85 ± 2.46	9.33 ± 1.22	8.86 ± 2.34	11.26 ± 3.98	12.77 ± 3.90	14.57 ± 1.41
5005	15.25 ± 15.25	15.01 ± 2.98	12.59 ± 3.25	11.20 ± 3.25	16.45 ± 2.59	13.43 ± 3.14	15.34 ± 2.91
5006	23.78 ± 23.78	24.39 ± 3.67	22.91 ± 3.03	19.16 ± 6.18	23.08 ± 6.26	26.18 ± 5.44	20.68 ± 2.06
5007	18.74 ± 18.74	16.33 ± 3.37	17.13 ± 1.83	15.00 ± 3.55	17.10 ± 5.33	16.67 ± 4.54	17.23 ± 2.29
5008	18.90 ± 18.90	18.06 ± 4.20	23.01 ± 2.82	12.55 ± 4.21	19.01 ± 3.80	18.37 ± 4.02	20.19 ± 2.57
5010	19.70 ± 19.70	14.02 ± 3.67	16.07 ± 2.97	14.74 ± 3.70	16.16 ± 5.43	18.74 ± 5.22	14.91 ± 2.20
5011	24.40 ± 24.40	22.78 ± 3.14	20.07 ± 4.43	24.00 ± 6.97	24.10 ± 3.66	23.71 ± 4.21	24.65 ± 5.12

Chest-in-lower back pitch range of motion (pitch ROM CH-LB)

Table 4.17: Mean ± standard deviation of pitch ROM CH-LB

pitch ROM CH-LB [*deg*]							
ID	Crossroad	Texting	Calling	Search	Fixed obstacle	Moving obstacle	In Lab SW
5001	9.24 ± 9.24	7.41 ± 1.63	7.70 ± 2.99	7.72 ± 2.02	8.77 ± 2.62	9.17 ± 2.44	5.59 ± 1.70
5004	5.34 ± 5.34	4.30 ± 0.92	4.37 ± 1.04	4.28 ± 1.28	4.69 ± 1.69	4.71 ± 1.81	6.53 ± 1.28
5005	5.33 ± 5.33	4.85 ± 1.81	5.71 ± 1.80	4.57 ± 1.82	5.28 ± 1.72	4.79 ± 1.37	4.52 ± 1.34
5006	14.70 ± 14.70	14.97 ± 2.49	12.79 ± 1.70	11.53 ± 3.12	12.33 ± 3.84	14.67 ± 3.42	6.13 ± 1.23
5007	8.22 ± 8.22	5.91 ± 2.18	5.46 ± 1.45	6.99 ± 2.62	7.80 ± 2.74	7.70 ± 2.66	4.82 ± 0.91
5008	3.49 ± 3.49	3.34 ± 0.81	4.80 ± 0.98	3.72 ± 1.45	3.87 ± 1.67	3.47 ± 1.18	3.87 ± 0.95
5010	6.13 ± 6.13	5.22 ± 2.06	6.43 ± 2.14	5.30 ± 1.86	5.99 ± 3.58	5.63 ± 1.93	4.72 ± 1.20
5011	10.08 ± 10.08	9.63 ± 2.25	10.34 ± 2.74	8.38 ± 2.12	10.32 ± 2.88	10.91 ± 3.17	10.45 ± 2.03

Head-in-chest yaw range of motion (yaw ROM HD-CH)

Table 4.18: Mean ± standard deviation of yaw ROM HD-CH

yaw ROM HD-CH [*deg*]							
ID	Crossroad	Texting	Calling	Search	Fixed obstacle	Moving obstacle	In Lab SW
5001	13.51 ± 13.51	6.67 ± 5.48	8.93 ± 2.96	35.08 ± 21.96	10.52 ± 10.30	9.79 ± 8.41	8.97 ± 4.36
5004	20.24 ± 20.24	5.85 ± 5.86	5.64 ± 3.48	20.65 ± 14.53	16.71 ± 14.83	21.09 ± 15.96	10.51 ± 1.87
5005	13.50 ± 13.50	7.66 ± 6.63	9.48 ± 6.17	18.33 ± 13.27	10.80 ± 7.60	9.66 ± 7.18	10.64 ± 10.10
5006	24.12 ± 24.12	12.43 ± 10.76	6.17 ± 4.37	24.55 ± 15.52	14.29 ± 14.14	11.59 ± 8.99	11.04 ± 6.21
5007	26.12 ± 26.12	10.67 ± 11.32	11.48 ± 3.83	45.27 ± 23.10	23.53 ± 17.01	19.01 ± 15.06	10.08 ± 2.76
5008	12.67 ± 12.67	4.78 ± 2.67	7.10 ± 2.31	18.41 ± 11.27	11.55 ± 7.58	7.34 ± 3.75	9.60 ± 2.90
5010	27.01 ± 27.01	13.23 ± 13.22	14.80 ± 8.44	39.92 ± 18.24	26.12 ± 17.60	22.70 ± 14.92	9.21 ± 6.31
5011	21.28 ± 21.28	8.07 ± 5.01	8.58 ± 6.17	28.17 ± 20.66	11.41 ± 6.43	11.64 ± 7.26	9.77 ± 3.14

Head-in-chest pitch range of motion (pitch ROM HD-CH)

Table 4.19: Mean ± standard deviation of pitch ROM HD-CH

pitch ROM HD-CH [*deg*]							
ID	Crossroad	Texting	Calling	Search	Fixed obstacle	Moving obstacle	In Lab SW
5001	17.56 ± 17.56	12.95 ± 12.47	11.09 ± 4.68	9.90 ± 4.47	15.53 ± 8.50	16.46 ± 9.93	10.27 ± 5.65
5004	11.10 ± 11.10	8.99 ± 6.77	6.09 ± 3.09	9.50 ± 5.14	10.49 ± 7.07	12.08 ± 8.14	6.15 ± 2.23
5005	11.89 ± 11.89	10.18 ± 8.19	9.52 ± 6.54	11.64 ± 7.99	12.45 ± 7.55	11.68 ± 6.67	12.21 ± 8.23
5006	16.55 ± 16.55	14.73 ± 10.90	8.90 ± 4.29	14.48 ± 9.02	12.61 ± 8.50	14.60 ± 9.06	6.16 ± 3.22
5007	18.85 ± 18.85	13.54 ± 11.10	15.84 ± 7.21	17.57 ± 5.65	17.88 ± 9.57	20.48 ± 10.66	9.13 ± 3.35
5008	9.55 ± 9.55	7.63 ± 7.63	6.46 ± 2.40	11.10 ± 6.73	10.27 ± 8.10	8.14 ± 4.72	6.98 ± 3.42
5010	12.74 ± 12.74	12.03 ± 11.00	14.64 ± 8.21	13.82 ± 7.36	12.83 ± 7.86	10.63 ± 7.56	8.42 ± 4.57
5011	12.33 ± 12.33	9.04 ± 6.40	7.59 ± 3.76	14.14 ± 6.34	11.45 ± 6.45	9.95 ± 5.64	8.43 ± 3.49

4.1.3 Attenuation

Vertical attenuation coefficient head-chest (ACV HD-CH)

Table 4.20: Mean ± standard deviation of ACV HD-CH

ACV HD-CH [%]							
ID	Crossroad	Texting	Calling	Search	Fixed obstacle	Moving obstacle	In Lab SW
5001	2.65 ± 2.65	14.08 ± 12.77	13.10 ± 7.46	-4.06 ± 13.59	6.12 ± 11.61	5.85 ± 14.26	11.16 ± 9.70
5004	16.45 ± 16.45	-1.04 ± 10.02	10.33 ± 6.43	13.57 ± 23.70	12.29 ± 22.68	18.91 ± 15.35	17.06 ± 7.86
5005	5.16 ± 5.16	6.43 ± 10.46	-4.37 ± 19.20	2.05 ± 13.60	6.98 ± 10.59	3.24 ± 9.41	15.04 ± 16.45
5006	-7.68 ± -7.68	-17.66 ± 38.25	29.57 ± 23.46	-28.29 ± 53.43	-9.40 ± 45.07	4.76 ± 36.33	17.49 ± 20.45
5007	13.54 ± 13.54	31.84 ± 16.43	10.39 ± 9.07	5.87 ± 9.80	7.39 ± 20.24	14.31 ± 14.86	2.18 ± 4.64
5008	30.64 ± 30.64	-18.67 ± 15.94	36.58 ± 10.52	19.20 ± 22.14	23.13 ± 21.56	22.01 ± 24.25	-4.54 ± 12.88
5010	1.51 ± 1.51	-12.83 ± 19.87	-8.29 ± 16.26	-11.34 ± 22.58	-2.69 ± 18.64	5.37 ± 17.06	9.08 ± 14.73
5011	-2.26 ± -2.26	-16.19 ± 9.07	-6.24 ± 12.35	9.14 ± 17.15	-0.73 ± 18.74	-3.41 ± 16.27	27.37 ± 14.15

Vertical attenuation coefficient head-lower back (ACV HD-LB)

Table 4.21: Mean ± standard deviation of ACV HD-LB

ACV HD-LB [%]							
ID	Crossroad	Texting	Calling	Search	Fixed obstacle	Moving obstacle	In Lab SW
5001	20.15 ± 20.15	31.61 ± 10.87	17.66 ± 7.32	-1.01 ± 15.70	18.38 ± 11.68	21.26 ± 11.68	17.32 ± 8.32
5004	30.69 ± 30.69	19.68 ± 7.90	28.45 ± 5.67	20.80 ± 29.71	25.77 ± 23.15	30.20 ± 15.07	34.24 ± 6.73
5005	34.01 ± 34.01	33.34 ± 8.04	29.33 ± 14.92	26.37 ± 13.49	36.59 ± 8.14	29.53 ± 8.86	37.22 ± 11.37
5006	37.95 ± 37.95	34.18 ± 20.79	57.16 ± 14.61	21.17 ± 40.06	34.41 ± 26.86	46.51 ± 20.40	42.47 ± 14.45
5007	29.46 ± 29.46	41.97 ± 14.88	27.73 ± 9.43	8.59 ± 11.93	16.16 ± 23.67	25.60 ± 14.30	22.00 ± 5.31
5008	48.17 ± 48.17	17.80 ± 8.33	57.97 ± 7.24	24.59 ± 28.64	41.19 ± 18.44	41.51 ± 18.23	24.17 ± 8.59
5010	24.31 ± 24.31	11.79 ± 13.35	6.73 ± 16.84	-0.93 ± 18.62	18.31 ± 17.89	26.31 ± 12.40	32.70 ± 10.03
5011	27.04 ± 27.04	25.30 ± 7.59	30.29 ± 10.04	3.48 ± 38.95	30.15 ± 14.23	31.17 ± 11.70	46.67 ± 11.13

Vertical attenuation coefficient chest-lower back (ACV CH-LB)

Table 4.22: Mean ± standard deviation of ACV CH-LB

ACV CH-LB [%]							
ID	Crossroad	Texting	Calling	Search	Fixed obstacle	Moving obstacle	In Lab SW
5001	17.72 ± 17.72	20.46 ± 4.50	5.13 ± 5.19	2.78 ± 8.88	12.85 ± 8.75	16.03 ± 8.00	6.70 ± 5.33
5004	17.05 ± 17.05	20.33 ± 5.29	20.18 ± 3.14	9.43 ± 10.39	15.56 ± 11.12	13.81 ± 9.05	20.65 ± 4.58
5005	30.34 ± 30.34	28.65 ± 5.04	32.04 ± 9.15	24.80 ± 8.47	31.59 ± 6.78	26.91 ± 8.63	25.75 ± 6.55
5006	41.98 ± 41.98	43.20 ± 9.61	39.28 ± 4.71	38.75 ± 14.29	38.53 ± 13.90	42.98 ± 9.12	30.12 ± 4.34
5007	18.36 ± 18.36	14.78 ± 7.86	19.50 ± 4.17	3.00 ± 6.09	8.68 ± 20.78	13.00 ± 9.28	20.21 ± 4.89
5008	24.95 ± 24.95	30.15 ± 6.63	33.73 ± 3.01	7.57 ± 15.35	23.71 ± 8.39	24.74 ± 5.95	27.26 ± 4.35
5010	23.14 ± 23.14	20.62 ± 12.28	13.76 ± 9.51	8.32 ± 11.89	20.06 ± 12.28	21.66 ± 7.27	25.43 ± 7.06
5011	28.53 ± 28.53	35.61 ± 5.59	34.19 ± 7.45	-5.48 ± 27.52	30.57 ± 7.64	33.23 ± 6.97	26.60 ± 6.33

Mediolateral attenuation coefficient head-chest (ACML HD-CH)

Table 4.23: Mean ± standard deviation of ACML HD-CH

ACML HD-CH [%]							
ID	Crossroad	Texting	Calling	Search	Fixed obstacle	Moving obstacle	In Lab SW
5001	13.89 ± 13.89	16.76 ± 14.78	10.25 ± 18.53	-10.92 ± 48.44	14.39 ± 19.19	22.80 ± 19.85	13.30 ± 14.83
5004	8.97 ± 8.97	31.82 ± 15.05	30.25 ± 8.67	9.09 ± 21.46	15.22 ± 22.06	7.20 ± 29.27	37.15 ± 9.28
5005	9.23 ± 9.23	14.40 ± 15.75	-5.22 ± 29.16	-8.32 ± 30.18	8.89 ± 26.34	2.39 ± 27.21	35.06 ± 20.84
5006	-67.80 ± -67.80	-55.30 ± 58.92	-46.36 ± 37.00	-49.80 ± 53.06	-39.90 ± 50.44	-48.87 ± 52.96	-9.20 ± 16.86
5007	-6.15 ± -6.15	-3.78 ± 28.30	23.94 ± 9.43	-14.39 ± 39.70	3.10 ± 33.81	6.90 ± 33.08	34.34 ± 13.70
5008	6.35 ± 6.35	-2.41 ± 16.24	-10.99 ± 14.30	-9.75 ± 27.01	9.87 ± 18.23	7.08 ± 20.04	34.22 ± 16.95
5010	-15.97 ± -15.97	-6.22 ± 18.67	-21.59 ± 19.83	-1.26 ± 23.48	-14.54 ± 22.20	-14.14 ± 25.97	-7.47 ± 17.57
5011	2.57 ± 2.57	21.75 ± 11.01	9.18 ± 23.26	1.64 ± 29.35	7.00 ± 29.65	1.05 ± 22.77	-2.30 ± 13.03

Mediolateral attenuation coefficient head-lower back (ACML HD-LB)

Table 4.24: Mean ± standard deviation of ACML HD-LB

ACML HD-LB [%]							
ID	Crossroad	Texting	Calling	Search	Fixed obstacle	Moving obstacle	In Lab SW
5001	38.71 ± 38.71	30.15 ± 11.62	25.14 ± 15.80	13.11 ± 37.07	36.14 ± 19.14	38.50 ± 18.12	17.57 ± 17.02
5004	52.60 ± 52.60	64.69 ± 10.55	66.90 ± 5.10	46.11 ± 18.50	53.24 ± 17.19	47.83 ± 22.08	62.77 ± 6.91
5005	36.45 ± 36.45	38.89 ± 13.31	13.91 ± 22.46	23.52 ± 21.08	37.50 ± 16.82	30.47 ± 21.04	46.08 ± 18.18
5006	-30.05 ± -30.05	-19.19 ± 46.67	-17.86 ± 29.60	2.60 ± 31.75	-23.05 ± 43.92	-29.34 ± 43.63	24.19 ± 15.42
5007	31.51 ± 31.51	35.61 ± 21.40	52.55 ± 8.30	12.71 ± 23.70	29.00 ± 33.83	37.58 ± 23.78	54.60 ± 12.89
5008	5.32 ± 5.32	20.60 ± 11.11	5.58 ± 14.53	14.68 ± 26.99	14.97 ± 19.83	14.13 ± 15.88	43.56 ± 13.54
5010	3.49 ± 3.49	10.52 ± 27.52	-4.90 ± 24.15	20.36 ± 22.55	8.47 ± 22.43	1.50 ± 27.61	12.52 ± 17.32
5011	27.36 ± 27.36	44.17 ± 8.60	33.16 ± 15.85	26.99 ± 21.52	25.63 ± 24.94	23.51 ± 19.28	27.99 ± 12.10

Mediolateral attenuation coefficient chest-lower back (ACML CH-LB)

Table 4.25: Mean ± standard deviation of ACML CH-LB

ACML CH-LB [%]							
ID	Crossroad	Texting	Calling	Search	Fixed obstacle	Moving obstacle	In Lab SW
5001	28.11 ± 28.11	14.78 ± 13.62	16.47 ± 7.84	19.87 ± 14.15	25.32 ± 15.30	19.44 ± 16.94	4.91 ± 11.12
5004	48.16 ± 48.16	47.60 ± 13.68	52.46 ± 5.28	40.89 ± 11.41	44.92 ± 13.74	44.12 ± 12.52	40.72 ± 6.70
5005	29.94 ± 29.94	28.30 ± 10.25	16.14 ± 18.28	28.04 ± 14.79	30.75 ± 9.90	28.15 ± 11.23	16.68 ± 7.76
5006	19.52 ± 19.52	22.35 ± 14.94	18.77 ± 11.13	32.49 ± 16.88	9.86 ± 20.29	10.05 ± 19.40	30.42 ± 10.23
5007	36.18 ± 36.18	37.64 ± 12.78	37.41 ± 9.88	20.69 ± 16.51	26.80 ± 20.32	32.16 ± 12.86	31.44 ± 9.03
5008	-1.84 ± -1.84	21.07 ± 14.32	14.87 ± 7.67	20.45 ± 23.64	3.86 ± 21.51	5.25 ± 18.22	13.05 ± 11.72
5010	16.10 ± 16.10	15.92 ± 18.76	13.22 ± 17.25	20.90 ± 14.63	19.42 ± 15.46	13.53 ± 14.18	18.32 ± 11.36
5011	24.49 ± 24.49	27.97 ± 10.86	24.67 ± 13.38	23.85 ± 19.99	19.89 ± 11.36	22.13 ± 12.03	29.19 ± 10.88

Anterior-posterior attenuation coefficient head-chest (ACAP HD-CH)

Table 4.26: Mean ± standard deviation of ACAP HD-CH

ACAP HD-CH [%]							
ID	Crossroad	Texting	Calling	Search	Fixed obstacle	Moving obstacle	In Lab SW
5001	24.34 ± 24.34	3.95 ± 22.00	-8.87 ± 25.10	-14.40 ± 40.90	18.81 ± 32.26	26.15 ± 26.23	10.54 ± 20.90
5004	-35.15 ± -35.15	5.37 ± 32.84	-63.36 ± 29.19	-15.85 ± 24.68	-34.19 ± 41.50	-23.29 ± 33.32	1.18 ± 9.88
5005	19.27 ± 19.27	23.88 ± 16.85	24.46 ± 19.81	16.89 ± 20.02	26.27 ± 16.22	27.81 ± 14.95	15.76 ± 17.93
5006	34.37 ± 34.37	42.75 ± 15.19	11.89 ± 13.63	5.94 ± 34.04	31.13 ± 32.82	33.82 ± 26.95	4.49 ± 14.32
5007	6.04 ± 6.04	-30.24 ± 33.90	-0.36 ± 28.38	5.98 ± 21.37	2.10 ± 54.50	7.62 ± 34.24	33.05 ± 20.89
5008	-9.57 ± -9.57	36.41 ± 13.79	-8.30 ± 4.17	1.41 ± 19.43	0.45 ± 18.81	-0.64 ± 17.45	29.73 ± 14.45
5010	17.59 ± 17.59	17.06 ± 24.68	18.05 ± 17.77	-5.31 ± 35.56	3.52 ± 38.51	12.78 ± 19.37	19.03 ± 11.14
5011	14.51 ± 14.51	28.83 ± 13.67	14.23 ± 17.06	25.66 ± 25.71	17.70 ± 21.79	23.13 ± 20.06	-1.87 ± 13.50

Anterior-posterior attenuation coefficient head-lower back (ACAP HD-LB)

Table 4.27: Mean ± standard deviation of ACAP HD-LB

ACAP HD-LB [%]							
ID	Crossroad	Texting	Calling	Search	Fixed obstacle	Moving obstacle	In Lab SW
5001	40.18 ± 40.18	24.79 ± 18.26	25.78 ± 17.04	24.76 ± 26.55	41.47 ± 20.76	39.05 ± 21.62	30.72 ± 17.83
5004	18.54 ± 18.54	48.17 ± 16.36	23.54 ± 13.81	24.73 ± 15.52	19.18 ± 26.66	16.58 ± 22.59	15.82 ± 13.94
5005	40.22 ± 40.22	43.67 ± 13.33	35.82 ± 15.69	34.17 ± 18.31	46.69 ± 15.14	42.79 ± 16.68	30.05 ± 16.40
5006	31.25 ± 31.25	41.84 ± 15.86	3.08 ± 15.26	11.33 ± 28.92	27.41 ± 32.35	27.86 ± 32.63	9.85 ± 14.43
5007	31.16 ± 31.16	-0.34 ± 26.36	31.58 ± 18.23	29.64 ± 14.35	25.33 ± 40.89	29.91 ± 25.14	51.31 ± 15.69
5008	-19.64 ± -19.64	27.52 ± 15.86	-29.82 ± 10.48	0.50 ± 23.95	-11.16 ± 22.01	-12.39 ± 21.09	8.44 ± 21.66
5010	16.99 ± 16.99	14.84 ± 27.14	-8.31 ± 44.88	7.43 ± 26.68	8.65 ± 33.82	7.97 ± 21.59	3.90 ± 15.36
5011	47.39 ± 47.39	61.10 ± 8.77	45.47 ± 15.96	55.44 ± 15.70	52.31 ± 14.35	54.57 ± 13.58	39.25 ± 10.11

Anterior-posterior attenuation coefficient chest-lower back (ACAP CH-LB)

Table 4.28: Mean ± standard deviation of ACAP CH-LB

ACAP CH-LB [%]							
ID	Crossroad	Texting	Calling	Search	Fixed obstacle	Moving obstacle	In Lab SW
5001	17.71 ± 17.71	21.43 ± 8.76	31.67 ± 4.55	33.62 ± 8.39	25.27 ± 15.09	16.62 ± 14.05	22.85 ± 6.69
5004	37.44 ± 37.44	44.28 ± 7.87	52.79 ± 6.01	34.53 ± 8.06	38.32 ± 11.63	30.25 ± 18.10	14.92 ± 10.28
5005	24.84 ± 24.84	25.63 ± 10.12	13.92 ± 14.02	20.74 ± 11.05	27.85 ± 11.03	21.07 ± 13.70	17.04 ± 6.85
5006	-7.75 ± -7.75	-2.15 ± 11.17	-10.30 ± 8.14	3.16 ± 19.61	-7.23 ± 18.21	-8.68 ± 16.62	5.38 ± 7.72
5007	25.97 ± 25.97	21.91 ± 13.87	30.79 ± 10.42	24.45 ± 9.15	22.12 ± 16.60	23.13 ± 10.68	27.51 ± 5.57
5008	-9.43 ± -9.43	-14.76 ± 15.14	-19.90 ± 8.89	-1.81 ± 19.78	-12.20 ± 12.83	-12.10 ± 11.81	-29.75 ± 9.30
5010	-2.09 ± -2.09	-3.87 ± 21.95	-30.99 ± 41.79	9.97 ± 15.11	3.00 ± 17.21	-5.90 ± 12.18	-18.68 ± 9.91
5011	38.30 ± 38.30	45.14 ± 8.55	37.02 ± 10.70	39.54 ± 8.47	42.11 ± 8.16	40.93 ± 8.98	40.22 ± 7.61

4.1.4 Symmetry

Vertical improved harmonic ratio (iHR V-LB)

Table 4.29: Mean ± standard deviation of iHR V-LB

iHR V-LB [/]							
ID	Crossroad	Texting	Calling	Search	Fixed obstacle	Moving obstacle	In Lab SW
5001	0.74 ± 0.74	0.76 ± 0.05	0.73 ± 0.06	0.65 ± 0.08	0.74 ± 0.08	0.77 ± 0.06	0.76 ± 0.05
5004	0.68 ± 0.68	0.71 ± 0.11	0.74 ± 0.08	0.68 ± 0.13	0.69 ± 0.12	0.69 ± 0.12	0.69 ± 0.12
5005	0.73 ± 0.73	0.75 ± 0.07	0.74 ± 0.09	0.71 ± 0.09	0.74 ± 0.08	0.74 ± 0.07	0.76 ± 0.07
5006	0.69 ± 0.69	0.71 ± 0.05	0.73 ± 0.04	0.60 ± 0.10	0.69 ± 0.09	0.71 ± 0.06	0.74 ± 0.04
5007	0.73 ± 0.73	0.75 ± 0.11	0.78 ± 0.07	0.71 ± 0.12	0.69 ± 0.13	0.74 ± 0.10	0.81 ± 0.05
5008	0.73 ± 0.73	0.73 ± 0.09	0.77 ± 0.08	0.65 ± 0.12	0.76 ± 0.10	0.75 ± 0.09	0.77 ± 0.07
5010	0.72 ± 0.72	0.66 ± 0.11	0.69 ± 0.10	0.60 ± 0.09	0.68 ± 0.11	0.73 ± 0.08	0.75 ± 0.08
5011	0.68 ± 0.68	0.72 ± 0.08	0.74 ± 0.07	0.60 ± 0.10	0.72 ± 0.07	0.71 ± 0.07	0.71 ± 0.04

Mediolateral improved harmonic ratio (iHR ML-LB)

Table 4.30: Mean ± standard deviation of iHR ML-LB

iHR ML-LB [/]							
ID	Crossroad	Texting	Calling	Search	Fixed obstacle	Moving obstacle	In Lab SW
5001	0.67 ± 0.67	0.69 ± 0.06	0.70 ± 0.08	0.65 ± 0.08	0.68 ± 0.07	0.68 ± 0.05	0.72 ± 0.05
5004	0.66 ± 0.66	0.69 ± 0.11	0.72 ± 0.07	0.67 ± 0.11	0.68 ± 0.11	0.68 ± 0.12	0.67 ± 0.13
5005	0.63 ± 0.63	0.65 ± 0.06	0.65 ± 0.07	0.63 ± 0.07	0.64 ± 0.07	0.64 ± 0.07	0.68 ± 0.06
5006	0.63 ± 0.63	0.66 ± 0.07	0.67 ± 0.07	0.58 ± 0.06	0.64 ± 0.08	0.65 ± 0.09	0.64 ± 0.05
5007	0.58 ± 0.58	0.61 ± 0.09	0.66 ± 0.09	0.62 ± 0.09	0.58 ± 0.08	0.59 ± 0.07	0.67 ± 0.04
5008	0.63 ± 0.63	0.60 ± 0.09	0.68 ± 0.07	0.61 ± 0.10	0.65 ± 0.10	0.65 ± 0.08	0.67 ± 0.07
5010	0.65 ± 0.65	0.63 ± 0.09	0.63 ± 0.09	0.62 ± 0.07	0.64 ± 0.08	0.65 ± 0.08	0.68 ± 0.06
5011	0.64 ± 0.64	0.64 ± 0.10	0.66 ± 0.08	0.58 ± 0.09	0.67 ± 0.08	0.66 ± 0.09	0.68 ± 0.08

Anterior-posterior improved harmonic ratio (iHR AP-LB)

Table 4.31: Mean ± standard deviation of iHR AP-LB

iHR AP-LB [/]							
ID	Crossroad	Texting	Calling	Search	Fixed obstacle	Moving obstacle	In Lab SW
5001	0.72 ± 0.72	0.73 ± 0.07	0.76 ± 0.06	0.68 ± 0.11	0.74 ± 0.09	0.77 ± 0.07	0.75 ± 0.05
5004	0.62 ± 0.62	0.63 ± 0.07	0.62 ± 0.04	0.64 ± 0.08	0.62 ± 0.08	0.62 ± 0.08	0.67 ± 0.09
5005	0.69 ± 0.69	0.71 ± 0.05	0.70 ± 0.08	0.67 ± 0.08	0.71 ± 0.05	0.70 ± 0.06	0.75 ± 0.06
5006	0.63 ± 0.63	0.64 ± 0.05	0.64 ± 0.05	0.55 ± 0.09	0.63 ± 0.07	0.64 ± 0.06	0.74 ± 0.04
5007	0.69 ± 0.69	0.70 ± 0.09	0.71 ± 0.05	0.67 ± 0.09	0.65 ± 0.11	0.69 ± 0.09	0.77 ± 0.04
5008	0.70 ± 0.70	0.68 ± 0.08	0.73 ± 0.08	0.64 ± 0.10	0.71 ± 0.09	0.70 ± 0.07	0.70 ± 0.04
5010	0.66 ± 0.66	0.64 ± 0.10	0.62 ± 0.10	0.63 ± 0.09	0.64 ± 0.12	0.67 ± 0.10	0.72 ± 0.08
5011	0.69 ± 0.69	0.69 ± 0.08	0.71 ± 0.07	0.58 ± 0.09	0.73 ± 0.09	0.72 ± 0.09	0.71 ± 0.05

4.1.5 Smoothness

Vertical head log dimensionless jerk (LDLJ V-HD)

Table 4.32: Mean ± standard deviation of LDLJ V-HD

LDLJ V-HD [/]							
ID	Crossroad	Texting	Calling	Search	Fixed obstacle	Moving obstacle	In Lab SW
5001	-4.74 ± -4.74	-4.65 ± 0.20	-5.09 ± 0.19	-4.89 ± 0.38	-4.77 ± 0.27	-4.81 ± 0.20	-4.91 ± 0.17
5004	-4.87 ± -4.87	-4.97 ± 0.28	-4.89 ± 0.20	-4.94 ± 0.33	-4.93 ± 0.37	-4.85 ± 0.29	-4.65 ± 0.21
5005	-4.90 ± -4.90	-4.99 ± 0.28	-4.96 ± 0.34	-4.96 ± 0.35	-4.87 ± 0.24	-4.92 ± 0.28	-4.63 ± 0.36
5006	-4.82 ± -4.82	-4.80 ± 0.19	-4.82 ± 0.18	-4.88 ± 0.55	-4.79 ± 0.34	-4.74 ± 0.24	-4.56 ± 0.17
5007	-4.97 ± -4.97	-4.83 ± 0.26	-5.05 ± 0.11	-4.78 ± 0.29	-5.05 ± 0.44	-4.97 ± 0.30	-4.83 ± 0.15
5008	-4.87 ± -4.87	-4.65 ± 0.25	-4.98 ± 0.19	-5.13 ± 0.51	-4.82 ± 0.25	-4.83 ± 0.24	-4.80 ± 0.20
5010	-4.92 ± -4.92	-5.04 ± 0.36	-4.71 ± 0.37	-5.20 ± 0.46	-4.95 ± 0.40	-4.85 ± 0.25	-4.68 ± 0.23
5011	-5.13 ± -5.13	-5.03 ± 0.21	-5.04 ± 0.20	-5.23 ± 0.39	-5.04 ± 0.20	-5.07 ± 0.23	-4.93 ± 0.19

Mediolateral head log dimensionless jerk (LDLJ ML-HD)

Table 4.33: Mean ± standard deviation of LDLJ ML-HD

LDLJ ML-HD [/]							
ID	Crossroad	Texting	Calling	Search	Fixed obstacle	Moving obstacle	In Lab SW
5001	-4.15 ± -4.15	-4.00 ± 0.25	-3.63 ± 0.25	-3.64 ± 0.46	-4.07 ± 0.33	-4.07 ± 0.39	-3.99 ± 0.36
5004	-3.93 ± -3.93	-3.88 ± 0.32	-3.79 ± 0.24	-3.92 ± 0.45	-3.90 ± 0.45	-3.81 ± 0.47	-3.38 ± 0.42
5005	-3.96 ± -3.96	-3.84 ± 0.30	-4.03 ± 0.38	-3.83 ± 0.39	-3.89 ± 0.34	-3.93 ± 0.31	-3.78 ± 0.34
5006	-3.76 ± -3.76	-3.61 ± 0.54	-3.95 ± 0.22	-3.56 ± 0.62	-3.70 ± 0.50	-3.74 ± 0.39	-3.38 ± 0.38
5007	-4.17 ± -4.17	-4.19 ± 0.49	-4.34 ± 0.39	-3.94 ± 0.52	-3.87 ± 0.64	-4.27 ± 0.48	-3.54 ± 0.51
5008	-4.17 ± -4.17	-4.07 ± 0.27	-4.14 ± 0.18	-4.09 ± 0.41	-4.07 ± 0.42	-4.14 ± 0.32	-4.05 ± 0.36
5010	-3.97 ± -3.97	-3.67 ± 0.39	-3.88 ± 0.43	-3.82 ± 0.53	-3.84 ± 0.52	-3.93 ± 0.33	-3.76 ± 0.32
5011	-4.01 ± -4.01	-3.92 ± 0.22	-3.89 ± 0.36	-3.63 ± 0.51	-3.97 ± 0.35	-4.01 ± 0.25	-3.83 ± 0.19

Anterior-posterior head log dimensionless jerk (LDLJ AP-HD)

Table 4.34: Mean ± standard deviation of LDLJ AP-HD

LDLJ AP-HD [/]							
ID	Crossroad	Texting	Calling	Search	Fixed obstacle	Moving obstacle	In Lab SW
5001	-4.42 ± -4.42	-4.23 ± 0.28	-5.00 ± 0.25	-4.23 ± 0.46	-4.48 ± 0.42	-4.40 ± 0.39	-4.66 ± 0.49
5004	-4.97 ± -4.97	-5.10 ± 0.44	-5.28 ± 0.34	-5.04 ± 0.37	-5.02 ± 0.45	-4.94 ± 0.46	-4.79 ± 0.40
5005	-4.93 ± -4.93	-4.83 ± 0.43	-5.05 ± 0.49	-4.90 ± 0.39	-4.88 ± 0.31	-4.94 ± 0.49	-4.58 ± 0.39
5006	-4.94 ± -4.94	-5.22 ± 0.46	-5.18 ± 0.33	-4.87 ± 0.45	-5.06 ± 0.47	-5.00 ± 0.42	-4.81 ± 0.35
5007	-4.67 ± -4.67	-4.47 ± 0.43	-4.71 ± 0.37	-4.30 ± 0.66	-4.75 ± 0.47	-4.59 ± 0.46	-4.90 ± 0.23
5008	-4.88 ± -4.88	-4.91 ± 0.31	-5.03 ± 0.25	-5.04 ± 0.39	-4.90 ± 0.34	-4.97 ± 0.31	-5.09 ± 0.33
5010	-5.07 ± -5.07	-4.88 ± 0.44	-5.03 ± 0.48	-4.85 ± 0.52	-5.07 ± 0.51	-5.03 ± 0.41	-5.09 ± 0.39
5011	-5.24 ± -5.24	-5.21 ± 0.35	-5.44 ± 0.30	-5.00 ± 0.41	-5.21 ± 0.42	-5.23 ± 0.39	-5.29 ± 0.34

4.1.6 Regularity

Vertical head refined composite multiscale entropy (RCME V-HD)

Table 4.35: Mean ± standard deviation of RCME V-HD

RCME V-HD [/]							
ID	Crossroad	Texting	Calling	Search	Fixed obstacle	Moving obstacle	In Lab SW
5001	1.15 ± 1.15	1.09 ± 0.15	1.34 ± 0.16	1.50 ± 0.52	1.22 ± 0.26	1.20 ± 0.15	1.30 ± 0.18
5004	1.19 ± 1.19	1.15 ± 0.20	1.27 ± 0.14	1.38 ± 0.34	1.29 ± 0.33	1.18 ± 0.22	1.24 ± 0.15
5005	1.28 ± 1.28	1.32 ± 0.17	1.47 ± 0.30	1.51 ± 0.32	1.30 ± 0.14	1.33 ± 0.25	1.23 ± 0.20
5006	1.25 ± 1.25	1.27 ± 0.13	1.29 ± 0.12	1.48 ± 0.42	1.31 ± 0.34	1.24 ± 0.14	1.00 ± 0.15
5007	1.22 ± 1.22	1.21 ± 0.18	1.31 ± 0.14	1.29 ± 0.31	1.48 ± 0.45	1.32 ± 0.33	1.18 ± 0.12
5008	1.11 ± 1.11	1.04 ± 0.20	1.29 ± 0.13	1.66 ± 0.49	1.18 ± 0.30	1.16 ± 0.19	1.18 ± 0.15
5010	1.17 ± 1.17	1.20 ± 0.28	1.17 ± 0.35	1.64 ± 0.34	1.36 ± 0.50	1.12 ± 0.20	0.95 ± 0.14
5011	1.15 ± 1.15	1.00 ± 0.14	1.06 ± 0.19	1.64 ± 0.56	1.11 ± 0.15	1.14 ± 0.18	1.20 ± 0.19

Mediolateral head refined composite multiscale entropy (RCME ML-HD)

Table 4.36: Mean ± standard deviation of RCME ML-HD

RCME ML-HD [/]							
ID	Crossroad	Texting	Calling	Search	Fixed obstacle	Moving obstacle	In Lab SW
5001	0.91 ± 0.91	0.81 ± 0.15	0.55 ± 0.14	0.83 ± 0.28	0.90 ± 0.19	0.90 ± 0.23	0.87 ± 0.12
5004	0.87 ± 0.87	0.85 ± 0.20	0.82 ± 0.14	0.83 ± 0.23	0.82 ± 0.22	0.79 ± 0.20	0.70 ± 0.12
5005	0.79 ± 0.79	0.80 ± 0.18	0.96 ± 0.24	0.78 ± 0.21	0.76 ± 0.16	0.81 ± 0.18	0.76 ± 0.23
5006	0.82 ± 0.82	0.81 ± 0.16	0.82 ± 0.12	0.77 ± 0.30	0.80 ± 0.22	0.83 ± 0.16	0.51 ± 0.11
5007	1.02 ± 1.02	1.03 ± 0.22	1.10 ± 0.23	1.05 ± 0.31	0.94 ± 0.31	1.02 ± 0.23	0.90 ± 0.23
5008	1.00 ± 1.00	0.97 ± 0.17	0.82 ± 0.14	1.03 ± 0.26	0.96 ± 0.21	0.98 ± 0.17	0.91 ± 0.16
5010	0.76 ± 0.76	0.66 ± 0.17	0.78 ± 0.22	0.74 ± 0.20	0.73 ± 0.23	0.74 ± 0.16	0.74 ± 0.13
5011	0.94 ± 0.94	0.85 ± 0.10	0.92 ± 0.19	0.82 ± 0.23	0.95 ± 0.17	0.96 ± 0.15	0.80 ± 0.12

Anterior-posterior head refined composite multiscale entropy (RCME AP-HD)

Table 4.37: Mean ± standard deviation of RCME AP-HD

RCME AP-HD [/]							
ID	Crossroad	Texting	Calling	Search	Fixed obstacle	Moving obstacle	In Lab SW
5001	1.21 ± 1.21	1.03 ± 0.19	1.46 ± 0.29	1.31 ± 0.32	1.28 ± 0.28	1.19 ± 0.26	1.41 ± 0.28
5004	1.33 ± 1.33	1.51 ± 0.27	1.50 ± 0.31	1.39 ± 0.28	1.35 ± 0.30	1.26 ± 0.28	1.27 ± 0.22
5005	1.40 ± 1.40	1.36 ± 0.28	1.62 ± 0.38	1.48 ± 0.29	1.33 ± 0.26	1.43 ± 0.32	1.21 ± 0.28
5006	1.39 ± 1.39	1.52 ± 0.23	1.55 ± 0.19	1.54 ± 0.40	1.48 ± 0.31	1.45 ± 0.22	1.19 ± 0.19
5007	1.13 ± 1.13	1.14 ± 0.23	1.31 ± 0.18	1.22 ± 0.46	1.37 ± 0.33	1.22 ± 0.31	1.24 ± 0.21
5008	1.11 ± 1.11	1.18 ± 0.23	1.12 ± 0.17	1.48 ± 0.41	1.17 ± 0.28	1.17 ± 0.23	1.13 ± 0.27
5010	1.50 ± 1.50	1.49 ± 0.32	1.64 ± 0.36	1.60 ± 0.40	1.56 ± 0.37	1.46 ± 0.30	1.31 ± 0.28
5011	1.61 ± 1.61	1.55 ± 0.22	1.67 ± 0.27	1.64 ± 0.31	1.62 ± 0.25	1.62 ± 0.27	1.40 ± 0.22

4.2 Differences in parameters across activities

Several parameters showed statistically significant differences among labels.
In the following sections are reported the boxplots of the aggregated parameters distributions that showed statistically significant differences.
They are described by their Median value (**Mdn**) and Interquartile range (**IQR**).

Table 4.38: Overview of statistical analyses performed, indicating the result of the normality test performed and the statistical test chosen with its p-value.

Statistical analysis				
Parameter	**Normality**	**ANOVA**	**Kruskal-Wallis**	**p-value**
stride speed	✓	✓		<0.001
stride length	✓	✓		<0.001
stride duration	✗		✓	<0.001
Froude number	✓	✓		<0.001
a-rms HD-V	✓	✓		<0.001
a-rms HD-ML	✗		✓	0.01
a-rms HD-AP	✗		✓	<0.001
a-rms CH-V	✓	✓		<0.001
a-rms CH-ML	✓	✓		0.003
a-rms CH-AP	✓	✓		0.005
a-rms LB-V	✓	✓		<0.001
a-rms LB-ML	✓	✓		<0.001
a-rms LB-AP	✓	✓		<0.001
yaw ROM HD-LB	✓	✓		<0.001
pitch ROM HD-LB	✓	✓		0.005
yaw ROM CH-LB	✓	✓		0.011
pitch ROM CH-LB	✓	✓		0.154
yaw ROM HD-CH	✓	✓		<0.001
pitch ROM HD-CH	✓	✓		<0.001
ACV HD-CH	✓	✓		0.301
ACV HD-LB	✓	✓		0.008
ACV CH-LB	✓	✓		0.005
ACML HD-CH	✗		✓	0.257
ACML HD-LB	✓	✓		0.132
ACML CH-LB	✓	✓		0.64
ACAP HD-CH	✓	✓		0.263
ACAP HD-LB	✓	✓		0.256
ACAP CH-LB	✓	✓		0.227
iHR V-LB	✓	✓		<0.001
iHR ML-LB	✓	✓		<0.001
iHR AP-LB	✓	✓		0.001
RCME V-HD	✓	✓		<0.001
RCME ML-HD	✓	✓		0.185
RCME AP-HD	✓	✓		0.011
LDLJ V-HD	✓	✓		0.04
LDLJ ML-HD	✓	✓		0.023
LDLJ AP-HD	✓	✓		0.044

4.2.1 Gait parameters

Stride speed

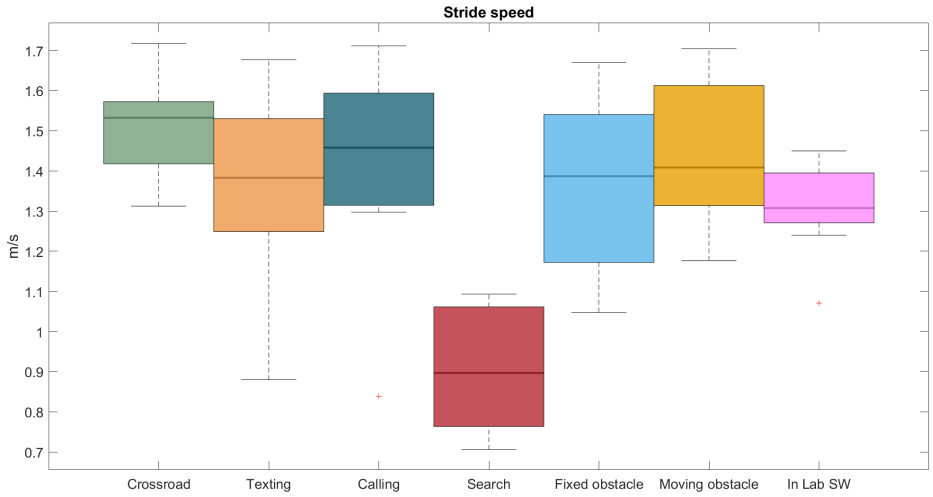

Figure 4.1: Stride speed

Stride speed distributions during visual search (mdn 0.90 IQR 0.30 m/s) significantly differed from all other labels (d>2.05).

Stride length

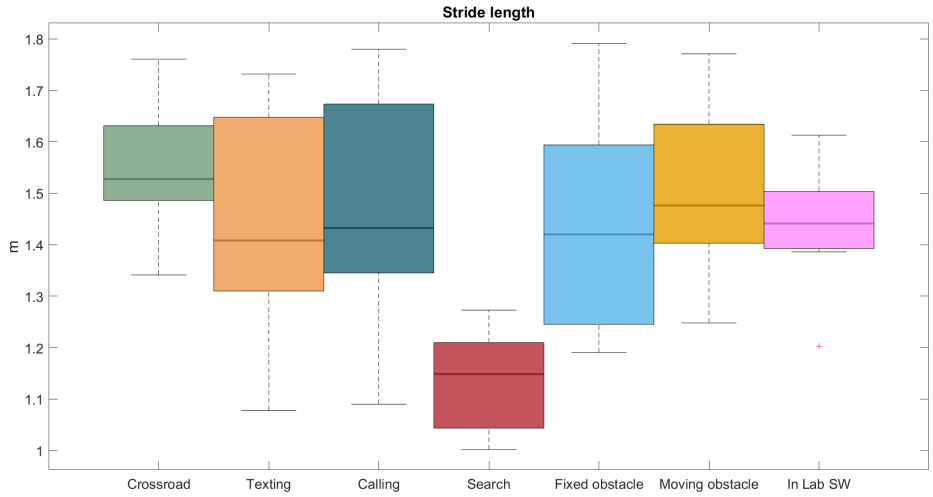

Figure 4.2: Stride length

Stride length distributions during visual search (mdn 1.15 IQR 0.17 m) significantly differed from all other labels (d>1.69).

Stride duration

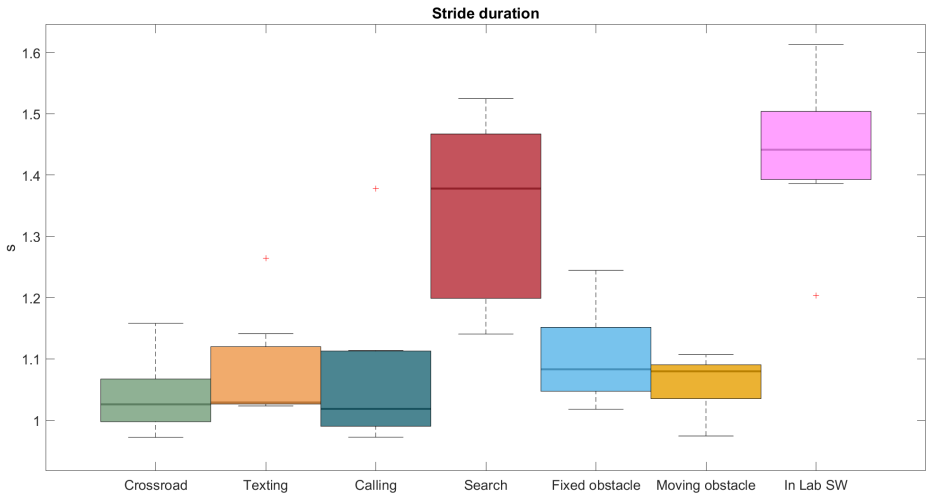

Figure 4.3: Stride duration

Stride duration distributions during visual search (mdn 1.38 IQR 0.27 s) significantly differed from crossroad (mdn 1.03 IQR 0.07 s, d=2.33) and calling(mdn 1.02 IQR 0.12 s, d=1.89). Distributions were significantly different also from Lab walking (mdn 1.44 IQR 0.11 s) and crossroad (d=3.95),calling (d=2.69), texting (mdn 1.03 IQR 0.09 s, d=3.23) and moving obstacle (mdn 1.08 IQR 0.06 s, d=3.23

Froude number

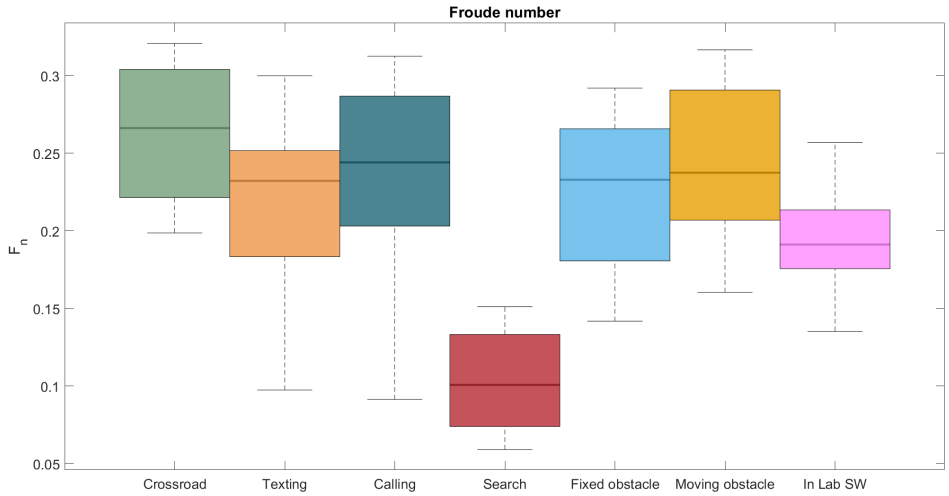

Figure 4.4: Froude number

Froude number distributions during visual search (mdn 0.10 IQR 0.06) significantly differed from all other labels (d>1.73).

4.2.2 Magnitude

a-rms HD-V

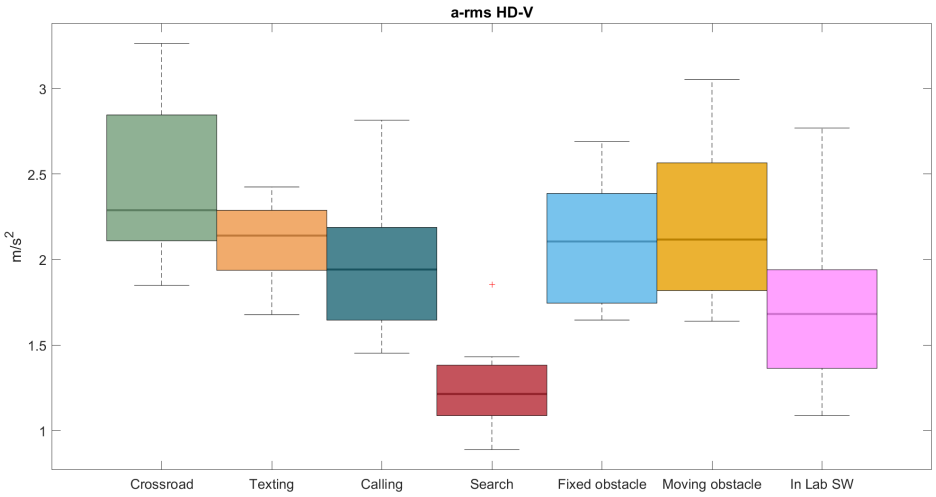

Figure 4.5: a-rms HD-V

a-rms HD-V distributions during visual search (mdn 1.21 IQR 0.30 m/s^2) significantly differed from all other labels (d>1.69) except lab walking (mdn 1.68 IQR 0.58 m/s^2). Lab walking was instead significantly different from crossroad (mdn 2.29 IQR 0.74 m/s^2, d=1,71).

a-rms HD-AP

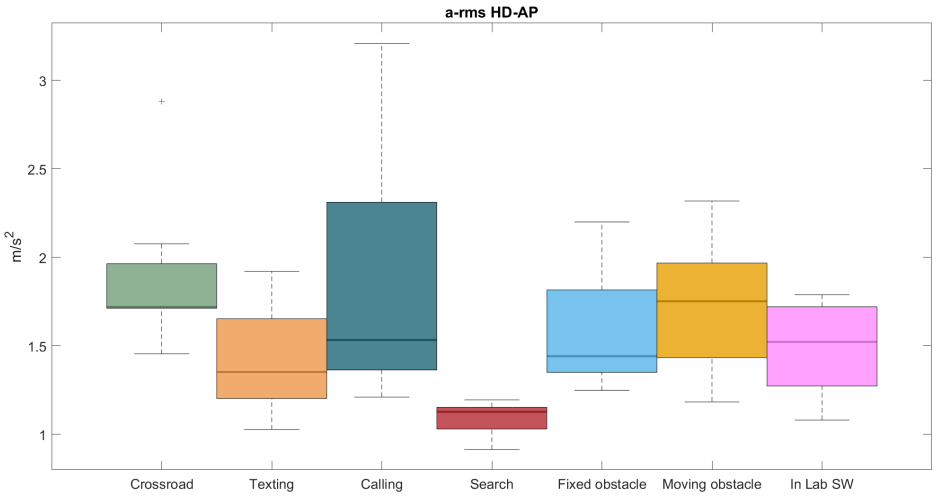

Figure 4.6: a-rms HD-AP

a-rms HD-AP distributions during visual search (mdn 1.21 IQR 0.30 m/s^2) significantly differed from crossroad (mdn 1.72 IQR 0.25 m/s^2, d=2.39), calling (mdn 1.53

IQR 0.95 m/s^2, d=1,40) and moving obstacle (mdn 2.29 IQR 0.74 m/s^2, d=2.22).

a-rms CH-V

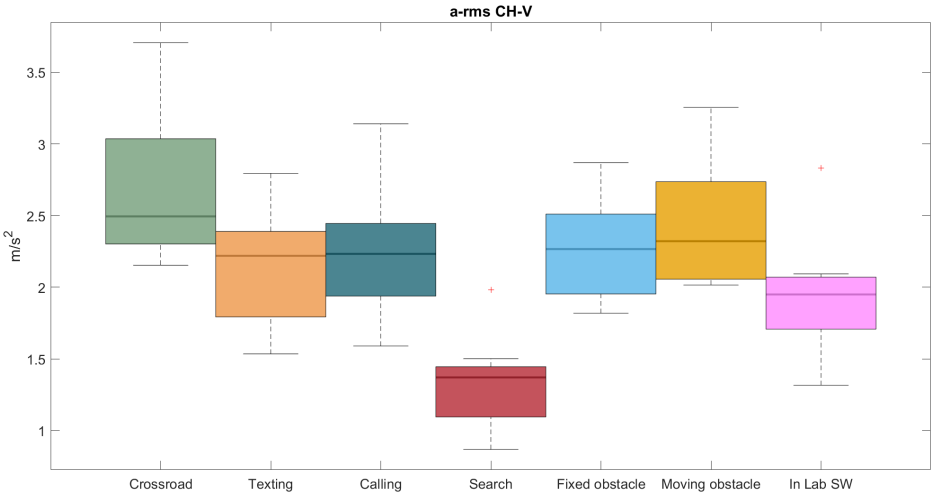

Figure 4.7: a-rms CH-V

a-rms CH-V distributions during visual search (mdn 1.37 IQR 0.35 m/s^2) significantly differed from all other labels (d>1.83) except lab walking (mdn 1.95 IQR 0.36 m/s^2). Lab walking was instead significantly different from crossroad (mdn 2.49 IQR 0.73 m/s^2, d=1,68).

a-rms CH-ML

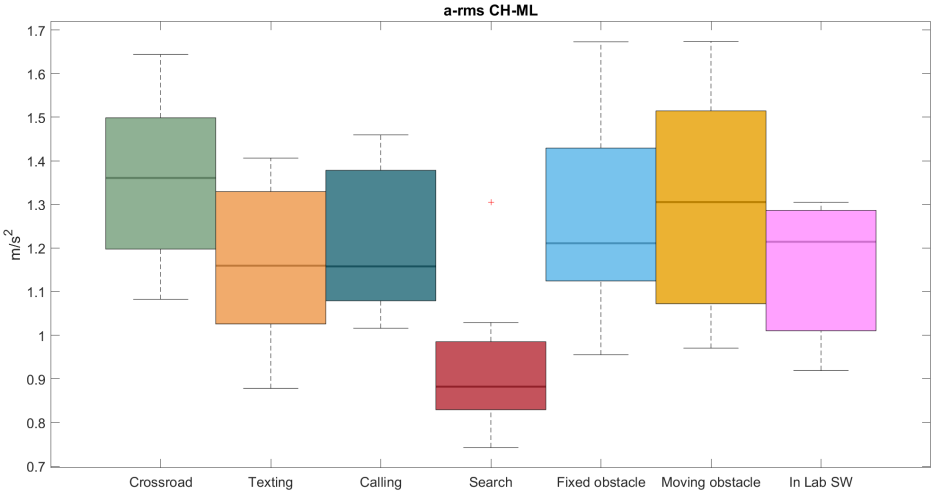

Figure 4.8: a-rms CH-ML

a-rms CH-ML distributions during visual search (mdn 0.88 IQR 0.16 m/s^2) significantly differed from crossroad (mdn 1.36 IQR 0.30 m/s^2, d=2.11), fixed obstacle (mdn 1.21 IQR 0.30 m/s^2, d=1.68) and moving obstacle (mdn 1.31 IQR 0.44 m/s^2, d=1,85).

a-rms CH-AP

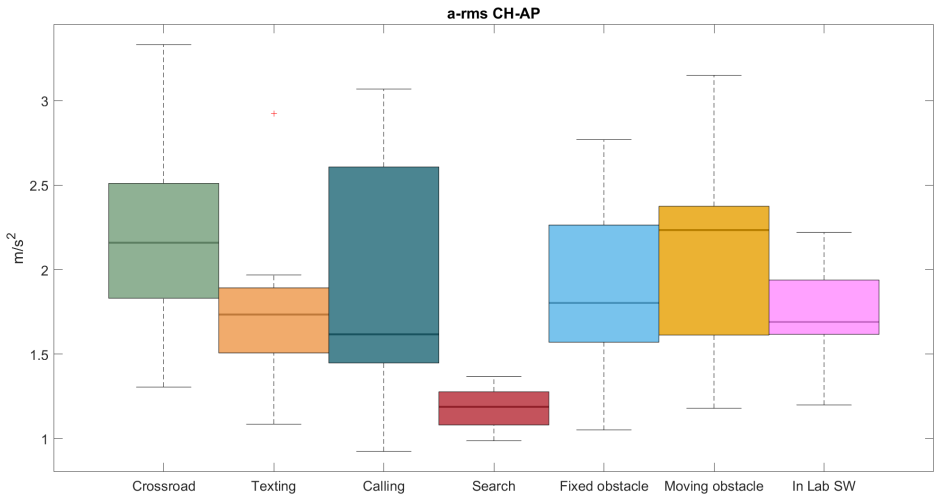

Figure 4.9: a-rms CH-AP

a-rms CH-AP distributions during visual search (mdn 1.19 IQR 0.20 m/s^2) significantly differed from crossroad (mdn 2.16 IQR 0.68 m/s^2, d=1.90) and moving obstacle (mdn 2.23 IQR 0.76 m/s^2, d=1,70).

a-rms LB-V

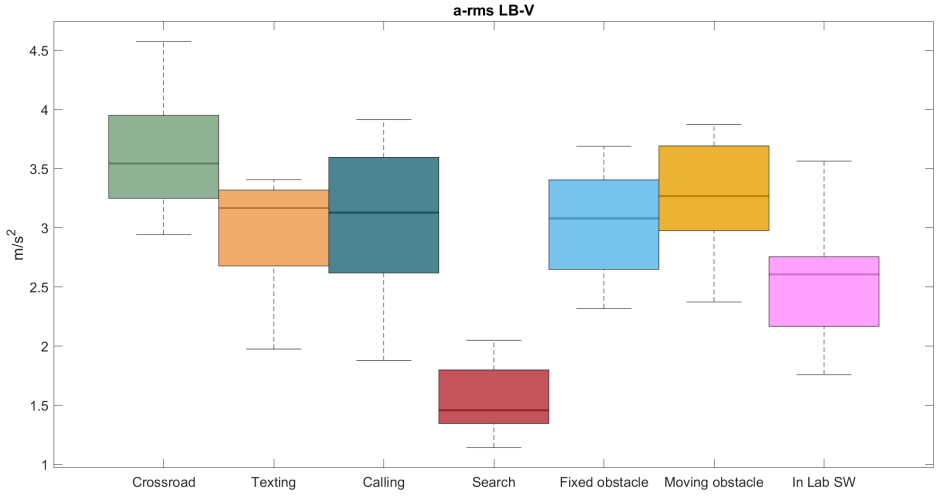

Figure 4.10: a-rms LB-V

a-rms LB-V distributions during visual search (mdn 1.46 IQR 0.45 m/s^2) significantly differed from all other labels (d>1.91).Lab walking (mdn 2.60 IQR 0.59 m/s^2) was significantly different from crossroad (mdn 3.54 IQR 0.70 m/s^2, d=2.06).

a-rms LB-ML

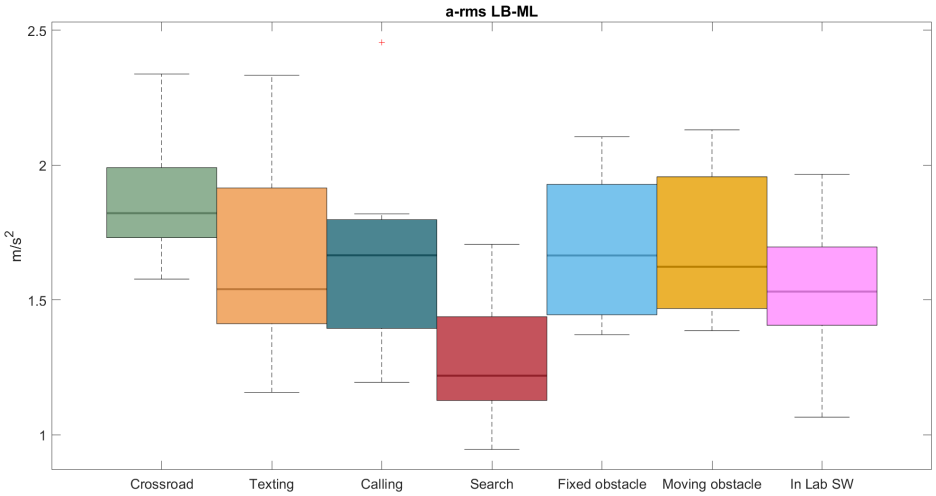

Figure 4.11: a-rms LB-ML

a-rms LB-ML distributions during visual search (mdn 1.22 IQR 0.31 m/s^2) significantly differed from crossroad (mdn 1.82 IQR 0.26 m/s^2, d=1.97).

a-rms LB-AP

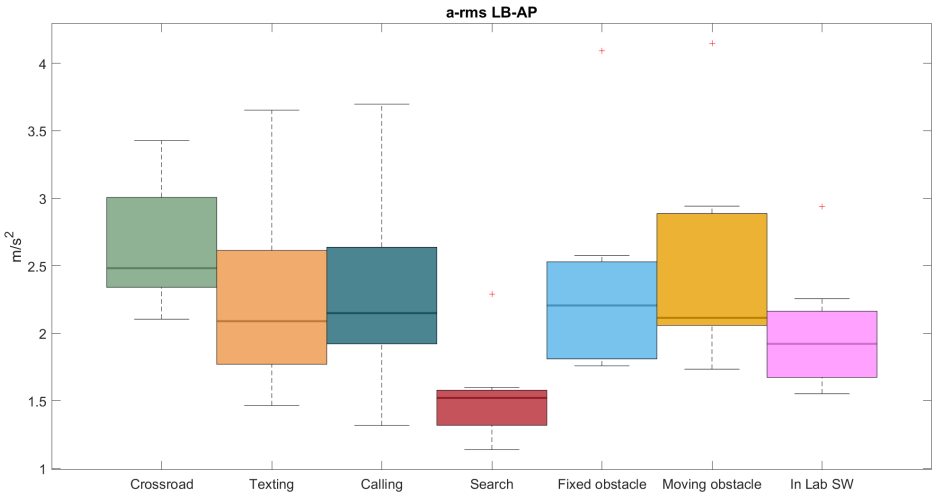

Figure 4.12: a-rms LB-AP

a-rms LB-ML distributions during visual search (mdn 1.52 IQR 0.26 m/s^2) significantly differed from crossroad (mdn 2.48 IQR 0.67 m/s^2, d=1.78) and moving obstacle (mdn 2.11 IQR 0.49 m/s^2, d=1,54).

Yaw ROM HD-LB

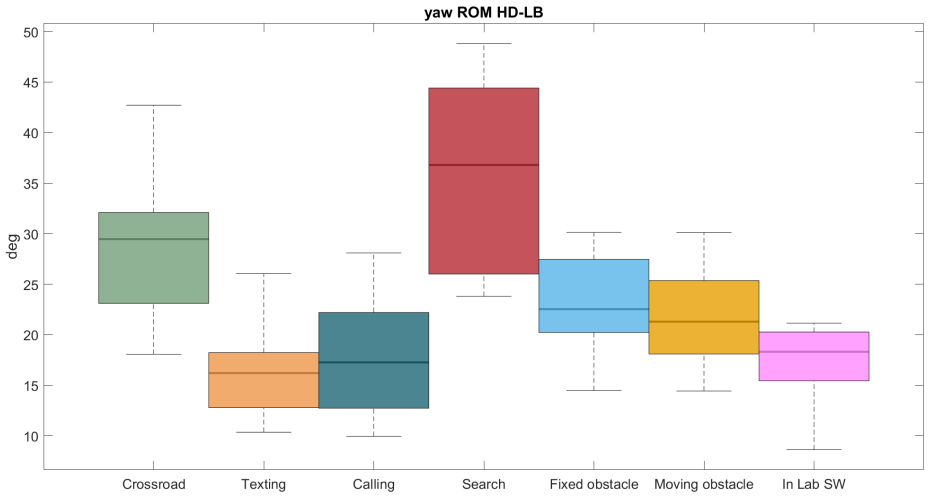

Figure 4.13: Yaw ROM HD-LB

Yaw ROM HD-LB distributions during visual search (mdn 36.80 IQR 18.41 deg) significantly differed form all other labels except crossroad (d>2.00). Crossroad (mdn 29.46 IQR 8.98 deg) instead differed significantly from texting (mdn 16.20 IQR 5.46 deg, d=1.94), calling (mdn 17.26 IQR 9.47 deg, d=1.72) and lab walking (mdn 18.31 IQR 4.82 deg, d=1.81).

Pitch ROM HD-LB

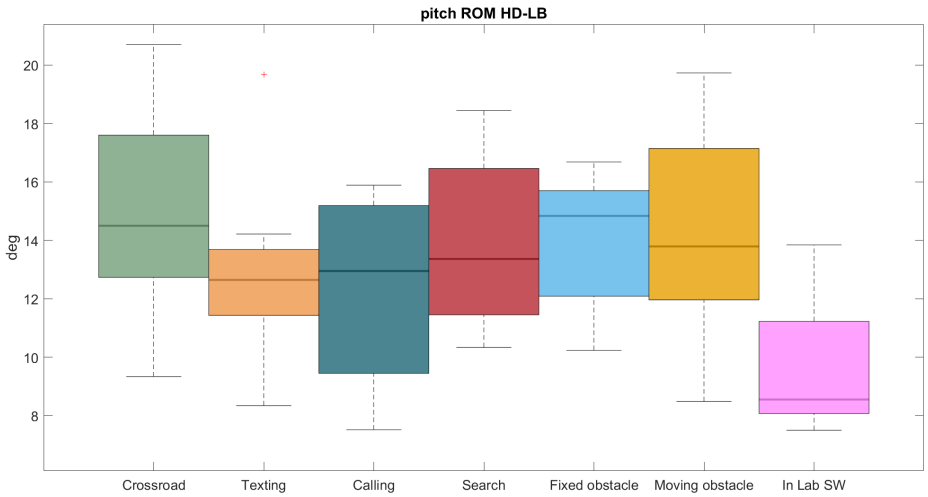

Figure 4.14: Pitch ROM HD-LB

Pitch ROM HD-LB distributions during crossroad (mdn 14.50 IQR 4.87 deg) significantly differed from lab walking (mdn 8.55 IQR 3.15 deg, d=1.72).

Yaw ROM HD-CH

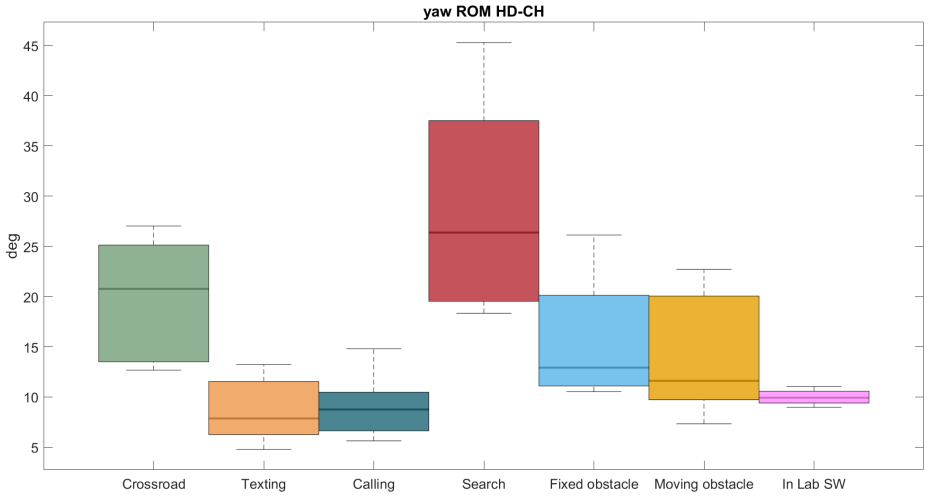

Figure 4.15: Yaw ROM HD-CH

Yaw ROM HD-CH distributions during visual search (mdn 26.36 IQR 17.97 deg) significantly differed form all other labels (d>1.57). Crossroad (mdn 20.76 IQR 11.61 deg) also differed significantly from texting (mdn 7.87 IQR 5.29 deg, d=1.94), calling (mdn 8.76 IQR 3.85 deg, d=1.88) and lab walking (mdn 9.92 IQR 1.17 deg, d=1.71).

Pitch ROM HD-CH

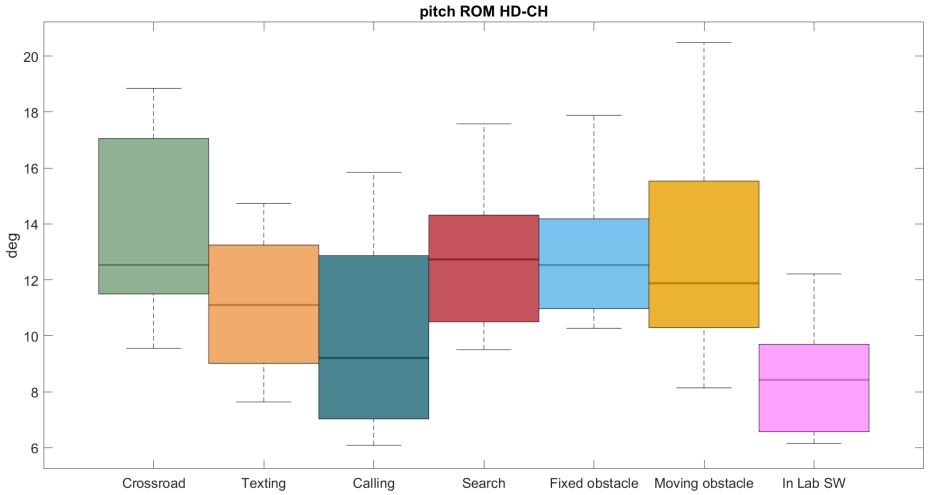

Figure 4.16: Pitch ROM HD-CH

Pitch ROM HD-CH distributions during crossroad (mdn 12.53 IQR 5.56 deg) significantly differed from lab walking (mdn 8.43 IQR 3.13 deg, d=1.75).

4.2.3 Attenuation

ACV HD-LB

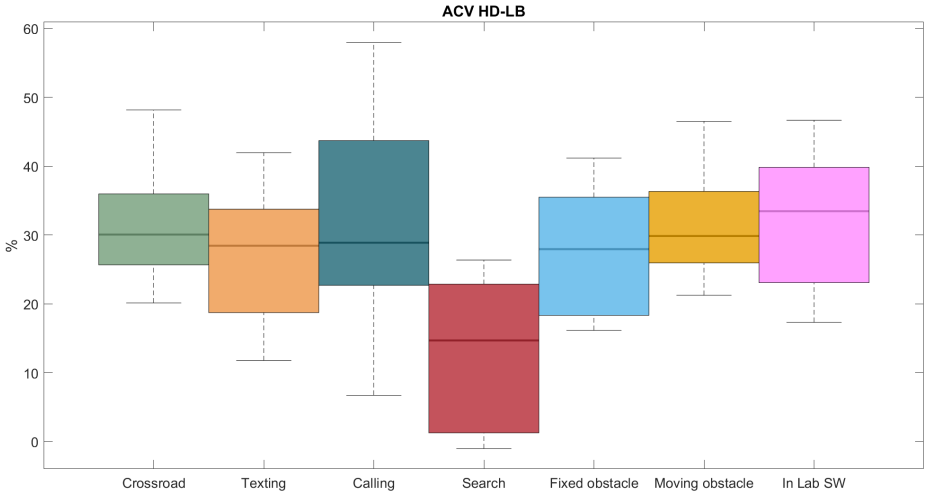

Figure 4.17: ACV HD-LB

ACV HD-LB distributions during visual search (mdn 14.70 IQR 21.60 %) differed from crossroad (mdn 30.07 IQR 10.31 %, d=1.65), calling (mdn 28.89 IQR 21.03 %, d=1.69), moving obstacle (mdn 29.87 IQR 10.38 %, d=1.65) and lab walking(mdn 33.47 IQR 16.76 %, d=1.70).

4.2.4 Symmetry

iHR V-LB

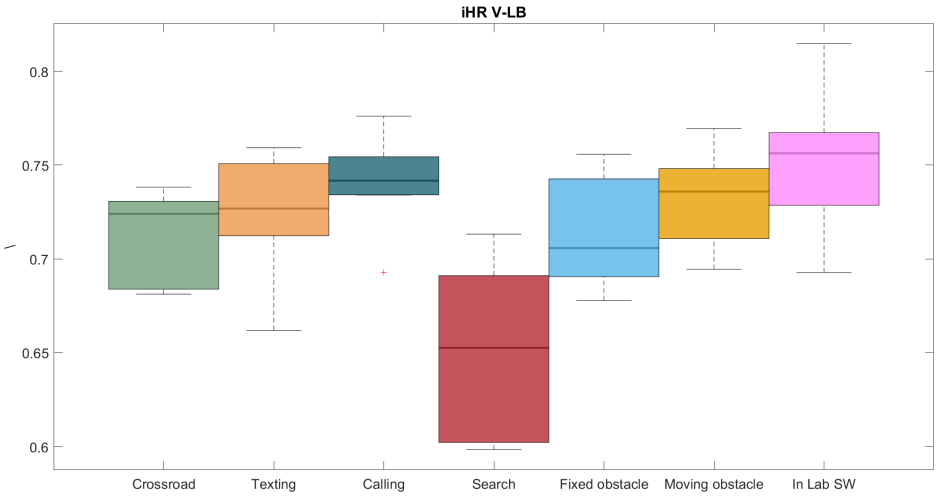

Figure 4.18: iHR V-LB

iHR V-LB distributions during visual search (mdn 0.65 IQR 0.09) differed significantly from all other labels (d>1.91).

iHR ML-LB

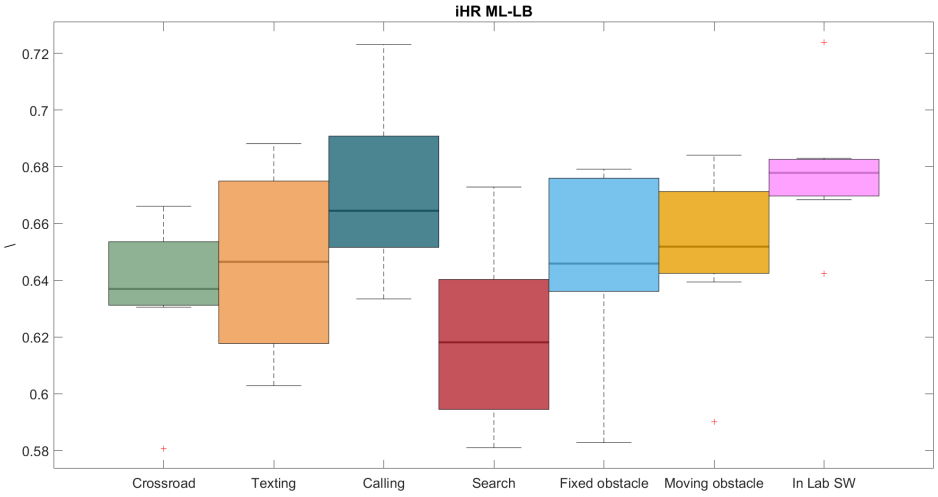

Figure 4.19: iHR ML-LB

iHR ML-LB distributions during visual search (mdn 0.62 IQR 0.05) differed significantly from calling (mdn 0.66 IQR 0.04, d=1.76) and lab walking (mdn 0.68 IQR 0.01, d=2.00).

iHR AP-LB

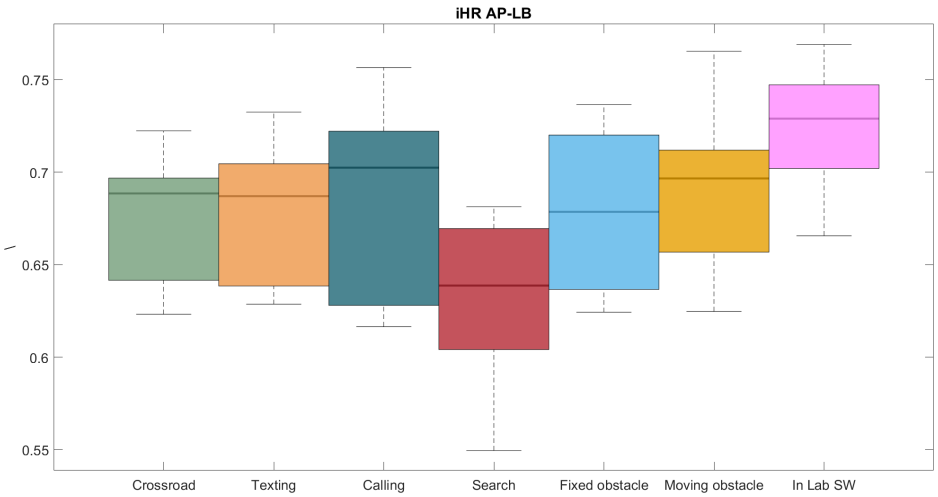

Figure 4.20: iHR AP-LB

iHR AP-LB distributions during visual search (mdn 0.64 IQR 0.07) differed significantly from straight walking (mdn 0.68 IQR 0.05, d=2.14).

4.2.5 Regularity

RCME V-HD

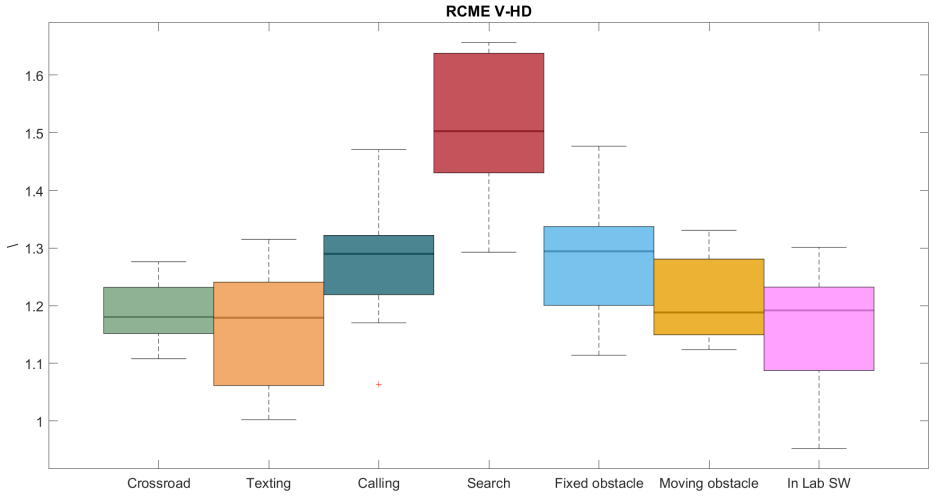

Figure 4.21: RCME V-HD

RCME V-HD distribution during visual search (mdn 1.50 IQR 0.21) differed significantly from all other labels (d>2.14).

Chapter 5

Discussion

The statistical analysis revealed significant differences across all examined domains, except for Smoothness. This highlights a widespread effect of the activities performed by the subjects during walking on the extracted parameters. The absence of differences in smoothness-related parameters could be attributed to the observed sample, which consisted solely of healthy young adults. This suggests that head movement fluidity may not be challenged or influenced by different activities in this population.
The gait parameters mainly highlighted the strong difference between the visual search task and the others. Several factors may have contributed to this result: the visual search task was performed inside a supermarket, a confined environment with limited space for movement and typically the presence of other individuals nearby, which likely reduced walking speed and stride length during navigation. Additionally, the increased cognitive load associated with actively searching for an item on crowded shelves may have influenced the difference compared to the other tasks, which involved a more passive interaction with the surrounding environment.
Stride duration in real-world was generally much shorter than in Lab walking, suggesting that different walking behaviors were adopted even for similar walking speeds.
RMS acceleration values exhibited patterns comparable to those of the gait parameters. Notably, accelerations were particularly elevated during street-crossing activities across all segments. This was probably due to the exploratory movements needed when checking incoming vehicles on the road. Generally people leaned forward when approaching and crossing the street, and this could have led to increased oscillations of head, chest and pelvis. The phenomenon described before could have also been augmented by the relatively higher stride speed of the road crossing activity.
Head yaw parameters showed the greatest number of significative differences among groups, for both the head-in-chest and the head-in-lower back metrics. This was the main indicator of difference in the active exploratory behavior that subjects adopted in the different activities.
Also improved harmonic ratio and entropy differed significantly for the visual search task, evidencing a reduction of gait symmetry and head motion regularity , especially in the vertical direction. This result could be influenced by the broad vertical distribution of products on supermarket shelves, that could have promoted the execution of additional movements to reach and/or identify the groceries.

Chapter 6

Conclusions

This study aimed to explore the integration of contextual information in the study of gait and head motion in real world scenarios.
Data from twenty-one young adults were collected and eleven of them were used to produce two highly detailed datasets for both the real-world, unconstrained acquisition and the In Lab reproduced tasks, by employing the most advanced available algorithms for event detection and orientation estimation.
Analysis of real-world gait showed many statistically significative differences across many of the evaluated parameters, confirming the initial hypothesis that motor behavior during walking is appreciably affected by the nature of the activities performed and the environmental stimuli encountered.

6.1 Limitations

This study had some limitations that should be considered when interpreting the results.

- The elaboration of video and audio data for the extraction of contextual information was made manually. The resulting process was highly time consuming and the label assignment was strongly influenced by the subjectivity of the labeler, even though many evaluation criteria were thoroughly described in the experimental protocol. Moreover, the temporal resolution of the labeling was relatively coarse (1 s), which may have affected the accurate assignment of labels to boundary strides and prevented the detection of very fast or brief events (duration $<$ 1s).

- The analyzed sample was very small (8 subjects) and constituted only by healthy young adults, limiting the generalizability of the observations. More subjects have been acquired and the elaboration of their data could improve this aspect.

- Data collection was carried out primarily in urban environments, with few or no observations conducted in domestic or natural settings. Expanding the analysis to these environments would also raise additional issues related to participant privacy.

- The passenger unit was approximated using only the head, chest, and lower back segments, neglecting the arms and other connecting parts such as the neck. Including them could have uncovered additional patterns with potential informational value.

- Visual exploration was evaluated only in terms of head and body motion, without considering the contribution of saccades and other eye movements. Accounting for the precise direction of gaze, rather than relying solely on head and torso orientation, could offer more detailed insights into the subject's actual interaction with the environment.

6.2 Future works

There are several potential improvements that could be applied to this study:

- The remaining subjects acquired should be included in the dataset. The development of an automatic labeling algorithm could be really useful and would also allow for subject observation in environments where personal privacy is an issue.

- Laboratory simulated activities have been acquired but were not included in the analysis. Confronting the unsupervised data from ecological acquisitions and lab tests for similar activities could confirm or confute the hypothesis that lab protocols struggle to catch the precise motor patterns adopted in real life situations.

- Older and pathological subjects could be observed using the proposed protocol, potentially evidencing more differences caused by the various activities.

- Gaze tracking devices should be integrated in the experimental setup, allowing a better evaluation of where and how the subjects attention is directed during gait and how the visual stimuli are managed.

- Future studies could focus on the motor response to specific sensory stimuli rather than on the type of activity performed. Stimulus-rich environments, such as busy urban streets, may influence gaze behavior and motor control differently compared to quieter indoor settings. Both the type and intensity of visual and auditory stimuli could have distinct effects on walking behavior.

Chapter 7

Appendix A - Orientation estimation

This study employed a Magdwick complementary filter for the orientation estimation from inertial data.

The used algorithm reliability was tested using a brief laboratory protocol that measured the performances compared to stereophotogrammetry (SP).

Experimental setup

The sensor configuration was the same of the In Lab acquisitions described in the study. A 3D-printed support housing the sensor and four markers for stereophotogrammetry was added to the head setup. Three of these markers were used to define the origin and axes of the plane on which the sensor lay during data acquisition. The fourth marker was added to facilitate the identification of the other three. The reference frame defined by the markers was aligned with the MIMu reference frame.
Inertial sensors sampled at 100 Hz and the SP system at 200 Hz.

Figure 7.1: Support with INDIP sensor and markers

The experiment was conducted in the stereophotogrammetry lab of Politecnico di Torino (Polito BioMedLab), equipped with a 12 camera Vicon system.

Experimental protocol

The experimental protocol consisted of a 12-minute acquisition of a single subject performing the following activities:

- 10 s slow head yaw
- 10 s standing, looking straight ahead
- 10 s slow head roll
- 10 s standing, looking straight ahead
- 10 s slow head pitch
- 10 s standing, looking straight ahead
- 10 s fast head yaw
- 10 s standing, looking straight ahead
- 10 s fast head roll
- 10 s standing, looking straight ahead
- 10 s fast head pitch
- 10 s standing, looking straight ahead
- 2 min standing, looking straight ahead
- 2 min walking with 90° turns, head aligned with trunk
- 2 min walking with 90° turns, free head movement
- 2 min walking in a figure-eight pattern

The tasks were selected to challenge the system and the orientation estimation algorithm, adopting a conservative approach to error estimation.

Data collection and synchronization

All data acquisition sessions were conducted using the custom-developed INDIP App, which enables the simultaneous connection and data logging of multiple INDIP MIMU via Bluetooth connection.Once each acquisition was completed, the data were manually retrieved from each device using a custom USB-based graphical user interface (INDIP GUI). This interface was also employed to synchronize the internal clocks of all INDIP units prior to data collection.
Simultaneously the position, in the lab reference frame, of markers on the head support was tracked with the Vicon system.
Using a custom matlab pipeline interfaced with the Vicon Nexus software, SP and inertial data were synchronized and stored in an organized `data.mat` file. In thi process SP data were downsampled to 100 Hz to match the MIMU sampling frequency.

Processing

SP data were filtered with a 4th order Butterworth low-pass filter with a 4 Hz cutoff frequency.
After this phase, the frame orientation was obtained with a geometric approach. Data were refined with a singular value decomposition(SVD) algorithm and then converted into quaternions.

The sensor orientation with inertial data was obtained applying the Magdwick algorithm. Both gyroscope and magnetometer were used in input to update the sensor angular position.
The computation was repeated with **17** different values of correction weight β obtaining a different quaternion matrix each time.

Error computation

For each β, the quaternion corresponding to the rotation from the first MIMU and SP quaternion was computed.
MIMU orientation was rotated of that quantity in order to impose the same starting orientation for both the MIMU and SP estimation. After that the orientation error was computed as the absolute relative position between the two estimations in an axis-angle notation.

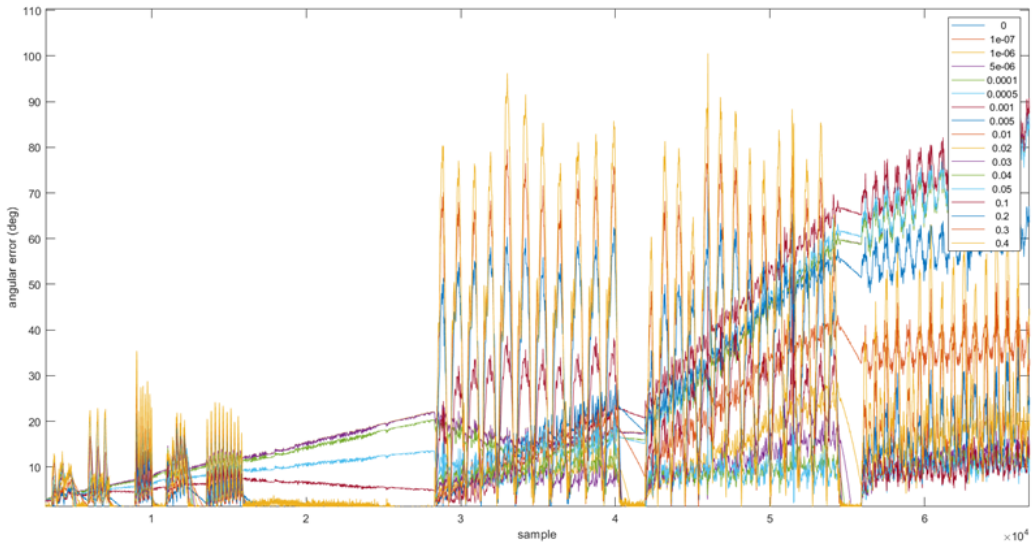

Figure 7.2: Plot of the orientation error in [deg] for the different β values

The rms value of the orientation error was used to choose the best β:

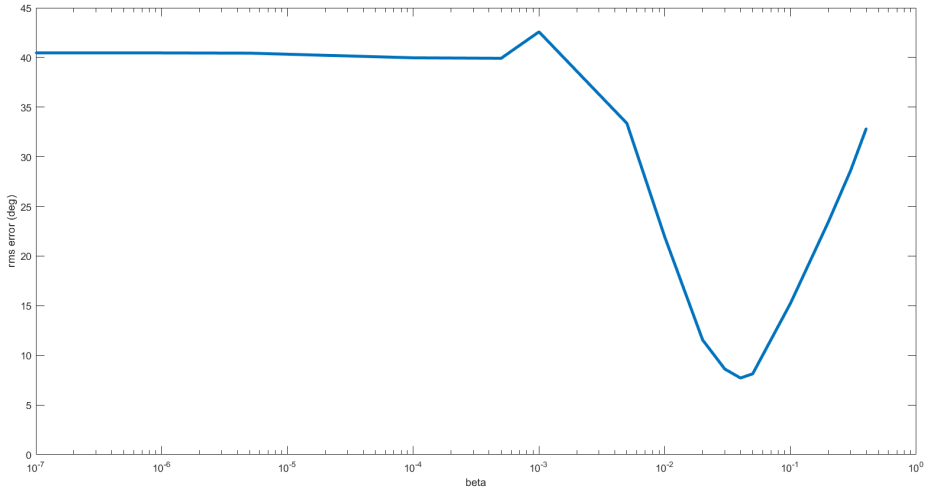

Figure 7.3: Root mean square value of the orientation error as a function of β

Results and Conclusions

The best β value was identified as 0.04 with and rms orientation error of 7.4°. The result was considered adequate to the precision required by the main study.

Bibliography

[1] Merriam-Webster. Gait. in merriam-webster.com dictionary. https://www.merriam-webster.com/dictionary/gait. Accessed 26/05/2025.

[2] Donald A. Neumann. *Kinesiology of the musculoskeletal system: Foundations for rehabilitation*. Mosby Elsevier, 2010.

[3] Michael W. Whittle. *Gait analysis: An introduction*. Butterworth-Heinemann, 1995.

[4] Cynthia C. Norkin Pamela K. Levangie. *Joint structure and function: A comprehensive analysis*. F.A. Davis Company, 2011.

[5] Physiopedia. The gait cycle. https://www.physio-pedia.com/The_Gait_Cycle. Accessed 26/05/2025.

[6] Judith M Burnfield Jacquelin Perry. *Gait Analysis: Normal and Pathological Function*. Slack Incorporated, 2010.

[7] MSD maluals. Gait disorders in older adults. https://www.msdmanuals.com/professional/geriatrics/gait-disorders-in-older-adults/gait-disorders-in-older-adults#Abnormal-Changes-in-Gait_v1136917. Accessed 06/06/2025.

[8] Thibault Warlop, Christine Detrembleur, Benjamin Bollens, Gaetan Stoquart, Frederic Crevecoeur, Anne Jeanjean, and Thierry M Lejeune. Temporal organization of stride duration variability as a marker of gait instability in parkinson's disease. *Journal of rehabilitation medicine*, 48(10):865–871, 2016.

[9] Stacy Fritz and Michelle Lusardi. White paper:"walking speed: the sixth vital sign". *Journal of geriatric physical therapy*, 32(2):2–5, 2009.

[10] Brian R Umberger. Stance and swing phase costs in human walking. *Journal of the Royal Society Interface*, 7(50):1329–1340, 2010.

[11] Ronita L Cromwell, Tina K Aadland-Monahan, Amy T Nelson, Sara M Stern-Sylvestre, and Bryan Seder. Sagittal plane analysis of head, neck, and trunk kinematics and electromyographic activity during locomotion. *Journal of Orthopaedic & Sports Physical Therapy*, 31(5):255–262, 2001.

[12] Ronita Cromwell, Jane Schurter, Scott Shelton, and Sagira Vora. Head stabilization strategies in the sagittal plane during locomotor tasks. *Physiotherapy Research International*, 9(1):33–42, 2004.

[13] Peter Hausamann, Martin Daumer, Paul R MacNeilage, and Stefan Glasauer. Ecological momentary assessment of head motion: Toward normative data of head stabilization. *Frontiers in human neuroscience*, 13:179, 2019.

[14] JJ Kavanagh, Steven Morrison, and RS Barrett. Coordination of head and trunk accelerations during walking. *European journal of applied physiology*, 94:468–475, 2005.

[15] Claudia Mazzà, Marco Iosa, Fabrizio Pecoraro, and Aurelio Cappozzo. Control of the upper body accelerations in young and elderly women during level walking. *Journal of neuroengineering and rehabilitation*, 5:1–10, 2008.

[16] JL Bellanca, KA Lowry, JM Vanswearingen, JS Brach, and MS Redfern. Harmonic ratios: a quantification of step to step symmetry. *Journal of biomechanics*, 46(4):828–831, 2013.

[17] John M Franchak, Brianna McGee, and Gabrielle Blanch. Adapting the coordination of eyes and head to differences in task and environment during fully-mobile visual exploration. *PLoS one*, 16(8):e0256463, 2021.

[18] Anshul Srivastava, Omar F Ahmad, Christopher Pham Pacia, Mark Hallett, and Codrin Lungu. The relationship between saccades and locomotion. *Journal of movement disorders*, 11(3):93, 2018.

[19] ScienceDirect. Saccadic velocity. `https://www.sciencedirect.com/topics/nursing-and-health-professions/saccadic-velocity`. Accessed 11/06/2025.

[20] Rainer Beurskens, Fabian Steinberg, Franziska Antoniewicz, Wanja Wolff, and Urs Granacher. Neural correlates of dual-task walking: Effects of cognitive versus motor interference in young adults. *Neural plasticity*, 2016(1):8032180, 2016.

[21] Nodoka Kimura and Robert van Deursen. The effect of visual dual-tasking interference on walking in healthy young adults. *Gait & Posture*, 79:80–85, 2020.

[22] Gabriella H Small, Lydia G Brough, and Richard R Neptune. The influence of cognitive load on balance control during steady-state walking. *Journal of biomechanics*, 122:110466, 2021.

[23] Prakruti Patel, Melissa Lamar, and Tanvi Bhatt. Effect of type of cognitive task and walking speed on cognitive-motor interference during dual-task walking. *Neuroscience*, 260:140–148, 2014.

[24] Emad Al-Yahya, Helen Dawes, Lesley Smith, Andrea Dennis, Ken Howells, and Janet Cockburn. Cognitive motor interference while walking: a systematic review and meta-analysis. *Neuroscience & Biobehavioral Reviews*, 35(3):715–728, 2011.

[25] Pritika Dasgupta, Jessie VanSwearingen, and Ervin Sejdic. "you can tell by the way i use my walk." predicting the presence of cognitive load with gait measurements. *Biomedical engineering online*, 17:1–18, 2018.

[26] Simon Ho, Amelia Mohtadi, Kash Daud, Ute Leonards, and Todd C Handy. Using smartphone accelerometry to assess the relationship between cognitive load and gait dynamics during outdoor walking. *Scientific reports*, 9(1):3119, 2019.

[27] Lisa A Zukowski, Jaclyn E Tennant, Gozde Iyigun, Carol A Giuliani, and Prudence Plummer. Dual-tasking impacts gait, cognitive performance, and gaze behavior during walking in a real-world environment in older adult fallers and non-fallers. *Experimental gerontology*, 150:111342, 2021.

[28] Edgar R Vieira, Hyun-Hwa Lim, Denis Brunt, Camilla Z Hallal, Laura Kinsey, Lisa Errington, and Mauro Gonçalves. Temporo-spatial gait parameters during street crossing conditions: a comparison between younger and older adults. *Gait & posture*, 41(2):510–515, 2015.

[29] Giuseppe Angelo Zito, Dario Cazzoli, Loreen Scheffler, Michael Jäger, René Martin Müri, Urs Peter Mosimann, Thomas Nyffeler, Fred W Mast, and Tobias Nef. Street crossing behavior in younger and older pedestrians: an eye-and head-tracking study. *BMC geriatrics*, 15:1–10, 2015.

[30] Valentina Agostini, Francesco Lo Fermo, Giuseppe Massazza, and Marco Knaflitz. Does texting while walking really affect gait in young adults? *Journal of neuroengineering and rehabilitation*, 12:1–10, 2015.

[31] Yue Luo, Haolan Zheng, Yuhao Chen, Wayne CW Giang, and Boyi Hu. Influences of smartphone operation on gait and posture during outdoor walking task. In *Proceedings of the Human Factors and Ergonomics Society Annual Meeting*, volume 64, pages 1723–1727. SAGE Publications Sage CA: Los Angeles, CA, 2020.

[32] Viktor Losing and Martina Hasenjäger. A multi-modal gait database of natural everyday-walk in an urban environment. *Scientific data*, 9(1):473, 2022.

[33] Abhishek Sharma, Vijeth Rai, Melissa Calvert, Zhongyi Dai, Zhenghao Guo, David Boe, and Eric Rombokas. A non-laboratory gait dataset of full body kinematics and egocentric vision. *Scientific Data*, 10(1):26, 2023.

[34] Vectornav. Inertial navigatio primer. `https://www.vectornav.com/resources/inertial-navigation-primer/theory-of-operation/theory-inertial`. Accessed 19/06/2025.

[35] Riccardo Antonello, Roberto Oboe, et al. *MEMS gyroscopes for consumers and industrial applications*. InTech, 2011.

[36] Dimosthenis E Bolanakis. *MEMS barometers toward vertical position detection: background theory, system prototyping, and measurement analysis*. Morgan & Claypool Publishers, 2017.

[37] Alessandra Audisio, Daniele Fortunato, Paolo Tasca, Marco Caruso, and Andrea Cereatti. Vertical displacement of the approximated body center of mass during typical daily activities: A transition-based complementary filter method using barometric and inertial data. *Journal of Biomechanics*, page 112711, 2025.

[38] S Santosh Kumar and BD Pant. Design principles and considerations for the 'ideal'silicon piezoresistive pressure sensor: a focused review. *Microsystem technologies*, 20:1213–1247, 2014.

[39] Javad Karamdel. Simulation and analysis different mems pressure sensor uses comsol multiphysics 5.2.

[40] Stefano Bertuletti, Andrea Cereatti, Daniele Comotti, Michele Caldara, and Ugo Della Croce. Static and dynamic accuracy of an innovative miniaturized wearable platform for short range distance measurements for human movement applications. *Sensors*, 17(7):1492, 2017.

[41] Rachele Rossanigo, Marco Caruso, Stefano Bertuletti, Franca Deriu, Marco Knaflitz, Ugo Della Croce, and Andrea Cereatti. Base of support, step length and stride width estimation during walking using an inertial and infrared wearable system. *Sensors*, 23(8):3921, 2023.

[42] ST Electronics. Vl6180x time-of-flight (tof) proximity sensor and ambient light sensing (als) module. `https://www.st.com/en/imaging-and-photonics-solutions/vl6180x.html`. Accessed 19/06/2025.

[43] Francesca Salis, Stefano Bertuletti, Tecla Bonci, Marco Caruso, Kirsty Scott, Lisa Alcock, Ellen Buckley, Eran Gazit, Clint Hansen, Lars Schwickert, et al. A multi-sensor wearable system for the assessment of diseased gait in real-world conditions. *Frontiers in Bioengineering and Biotechnology*, 11:1143248, 2023.

[44] M Encarna Micó-Amigo, Tecla Bonci, Anisoara Paraschiv-Ionescu, Martin Ullrich, Cameron Kirk, Abolfazl Soltani, Arne Küderle, Eran Gazit, Francesca Salis, Lisa Alcock, et al. Assessing real-world gait with digital technology? validation, insights and recommendations from the mobilise-d consortium. *Journal of neuroengineering and rehabilitation*, 20(1):78, 2023.

[45] Cameron Kirk, Arne Küderle, M Encarna Micó-Amigo, Tecla Bonci, Anisoara Paraschiv-Ionescu, Martin Ullrich, Abolfazl Soltani, Eran Gazit, Francesca Salis, Lisa Alcock, et al. Mobilise-d insights to estimate real-world walking speed in multiple conditions with a wearable device. *Scientific reports*, 14(1):1754, 2024.

[46] Robbin Romijnders, Francesca Salis, Clint Hansen, Arne Küderle, Anisoara Paraschiv-Ionescu, Andrea Cereatti, Lisa Alcock, Kamiar Aminian, Clemens Becker, Stefano Bertuletti, et al. Ecological validity of a deep learning algorithm to detect gait events from real-life walking bouts in mobility-limiting diseases. *Frontiers in Neurology*, 14:1247532, 2023.

[47] P Tasca, F Salis, S Rosati, G Balestra, C Mazzà, and A Cereatti. Estimating gait speed in the real world with a head-worn inertial sensor. *IEEE Transactions on Neural Systems and Rehabilitation Engineering*, 2025.

[48] Luca Palmerini, Luca Reggi, Tecla Bonci, Silvia Del Din, M Encarna Micó-Amigo, Francesca Salis, Stefano Bertuletti, Marco Caruso, Andrea Cereatti, Eran Gazit, et al. Mobility recorded by wearable devices and gold standards:

the mobilise-d procedure for data standardization. *Scientific Data*, 10(1):38, 2023.

[49] Sebastian OH Madgwick et al. An efficient orientation filter for inertial and inertial/magnetic sensor arrays. 2010.

[50] Christopher Buckley, Brook Galna, Lynn Rochester, and Claudia Mazzà. Upper body accelerations as a biomarker of gait impairment in the early stages of parkinson's disease. *Gait & posture*, 71:289–295, 2019.

[51] Christopher L Vaughan and Mark J O'Malley. Froude and the contribution of naval architecture to our understanding of bipedal locomotion. *Gait & posture*, 21(3):350–362, 2005.

[52] Claudia Mazzà, Marco Iosa, Pietro Picerno, and Aurelio Cappozzo. Gender differences in the control of the upper body accelerations during level walking. *Gait & posture*, 29(2):300–303, 2009.

[53] Ilaria Pasciuto, Elena Bergamini, Marco Iosa, Giuseppe Vannozzi, and Aurelio Cappozzo. Overcoming the limitations of the harmonic ratio for the reliable assessment of gait symmetry. *Journal of biomechanics*, 53:84–89, 2017.

[54] Paolo Brasiliano, Gaspare Pavei, and Elena Bergamini. Smooth moves: Comparing log dimensionless jerk metrics from body center of mass trajectory and wearable sensor acceleration during walking. *Sensors*, 25(4):1233, 2025.

[55] Sivakumar Balasubramanian, Alejandro Melendez-Calderon, and Etienne Burdet. A robust and sensitive metric for quantifying movement smoothness. *IEEE transactions on biomedical engineering*, 59(8):2126–2136, 2011.

[56] Alejandro Melendez-Calderon, Camila Shirota, and Sivakumar Balasubramanian. Estimating movement smoothness from inertial measurement units. *Frontiers in bioengineering and biotechnology*, 8:558771, 2021.

[57] Shuen-De Wu, Chiu-Wen Wu, Shiou-Gwo Lin, Kung-Yen Lee, and Chung-Kang Peng. Analysis of complex time series using refined composite multiscale entropy. *Physics Letters A*, 378(20):1369–1374, 2014.

[58] Espen AF Ihlen, Aner Weiss, Alan Bourke, Jorunn L Helbostad, and Jeffrey M Hausdorff. The complexity of daily life walking in older adult community-dwelling fallers and non-fallers. *Journal of biomechanics*, 49(9):1420–1428, 2016.